LA-8352-MS
Informal Report

2

The Premature Detonation Problem

LOS ALAMOS SCIENTIFIC LABORATORY
Post Office Box 1663 Los Alamos, New Mexico 87545

This report was not edited by the Technical Information staff.

This program was supported by the Department of Defense Joint Services Explosive Program and the US Army Armament Research and Development Command In-Bore Premature Study.

LA-8352-MS
Informal Report
UC-45
Issued: May 1980

The Premature Detonation Problem

George H. Pimbley
Elisabeth F. Marshall

CONTENTS

THE PREMATURE DETONATION PROBLEM

by

George H. Pimbley and Elisabeth F. Marshall

ABSTRACT

Determining how cavities or voids in the explosive loads of artillery shells cause in-bore premature detonations is important to military authorities. Though answers continue to be elusive, in detailing recent studies of the problem at LASL, we have examined some traditional approaches and suggest a new direction of investigation.

The aquarium experiment and the pipe test have been devised at LASL to model the events taking place in a base gap, or in an internal cavity, in the load of an accelerating artillery shell. To assess the data from these experiments we use numerical simulation.

This report describes both the experimental and the numerical simulation phases of the project. The commonly accepted gas compression, thermal ignition mechanism is not consistent with the results of this study. The dominant mechanism or mechanisms have not been identified.

I. INTRODUCTION

A. History of the Problem

1. Recognition of the Problem. Shell-type elongated projectiles containing bursting charges, fired from rifled cannon, were in general use by the time of the American Civil War. We have no record as to whether the Union or Confederate forces had any organized awareness of the problem of premature explosions within the bore of a gun. Similarly, if there was a "premature" problem during the Spanish-American conflict of 1898, or in World War I, we may guess that it escaped official notice. The lack of detonation in the black-powder charges of the former, and the slow detonation in the TNT and similar charges of the latter, precluded any great problem.

It was during World War II and in later conflicts, with the introduction of Composition B (Comp. B) as a load for shells, that premature detonation became a recognized problem. Comp. B, which is a mixture of 40% TNT and 60% RDX, is of sufficient sensitivity, and its detonation velocity is sufficiently high, to make the in-bore premature explosion a statistically significant risk.

2. Previous Experimental Work. In a classic demonstration, Bowden and Yoffe[1] showed in 1952 that trapped air in bubbles tended to sensitize nitroglycerin. A 40-gram hammer, which was dropped from 3 cm on an air bubble in nitroglycerin smeared on a plate, would initiate an explosion; in the absence of air bubbles, no explosion occurred even when a 1000-gram weight was dropped from 150 cm. Similar, though less marked, results were obtained by these investigators with voids in solid explosives. For a bubble-like void in PETN, the energy required to explode 50% of samples was 2.8×10^4 g-cm, while with no bubble it was 7.1×10^4 g-cm.

Firing tests with actual guns have been conducted with shells containing both artificial and known natural cavities in their charges. Generally, prematures have occurred with relatively large voids ($\sim$½ inch) at the base of the shell. The setback pressure of the charge resulting from the acceleration of the shell, and the consequent collapse of the void, is usually blamed.

Experiments reported in 1957 by the Arthur D. Little Co. served further to connect the occurrence of premature explosions with voids or cavities in the load of the shell.[2] Samples of Comp. B with artificial internal and surface cavities of various shapes and sizes were subjected to known shock pressures transmitted hydraulically to the sample. Frequencies of detonations for the various types of cavities were cataloged and studied.

Up to now the generally accepted mechanism whereby voids and cavities cause premature explosion of a loaded shell has been the supposed adiabatic compression of trapped air in collapsed cavities, with heating to the thermal ignition point. This viewpoint has been called into question during the course of our work at LASL. This is what the present report is about.

The question of the effect of voids and cavities has often been of interest in meetings of the High Explosive Working Group at LASL in recent years. In 1973-1974 the aquarium technique for experimenting with explosive samples was pioneered by B. G. Craig. Extensive tests were then conducted at LASL on simulated base gaps in cylinders of pressed TNT.[3,4] The results are used to help support the conclusions of this report, along with those of more recent aquarium tests.

B. Recent Studies at LASL

1. Aquarium Tests. Experiments were performed at LASL on the premature explosion problem, beginning in 1973-1974, using the aquarium technique and TNT samples. Further aquarium studies using Comp. B samples were done in 1978-1979. Known charges of explosive were detonated under water, and samples of pressed TNT or of Comp. B were thus subjected to water-transmitted shocks of known strength. These cylindrical samples were placed on a Plexiglas ring at calibrated distances from the center of detonation. Then the ring was submerged at a depth such that, upon detonation, the gas bubble vented before reaching maximum radius; thereby bubble oscillations were prevented. Each sample was enclosed in a Plexiglas cylinder, the latter being extended slightly beyond the sample face so that when capped with a Plexiglas cover, a gap was formed. The samples

were so mounted on the ring that these gaps were directly exposed to the oncoming shock wave. The gaps were thus designed to simulate the base cavity in a defective shell.

With the aquarium technique, a number of samples can be studied simultaneously under the same conditions in one experiment.

2. Pipe Tests. Yet another type of test performed at LASL in 1978-1979, involving cavities in an explosive, is the pipe test. This test was designed to study internal cavities and their possible role in causing in-bore premature explosions. A cylinder of explosive with an internal cavity is enclosed in an upright thick steel pipe, with a witness plug beneath it and a charge of propellant above it. The effects of various internal cavities, and the collapse thereof in a detonation, are read by measuring the deformation of the witness plug. These tests were also pioneered by B. G. Craig.

3. Computer Simulations. The two general types of experiments discussed above were simulated in a series of computer runs using the SIN,[5,8] 2DL,[6,8] and 2DE[7,8] codes that were developed at LASL. The SIN and 2DL codes employ difference analogs of the reactive hydrodynamic equations in Lagrangian coordinates. The SIN code was used with an assumption of spherical symmetry, whereas the 2DL code was applied without this assumption. The 2DE code is an Eulerian code and was used with an assumption of cylindrical symmetry. Numerical simulation is the current method for attempting to assess the chain of events in an experiment.

II. AQUARIUM TESTS

A. Methodology

1. The TNT Tests. A number of test cylinders of pressed TNT were mounted on a Plexiglas ring, the axis of each cylinder being directed toward the center of the ring. Each cylinder of explosive was 2.54 cm in diameter and 2.54 cm long, and the TNT was of density 1.611 g/cc. An undersize O-ring was shrunk on each sample at the end nearest the center of the ring, and a Plexiglas cylindrical shell was slipped over each O-ring and glued so as to extend a given distance beyond the TNT. Silicone grease was used to extend the plane of the TNT face to the inside of the Plexiglas cylinder without contaminating the face of the TNT. Plexiglas disks, 0.15 cm thick, were glued inside the extended ends of the Plexiglas cylinders so as to form the desired gaps. A Plexiglas disk was used also when a particular sample had no gap.

At the center of the ring was a sphere of explosive, consisting of an initiator at the center with a surrounding shell of PETN, density 1.55 g/cc, 0.635 cm thick. This ball was in turn enclosed in a shell of PBX-9404 of thickness 0.635 cm and density 1.844 g/cc. The water distance between the PBX-9404 surface of the central ball and the exposed face of each TNT sample cylinder was 9.754 cm.

With this apparatus, peak shock pressure transmitted to the exposed end of a cylindrical sample was estimated to be 2 kbar with a moderate air gap and 3 kbar with no air gap.

A total of 29 samples of pressed TNT were thus tested by water-transmitted shocks. As shown in Table I, these tests were conducted under various conditions of ambient temperature, with various widths for the base gaps, and assorted gases filling the gaps, including air, methane, and krypton. (The two experiments with

TABLE I

SUMMARY OF OBSERVATIONS OF TNT GAP IGNITION

Shot	Sample	T (°C)	Base Gap (mm)	Gas Gap (mm)	HE Surface Finish	HE Surface Coating	Condition of HE Sample
E-3822	1	36	0	Air	600 wet	None	No reaction
E-3851	2	29	0	Air	Polished	None	No reaction
E-3868	3	12	0	Air	Polished	None	No reaction
E-3851	4	29	1	Air	Polished	None	Blackened and cracked
E-3858	5	11.5	1	Air	Polished	None	Less blackened and cracked than sample 4.
E-3858	6	11.5	1	Air	600 dry	None	Blackened and cracked
E-3858	7	11.5	1	Air	120 dry	None	Blackened and more cracked than sample 4
E-3857	8	11	1	Air	Polished	Al	No reaction
E-3857	9	11	1	Air	120 dry	Al	No reaction
E-3857	10	11	1	Vac + H_2O	Polished	None	Larger cracks and blackened on half
E-3859	11	12	1	Kr	Polished	None	Blackened and cracked
E-3859	12	12	1	Me	Polished	None	Blackened and cracked
E-3859	13	12	1	Air	Polished	None	Least blackened of any of above
E-3868	14	12	1	Air	Polished	Krylon	Blackened and cracked
E-3868	15	12	1	Air	Polished	None	Not defined
E-3851	16	29	2	Air	Polished	None	Slightly more blackened and cracked than sample 4
E-3851	17	29	3	Air	Polished	None	Slightly more blackened and cracked than sample 16
E-3851	18	29	4	Air	Polished	None	Slightly more blackened and cracked than sample 17, some pitting near center
E-3822	19	36	5	Air	600 wet	None	Blackened and cracked a little more than sample 18
E-3858	20	11.5	5	Air	Polished	None	Blackened a little more than sample 19
E-3858	21	11.5	5	Air	120 dry	None	Blackened a little more than sample 19
E-3857	22	11	5	Air	Polished	Al	Significantly less blackening than sample 20
E-3857	23	11	5	Vac + H_2O	Polished	None	Blackened and deeply pitted on half
E-3859	24	12	5	Kr	Polished	None	Blackened a little more than sample 19
E-3859	25	12	5	Me	Polished	None	Blackened a little more than sample 19
E-3868	26	12	5	Air	Polished	None	Not defined
E-3868	27	12	5	Air	Polished	Krylon	Blackened and cracked a little more than sample 18
E-3822	28	36	10	Air	600 wet	None	More burned than any above
E-3822	29	36	15	Air	600 wet	None	Badly broken - almost exploded

vacuum gaps developed leaks and water was present in the gap.) The test samples had various finishes and a few had surface coatings, as noted in Table I.

2. The Comp. B Tests. Except for the use of Comp. B, density 1.715 g/cc, instead of TNT, the methodology was quite similar at first. There was a fixed number of test specimens of Comp. B mounted on the Plexiglas ring in each experiment, but in one of the experiments (shot #3221) the water distances between the PBX-9404 surface and the exposed faces of the Comp. B specimens were set at various amounts as shown in Table II. For shots #3222 and #3234, this distance was fixed at 8.5 cm. The arrangement of cylinders on the ring for these three shots, together with gap size and type, is shown in Fig. 1.

Experimental shot #3221 had one specimen with no gap. This was intended as a control. Four specimens, set on the ring with distances from the central ball of 8 cm, 8.5 cm, 9 cm, and 9.5 cm, each had air gaps of 0.5 cm. The last sample had a 0.5-cm vacuum gap of 1000 μm of mercury. Five samples were thus intended to simulate base cavities in shells (Fig. 1a).

Shot #3222, with six samples on the ring (8.5 cm from the ball), had gaps as follows: (a) three 5-mm gaps with, respectively, air, Comp. B powder at tapped pour density, and a vacuum of 180 μm of mercury; (b) two 2.5-mm gaps with, respectively, air and loosely packed Comp. B powder; (c) one gap with only 1 mm of very loosely packed Comp. B powder (Fig. 1b).

Shot #3234 was somewhat apart from the preceding shots. The Plexiglas holder for the Comp. B specimens was redesigned, as shown in Fig. 2, to have air-filled side gaps 2.5 mm wide. A suspicion had developed after the previous shots that two-dimensional effects might be important; that is, it was suspected that secondary shock pressure might be compressing the sides of a cylindrical specimen at a time prior to the arrival of the direct shock through the gap at the front face. The progress of a direct shock is generally slower in an air gap than in the surrounding water. Thus, all but one of the samples in shot #3234 had these redesigned Plexiglas holders.

Some of the samples in #3234 had grooved front covers, designed to break in a symmetrical manner upon arrival of the front shock. This was in response to suspicion that the manner of breakup of the front cover might be affecting the results (Fig. 1c).

All samples in shot #3234 had front gaps of 2.5 mm and the distance to the center ball was 8.5 cm in each case. See Table II and Fig. 1c.

B. Experimental Results

1. The TNT Tests. The results of all 29 tests are shown in Table I. In Table III we attempt to group these experimental results for easier interpretation. As seen in Table III, wider air gaps seem to be correlated with more damage to the sample (that is, more reaction), though this tendency may be reversed for krypton- and methane-filled gaps. There is some tendency for a rough surface to give more reaction than a smooth surface. Vacuum-plus-H_2O gaps produce about the same amount of reaction as air-filled gaps. An aluminum coating on the sample seems to result in less reaction, while a krylon coating results in more. There is more of a reaction when the aquarium test is performed at a significantly higher ambient temperature.

Figures 3-8 show the effects on the TNT samples that underwent the aquarium tests listed in Tables I and III.

TABLE II

RESULTS OF AQUARIUM EXPERIMENTS WITH COMP. B

Shot and Cylinder No.	Distance from Center of 9404 (mm)	Gap	Comments
3221-1	80	5 mm, air	Appreciable decomposition with blackened conical pit at center
3221-2	90	No gap	No reaction
3221-3	90	5 mm, vacuum (1000 μs)	More decomposition than corresponding air gap, 3221-4, pit almost obscured
3221-4	90	5 mm, air	Appreciable decomposition with pit
3221-5	95	5 mm, air	Appreciable decomposition with pit, less than 3221-1
3221-6	85	5 mm, air	Appreciable decomposition with pit
3221-1	85	5 mm filled with powdered Comp. B	No decomposition, cake of compacted powder recovered
3222-2	85	5 mm, air	Repeat of 3221-6, same result
3222-3	85	5 mm, vacuum (180 μs)	More decomposition than corresponding air gap, 3221-6 and 3222-2, no pit
3222-4	85	2.5 mm, air	Appreciable decomposition with pit
3222-5	85	2.5 mm filled with powdered Comp. B, not as tightly packed as 3222-1	Pale discoloration of both materials at powder-solid interface, surface smooth, portion of cake of compacted powder recovered
3222-6	85	1 mm loosely filled with powdered Comp. B	Pronounced discoloration of both materials at powder-solid interface, surface generally smooth, most of compacted powder recovered
3234-1	85	2.5 mm, air, grooved cover, coarse Comp. B particles glued on surface of Comp. B, side gaps	Extensive decomposition, sides splayed, more than in 3221-3
3234-2	85	2.5 mm, air, side gaps plain cover	Light blackening, small black pit, less than 3234-4
3234-3	85	2.5 mm, air, side gaps plain cover, vacuum (155 μs)	Fairly smooth, irregular 7-mm dark area
3234-4	85	2.5 mm, air, side gaps, grooved cover	Medium darkening, more pronounced in a 14-mm area at center, like 3221-1
3234-5	85	2.5 mm, air, side gaps, grooved cover, smeared with vacuum grease[a]	Smooth dent in center, no sign of reaction
3234-6	85	2.5 mm, air, no side gaps, grooved cover	Darkened about like 3222-6, irregular pits, one at center

[a] Dow-Corning high vacuum grease, Cat. No. 970V.

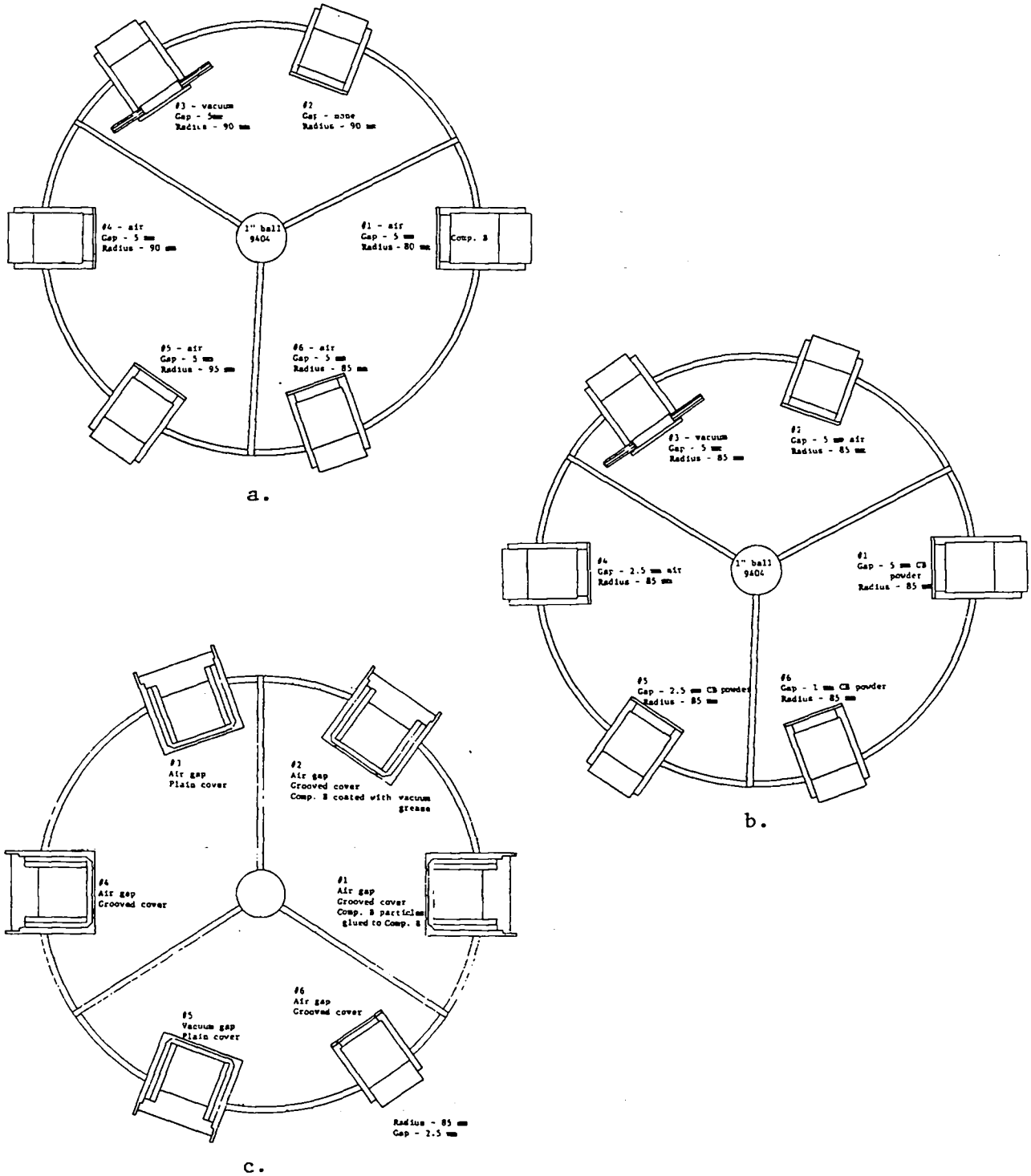

Fig. 1.
Arrangement of sample cylinders in Comp. B aquarium experiments.

TABLE III

COMPARISON OF OBSERVATIONS OF TNT GAP IGNITION

1. Gap Size

Polished Surface (29°C ambient temperature, no coating)

E-3851	No gap	No reaction
E-3851	1 mm air	Blackened and cracked
E-3851	2 mm air	Slightly more blackened and cracked
E-3851	3 mm air	Yet slightly more blackened and cracked
E-3851	4 mm air	More blackened and cracked, pitted near center

600 Wet Surface (36°C ambient temperature, no coating)

E-3822	No gap	No reaction
E-3822	5 mm air	Blackened and cracked
E-3822	10 mm air	Considerably burned
E-3822	15 mm air	Badly broken, almost exploded

Polished Surface (12°C ambient temperature, air in gap)

E-3868	No gap	No reaction
E-3868	1 mm, with krylon	Blackened and cracked
E-3868	1 mm, no coat	Not defined
E-3868	5 mm, no coat	Not defined
E-3868	5 mm, with krylon	Blackened and cracked

Polished Surface (12°C ambient temperature, no coating)

E-3859	1 mm, with krypton	Blackened and cracked
E-3859	1 mm, with methane	Blackened and cracked
E-3859	1 mm, with air	Less blackened and cracked
E-3859	5 mm, with krypton	Blackened
E-3859	5 mm, with methane	Blackened

2. Various Surface Finishes (no coating, 11.5°C ambient temperature, air in gap)

E-3858	1 mm, polished	Blackened and cracked
E-3858	1 mm, 600 dry	Blackened and cracked
E-3858	1 mm, 120 dry	Blackened and more cracked
E-3858	5 mm, polished	Blackened
E-3858	5 mm, 120 dry	Blackened

3. Vacuum - No Vacuum (polished, no coating)

E-3858	1 mm air, 11.5°C	Blackened and cracked
E-3857	1 mm vacuum + H_2O, 11°C	Large cracks, blackened on half
E-3858	5 mm air, 11.5°C	Blackened
E-3857	5 mm vacuum + H_2O, 11°C	Blackened and deeply pitted on half

4. Coating - No Coating (polished, air in gap)

E-3857	1 mm, Al, 11°C	No reaction
E-3858	1 mm, no coating, 11.5°C	Blackened and cracked
E-3868	1 mm, krylon, 12°C	Blackened and cracked
E-3857	5 mm, Al, 11°C	Less blackened
E-3858	5 mm, no coating, 11.5°C	Blackened
E-3868	5 mm, krylon, 12°C	Blackened and cracked

5. Ambient Temperature (polished, no coating)

E-5851	1 mm air, 29°C	Blackened and cracked
E-5858	1 mm air, 11.5°C	Less blackened and cracked
E-5859	1 mm air, 12°C	Least blackened

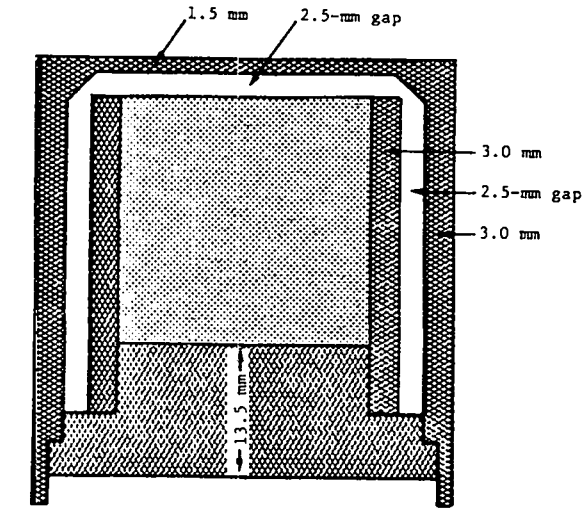

Fig. 2.
Specimen holder for aquarium shots, isolation type.

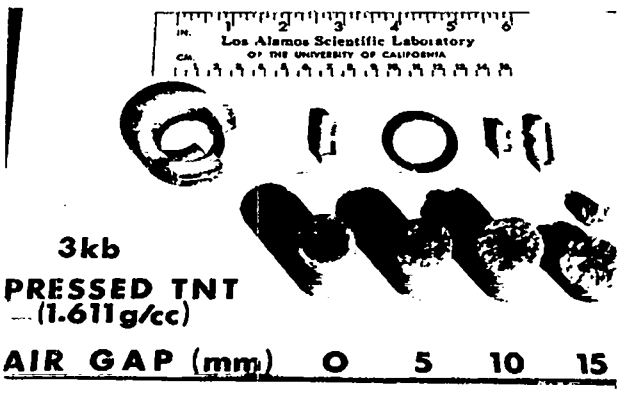

Fig. 3.
Appearance of samples and typical parts recovered from shot E-3822. The air gap is the thickness in millimeters of the base gap.

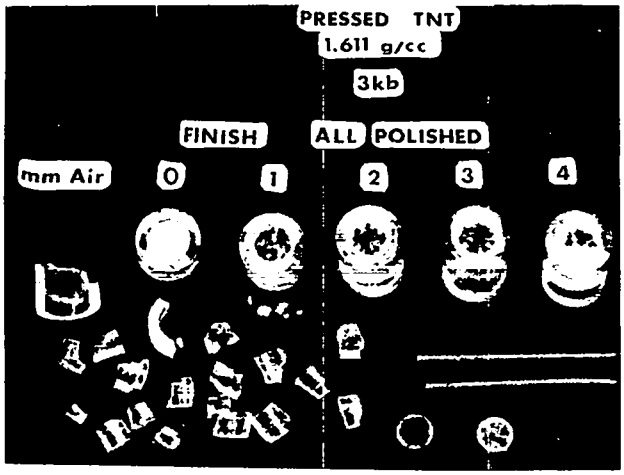

Fig. 4.
Appearance of samples and typical parts recovered from shot E-3851.

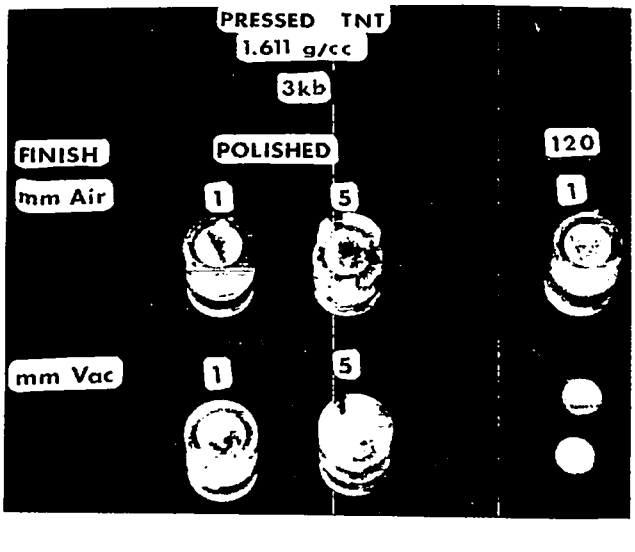

Fig. 5.
Appearance of samples recovered from shot E-3857. The two samples in the upper left were polished and coated with thin aluminum foil. The sample in the upper right was roughened with 120-grit carborundum and coated with aluminum.

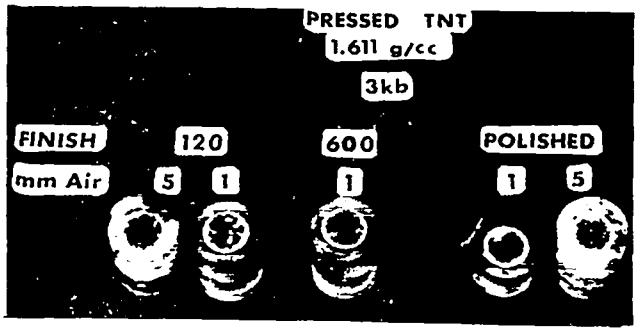

Fig. 6.
Appearance of samples recovered from shot E-3858.

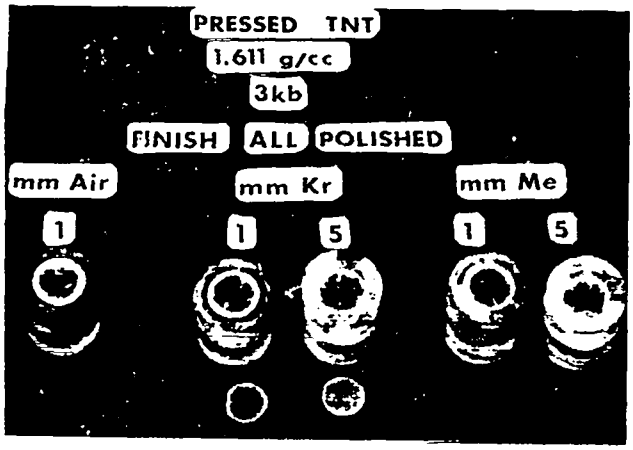

Fig. 7.
Appearance of samples recovered from shot E-3859.

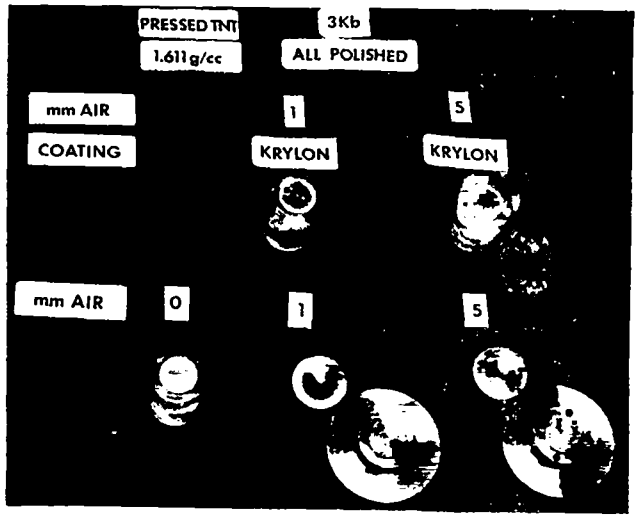

Fig. 8.
Appearance of samples recovered from shot E-3868.

2. The Comp. B Tests. In Table IV the results of all the Comp. B aquarium shots to date are classified and grouped.

Figures 9-13 are photographs showing the effects on the Comp. B samples listed in Tables II and IV.

A study of Table IV leads to the following conclusions for Comp. B specimens:

- The amount of decomposition in a cylindrical sample decreases with an increase in the water distance between the surface of the sample and the central ball.
- There is much more decomposition and pitting of a sample with an air gap than there is without any gap.
- There may be slightly more decomposition of a sample with a vacuum gap than of a sample with an air gap of the same size, but there is ambiguity. Air gaps seem to give slightly more pitting.
- There is slightly less decomposition and pitting of a sample with a grooved cover plate, particularly the center pit, than there is if the cover plate has no grooves.

TABLE IV

COMPARISON OF EFFECTS - COMP. B AQUARIUM TESTS

1. Various Radii from Center (identical assemblies, 5 mm air)		
3221-1	80 mm	Appreciable decomposition, blackened pit at center
3222-2	85 mm	Appreciable decomposition with pit
3221-6	85 mm	Appreciable decomposition with pit
3221-4	90 mm	Appreciable decomposition with pit
3221-5	95 mm	Appreciable decomposition with pit, but less than 3221-1
2. Gap and No Gap		
3221-4	No gap	No reaction
3221-2	5-mm gap	Appreciable decomposition with pit
3. Vacuum or Air		
90 mm, no side gap		
3221-4	5-mm air gap	Appreciable decomposition with pit
3221-3	5-mm vacuum, 1000 μm	More decomposition, pit almost obscured
85 mm, no side gap		
3221-6	5-mm air gap	Appreciable decomposition with pit
3222-3	5-mm vacuum, 180 μm	More decomposition but no pit
85 mm, with side gap		
3234-2	2.5-mm air gap	Light blackening, small black pit
3234-3	2.5-mm vacuum, 155 μm	Irregular dark area, fairly smooth
4. Grooved Cover Plate - No Grooves		
85-mm radius, no side gap		
3222-4	2.5-mm air gap, plain	Appreciable decomposition with pit
3234-6	2.5-mm air gap, grooved	Pronounced discoloration; irregular pits, one at center
85-mm radius, with side gap		
3234-2	25-mm air gap, plain	Light blackening, small black pit
3234-4	25-mm air gap, grooved	Medium darkening, more pronounced in a 14-mm area near center
5. Comp. B Powder or Particles, etc.		
85-mm radius, no side gap, no grooves		
3222-6	1 mm powder	Pronounced discoloration of both materials at powder-solid interface, surface generally smooth, most of compacted powder recovered
3222-4	2.5-mm air gap	Appreciable decomposition with pit
3222-5	2.5 mm powder	Pale discoloration of both materials at the powder-solid interface, surface smooth, portion of cake of compacted powder recovered
3222-2	5-mm air gap	Appreciable decomposition with pit
3221-6	5-mm air gap	Appreciable decomposition with pit
3222-1	5 mm powder	No decomposition, cake of compacted powder recovered
85-mm radius, grooved cover, 2.5-mm side gap		
3234-4	2.5-mm air gap	Medium darkening, more pronounced in a 14-mm area at center
3234-1	2.5-mm air gap, Comp B particles glued on face	Extensive decomposition, sides splayed
6. Vacuum Grease - No Vacuum Grease on Face (Dow-Corning, Cat. No. 970V)		
85-mm radius, 2.5-mm side gap, grooved cover		
3234-4	2.5-mm air gap	Medium darkening, more pronounced in a 14-mm area at center
3234-5	2.5-mm air gap, vacuum grease on face	Smooth dent in center, no sign of a reaction

•There is far less decomposition of a sample if the gap is filled with Comp. B powder than there is with an air filling. When coarse particles of Comp. B are glued on the face of the sample, however, the reaction is the most violent experienced in any of the Comp. B tests.

•For a sample with an air gap, there is slightly less decomposition and pitting if side gaps are present than there is if side gaps are absent.

•With side gaps, and in the presence of an air gap, there is no observable decomposition if the sample face is coated with vacuum grease.

The important results of the Comp. B experiments were that the presence of powdered Comp. B in a gap, or the coating of the sample surface with vacuum grease in the case of an air gap, each seem to nullify completely the presence of the gap. If the sample with an air gap has coarse particles of Comp. B glued on its face, however, the reaction is intense.

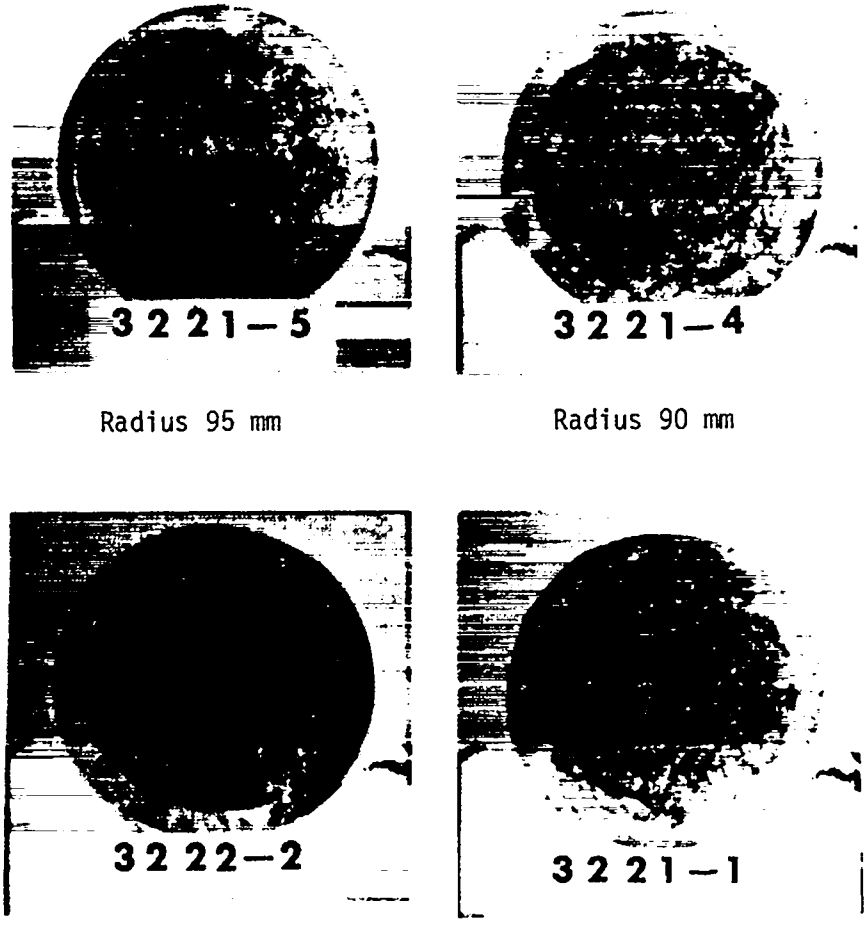

Fig. 9.
Effect of radius. All assemblies had a type-B specimen holder with an air-filled 5-mm base gap.

C. Numerical Modeling of the Aquarium Experiments

1. TNT Computations. Three one-dimensional Lagrangian calculations were performed using the SIN code[5] developed at LASL. These calculations (and the Comp. B calculations) were designed to model computationally the aquarium experiments described above.

A spherically symmetric geometry described by spherical coordinates was assumed. There is much in the concept of the aquarium experiment, however, that violates an assumption of spherical symmetry, such as the water surface and an essentially two-dimensional arrangement of cylindrical specimens of intermittent azimuthal occurrence. A cylinder itself is rather ill-fitting in a

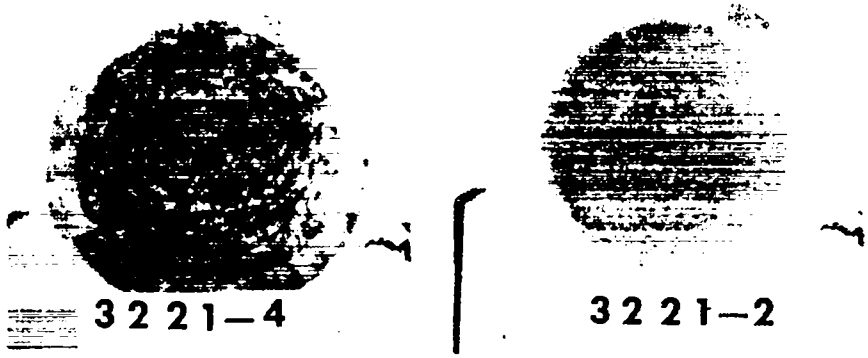

Type B specimen holder
5-mm base gap
Radius 90 mm

Type A specimen holder
No base gap
Radius 90 mm

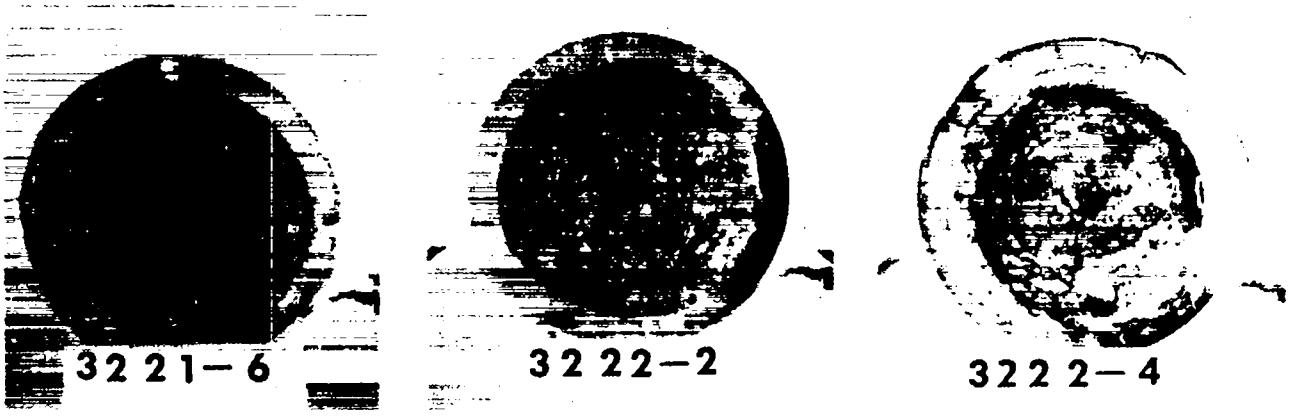

Type B specimen holder
5-mm base gap
Radius 85 mm

Type B specimen holder
5-mm base gap
Radius 85 mm

Type B specimen holder
2.5-mm base gap
Radius 85 mm

Fig. 10.
Effect of size of base gap. All gaps were filled with air.

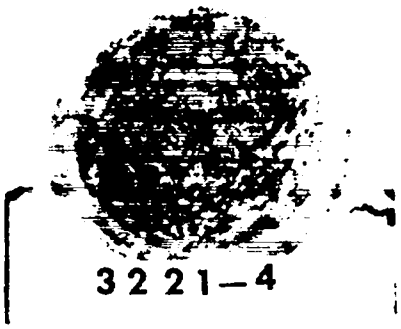

Base gap, 5 mm, air
Radius 90 mm
Type B specimen holder

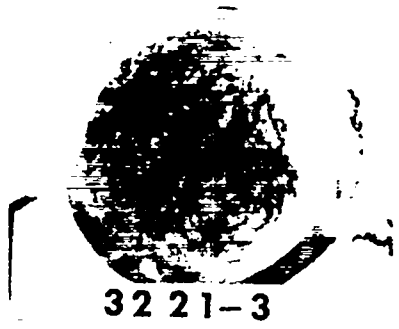

Base gap, 5 mm, vacuum (1000 μ)
Radius 90 mm
Type B specimen holder

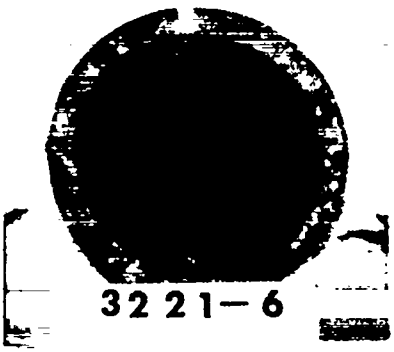

Base gap, 5 mm,air
Radius 85 mm
Type B specimen holder

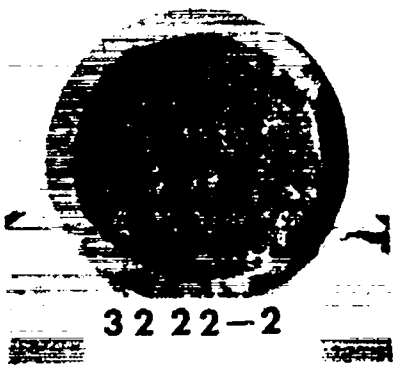

Base gap, 5 mm, air
Radius 85 mm
Type B specimen holder

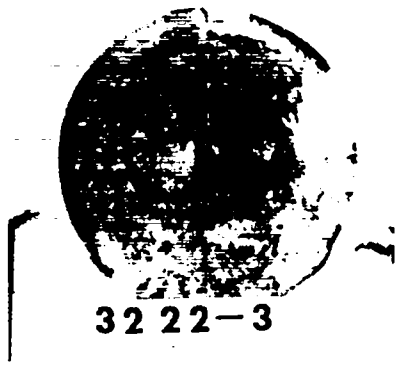

Base gap, 5 mm, vacuum (180 μ)
Radius 85 mm
Type B specimen holder

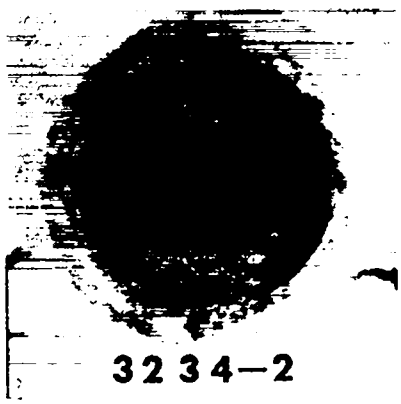

Base and side gaps, 2.5 mm, air
Radius 85 mm
Type D specimen holder

Base and side gaps, 2.5 mm, vacuum (155 μ)
Radius 85 mm
Type D specimen holder

Fig. 11.
Effect of vacuum.

spherical geometry. Our use of the SIN code and spherically symmetric coordinates was dictated by the availability, convenience, and efficiency of this code, with the thought that the results would probably be a very good first approximation.

The SIN code provides for sandwich-like layers of materials. Along the radial coordinate, starting from the center, one may prescribe materials in layers identical with those in the experiment. The code accepts physical data, etc., for each layered component material in sequence. Moving out from the center, the following three layers are common to all of our one-dimensional Lagrangian aquarium calculations: 0.1588 cm of hot spot PETN burned with the Arrhenius rate law, 0.4762 cm of PETN (again with the Arrhenius rate law), and 0.635 cm of PBX-9404 with the CJ volume burn. Out from this point, the layering varies with the particular calculation being done.

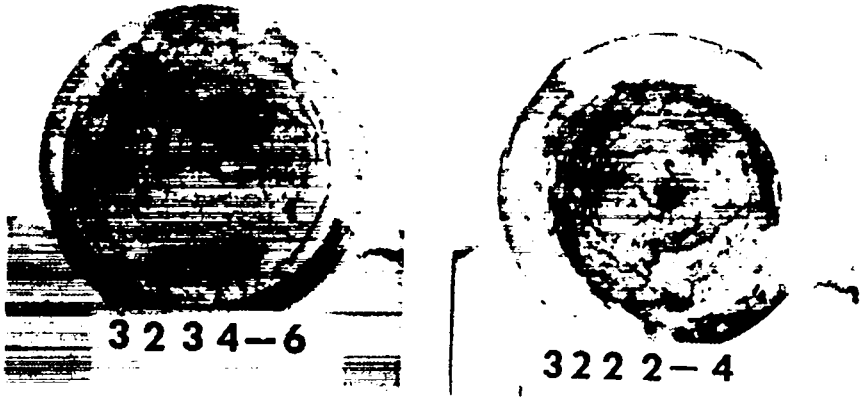

Type C specimen holder

Type B specimen holder

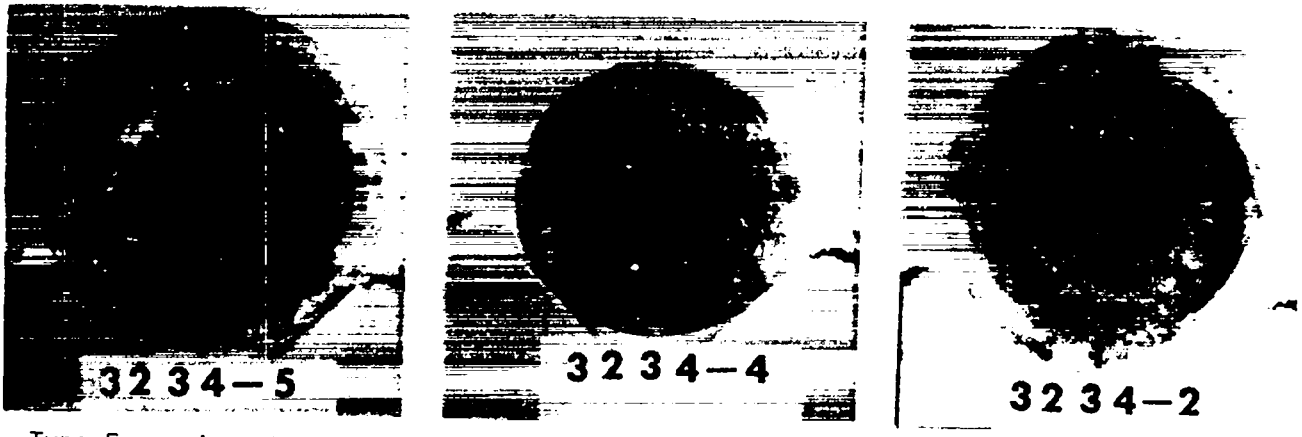

Type E specimen holder
Sample coated with
vacuum grease

Type E specimen holder

Type D specimen holder

Fig. 12.
Effects of various types of specimen holders and of vacuum grease on specimen. All assemblies had air-filled 2.5-mm base gaps and were at a radius of 85 mm.

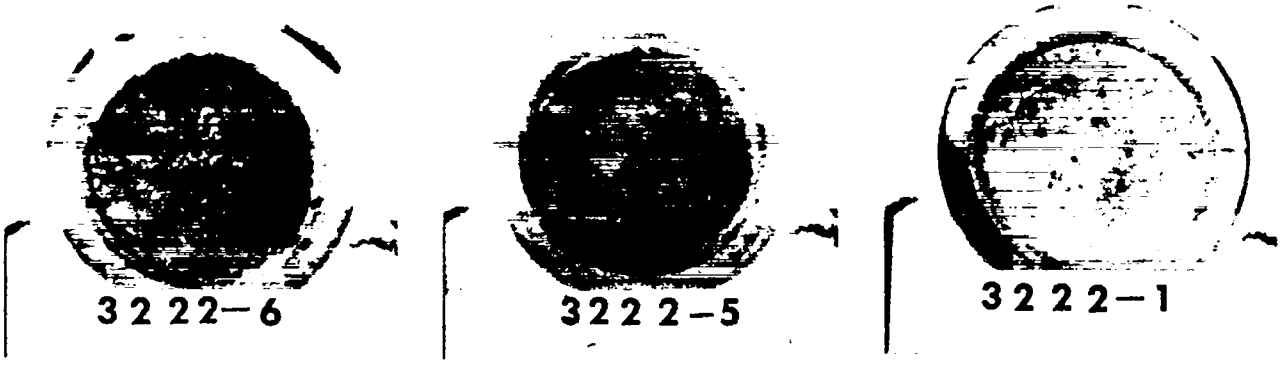

Base gap 1 mm
Type B specimen holder

Base gap 2.5 mm
Type B specimen holder

Base gap 5 mm
Type B specimen holder

Base gaps filled with sifted Comp. B

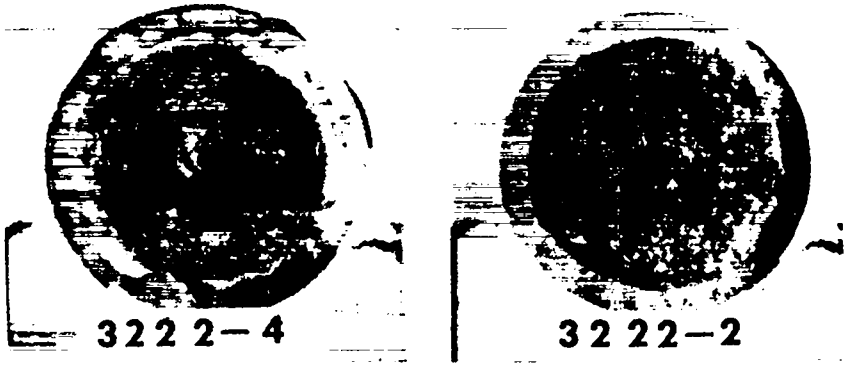

Base gap 2.5 mm
Type B specimen holder

Base gap 5 mm
Type B specimen holder

Air-filled base gaps

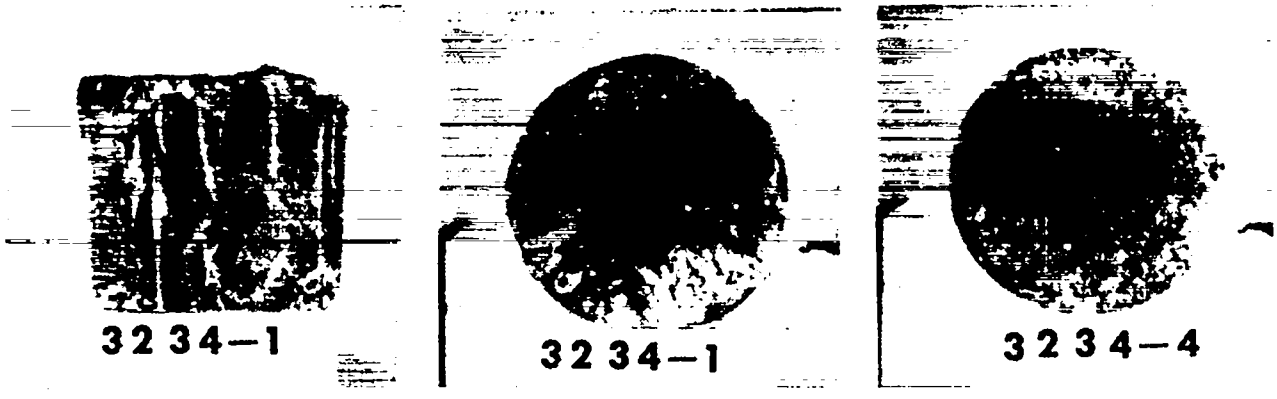

Coarse particles of Comp. B were glued on the face of the specimen.
Type E specimen holder

Plain
Type E specimen holder

Air-filled 2.5-mm base and side gaps

Fig. 13.
Effect of Comp. B powder and particles. All assemblies were at a radius of 85 mm.

The three TNT calculations involved, respectively, an air gap, a krypton-filled gap, and a methane-filled gap. In the first of these the PBX-9404 was followed by 9.68 cm of water, 0.15 cm of Plexiglas, 0.25 cm of air, and 2.0 cm of pressed TNT (with its relevant physical attributes). The other two TNT calculations were similar except for the substitution, respectively, of krypton and methane for the air. The data used for these materials is found in Appendix I.

The SIN code incorporates finite-difference schemes which date back to the pioneering work of J. von Neumann in Los Alamos. These schemes approximate the initial-boundary value problems for the reactive hydrodynamic equations (differential systems of high-order parabolic type) with options for plane, cylindrical, or spherically symmetric geometry. Though our understanding of these equations remains spotty, there is an accumulation of experience at Los Alamos with the computer simulation of such problems. Moreover, serious efforts have been made to test the SIN and other hydrodynamic codes and to compare the results with the few analytically derived solutions that are known for special cases.

The results of these calculations are given in Figs. 14-16. In Fig. 14, the four functions of time depict, respectively, the TNT shock pressure, the pressure at the air/TNT interface, the air temperature at the air center, and the air pressure at the air center. At 62 μs the temperature in the air gap builds up to about 3500 K and the pressure in the air gets to about 4.25 kbar. The pressure in the adjacent TNT peaks at about 63 μs and reaches about 3.33 kbar at that time. With test specimens #3851-2 and #3851-3 shown in Fig. 4, which may correspond, Table I lists blackening and cracking as the damage.

In Fig. 15 there are again four functions showing, with a krypton-filled gap, the calculated behavior in time of the TNT shock pressure, the pressure at the TNT/krypton interface, the krypton temperature at the krypton center, and the krypton pressure at the krypton center. The obvious feature of this calculation was the rise of the krypton temperature to 9250 K at about 62.25 μs. This was accompanied, however, by a krypton pressure that rises only to about 3.1 kbar. Apparently because of the low heat capacity of krypton, the available energy goes more into temperature rise in the gap and less into mechanical work. The samples from the corresponding shot (#3859), shown in Fig. 7, do have blackening and cracking. The transmitted pressure to the adjacent TNT reaches a peak of about 3 kbar at 64 μs. This is a lower peak than was obtained with the presence of an air gap.

In Fig. 16 the three functions show the computed time dependence of, respectively, the TNT shock pressure, the methane temperature at the methane center, and the methane pressure at the methane center. The peak methane pressure is 5.8 kbar and the peak temperature is 1350 K. The pressure decays rapidly to 3.4 kbar.

2. Comp. B Computations. Our Comp. B aquarium calculations come under two headings: one-dimensional Lagrangian and two-dimensional Lagrangian.

a. One-Dimensional Lagrangian Computations. Three basic one-dimensional SIN calculations were made assuming a spherically symmetric geometry with spherical coordinates.

The code accepts the same data for the layers of explosive in the central ball as given in the description of the TNT calculation.

For the Comp. B aquarium calculations the water distance between the surface of the PBX-9404 and the Plexiglas cover of the cylindrical sample was a constant 7.32 cm (in constrast with the experiments) and the Plexiglas cover was again 0.15 cm wide.

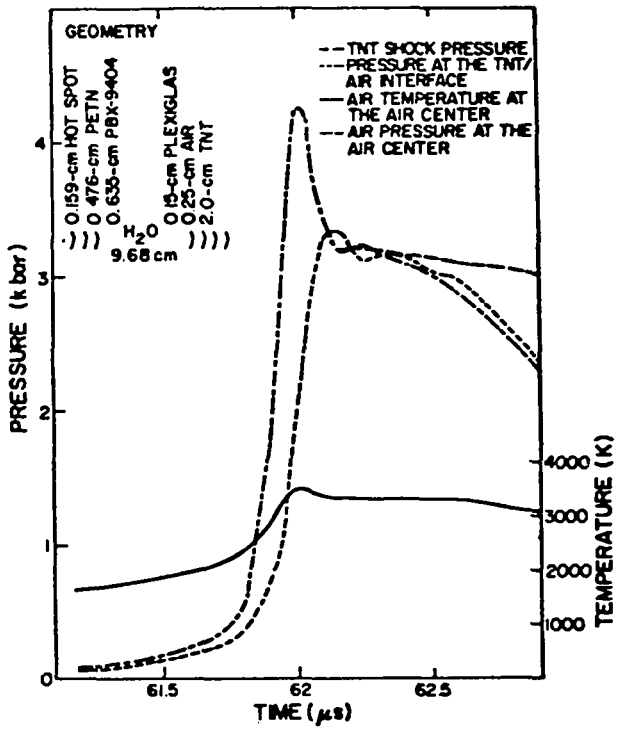

Fig. 14.
Calculated behavior in time of variables in the case of an air gap for TNT.

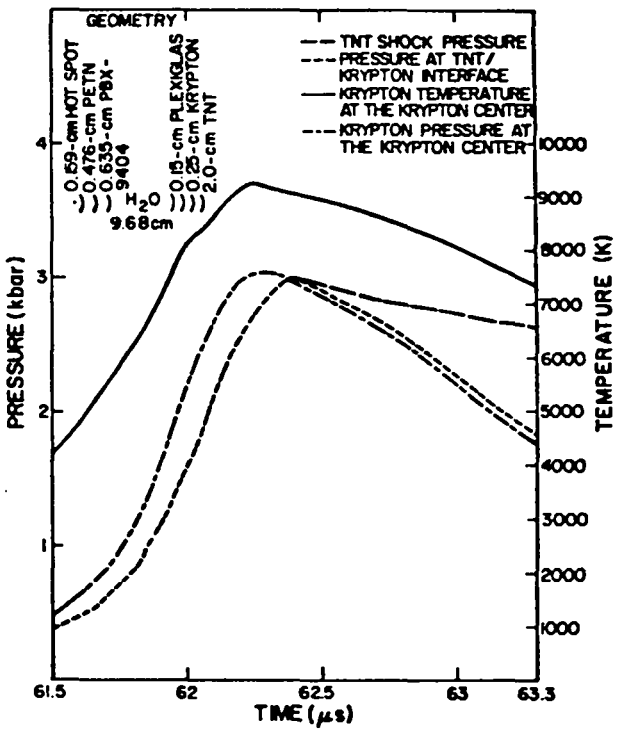

Fig. 15.
Calculated behavior in time of variables in the case of a krypton gap for TNT.

In the first Comp. B calculations, after the Plexiglas (going out from the center) came 0.25 cm of air and then 1.72 cm of Comp. B with heat conduction in the Comp. B coupled into the difference equations (but with no burning permitted). In the second calculation, after the Plexiglas came 0.25 cm of air, then 0.5 cm of Comp. B powder (with the reaction flag off), and then 3.0 cm of solid Comp. B (with no burning permitted). For the third run, which was for control, after the Plexiglas came 3.0 cm of Comp. B with the Forest Fire burn coupled in; thus there was no gap in the third calculation.

The results of these computer runs are shown in Figs. 17-19. Figure 17 shows five functions of time associated with the case of an air gap of 2.5 mm and a 17.2-mm-thick layer of Comp. B. Thus, Fig. 17 might correspond roughly with shots #3234-3 or #3234-4 in Table II. The five functions are, respectively, the shock pressure in the Comp. B, the pressure at the Comp. B/air interface in the Comp. B, the temperature in the middle of the air gap, the pressure in the middle of the air gap, and the Comp. B temperature with heat conduction considered.

The significant observation to be made in Fig. 17 is that the peaks of temperature and pressure in the air gap, which occur approximately together just before 44 μs have elapsed from the start of the run, are sufficiently strong to have caused detonation in the adjacent Comp. B through adiabatic compression and thermal ignition with Arrhenius kinetics. The rise in pressure in the Comp. B, peaking at about 44.1 μs, is 4.5 kbar.

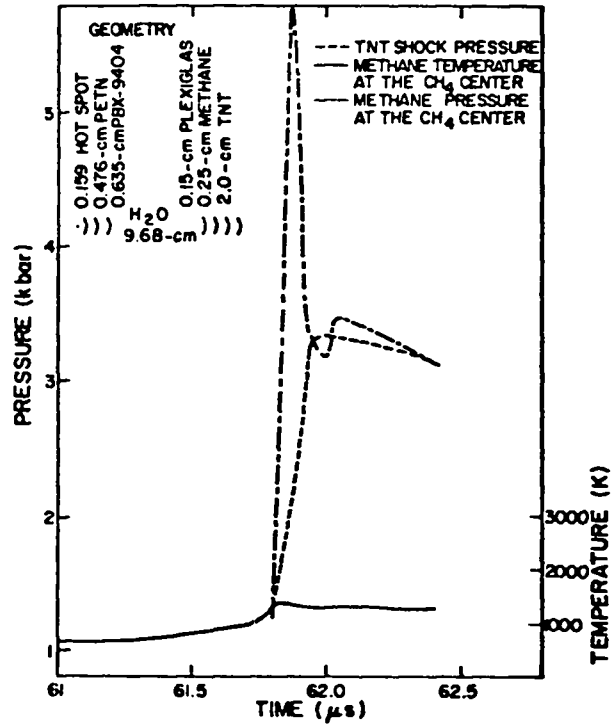

Fig. 16.
Calculated behavior in time of variables in the case of a methane gap for TNT.

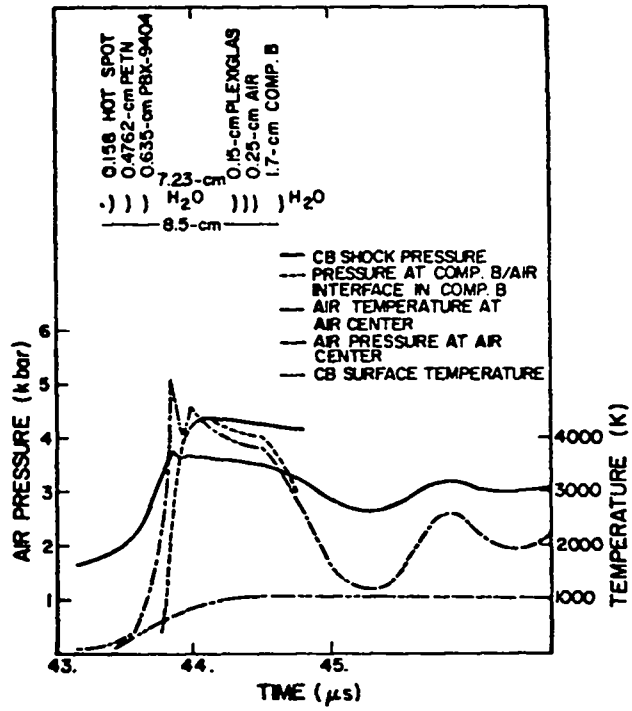

Fig. 17.
Calculated behavior in time of variables in the case of an air gap (heat conduction included) for Comp. B.

Figure 18 shows three functions of time associated with the case of a 2.5-mm air gap, a 5-mm-wide layer of Comp. B powder, and a 30-mm-thick layer of Comp. B solid. These functions are, respectively, the pressure at the Comp. B/air interface in the Comp. B, the air temperature at the center of the air gap, and the air pressure at the center of the air gap. In Fig. 18 we see that events are slightly delayed relative to events in Fig. 17 because the combined air and Comp. B powder gaps present more space into which the shock wave can expand.

The important observation to be made in Fig. 18 is that the peaks of temperature and pressure in the air gap, which occur at about 44.1 μs, are not sufficient to result in detonation by Forest Fire shock mechanisms in the solid Comp. B. The temperature in the air gap does not exceed 3500 K and the pressure in the air reaches only 2.98 kbar. The pressure at the Comp. B/air interface in the Comp. B is exceedingly modest.

Figure 19 shows three functions of time for the situation where there is no gap and the solid Comp. B is next to the 1.5-mm layer of Plexiglas. This calculation might correspond roughly to shot #3221-2. The functions are, respectively, the Comp. B shock pressure, the pressure at the Plexiglas/Comp. B interface in the Comp. B, and the Comp. B surface temperature. The steep rise in pressure in the Comp. B at the Plexiglas/Comp. B interface occurs quite early compared with the previously described runs. The peak pressure appears now at about 35 μs. This early rise in the Comp. B pressure when there is no air gap was to have

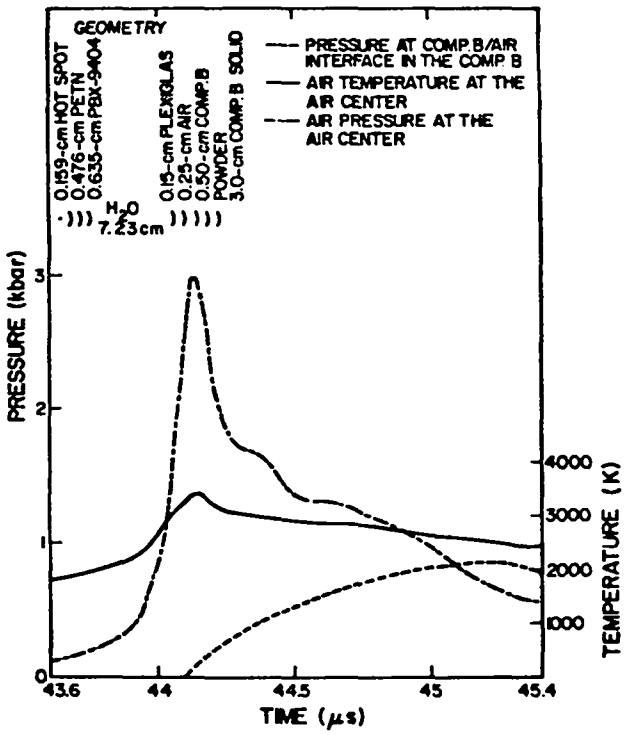

Fig. 18.
Calculated behavior in time of variables in the case of a gap with a layer of air and a layer of Comp. B powder.

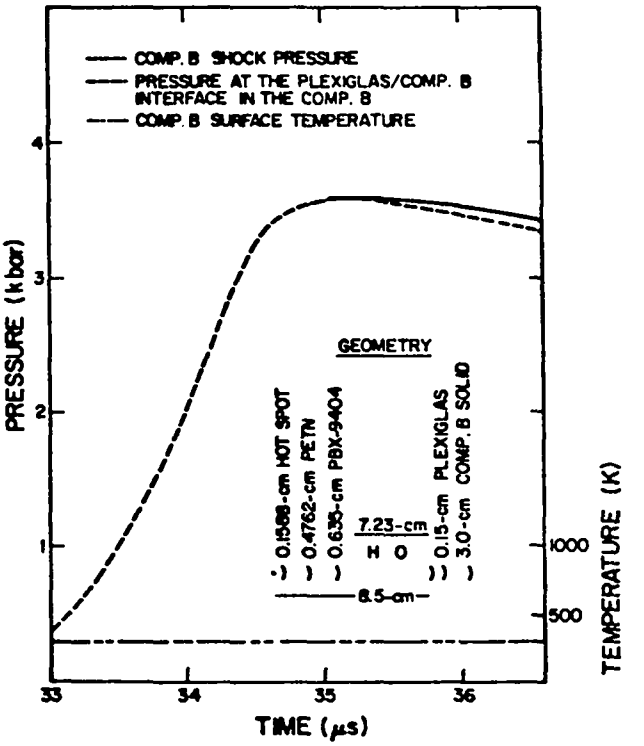

Fig. 19.
Calculated behavior in time of variables in the case of no gap for Comp. B.

been expected. Note, however, that the pressure now builds up only to about 3.6 kbar, in contrast to the run depicted in Fig. 17 where there was a simple air gap. In Fig. 17 the pressure at the air/Comp. B interface came up to about 4.35 kbar.

An air gap permits the Plexiglas cover to reverberate and to move faster, so that, upon collapse of the void, the matched shock results in a pressure buildup at the front face of the Comp. B sample.

The calculations plotted in Fig. 19 indicate that neither shock-induced decomposition (calculated by Forest Fire) nor thermal decomposition (using Arrhenius kinetics) should occur. Hence, this result tends to be in line with the experimental result of shot #3221-2 where no decomposition was observed. (This observation might be strengthened if there is any validity to the side-shock hypothesis. Shot #3221-1 had no side gaps to shield the sample from a side shock. Experiment #3234, as indicated in Table IV, did show that decomposition is slightly less with side gaps. Sample #3221-2 did not decompose even though side shocks may have been present as well as the front shock.)

b. Two-Dimensional Lagrangian Computations. The SIN calculations, as noted above, were based on an assumption of spherical symmetry, which does not really exist in the aquarium-type experiment. Some two-dimensional effects are to be expected. Our use of the SIN code in the foregoing computations was as a first approximation.

The two-dimensional effect we would like to assess, in using a two-dimensional Lagrangian code, is that of secondary shock waves in the water that might get around the faces of the sample cylinders and penetrate the cylinders at their sides. In samples with air gaps, it may be that a substantial part of the damage to the Comp. B specimen results from such side penetration. (In Table II compare shot #3222-4 with shot #3234-2.) In the calculation shown in Fig. 17 (where the gap was 2.5 mm wide) 9 μs were spent by the direct shock in traversing the air gap. During this time, secondary shocks penetrating the sides may have been having an effect.

It was this concern that motivated the #3234 series of aquarium tests (illustrated in Figs. 1c, 2, and 9-13). The air gaps at the sides (Fig. 2) were designed to delay the side shocks until the direct shock arrives at the face of the Comp. B. Shot #3222-4 compared with #3234-2 in Table II indicates little effect, however.

SIN-type computations might be expected to model experiments with side gaps better than they do experiments without side gaps, while the LASL two-dimensional Lagrangian code (2DL) would be expected to model more closely the experiments with no side gaps. Figure 17, showing results obtained with SIN, indicates that a detonation of the sample is possible through Arrhenius kinetics, but sample #3234-2 with side gaps had only light blackening with a small black pit.

We are hampered in our presentation of two-dimensional numerical results, that are distributed in time, by their bulk. Presumably one could plot only the pressure and temperature data along the axis of a sample, but this would discard a vast amount of data.

In Fig. 20 there is a sequence of two-dimensional plots (radial distances plotted horizontally, axial distances plotted vertically), each of which represents the situation at a discrete time. The cylindrical sample of Comp. B is shown at a sequence of discrete times as a 2.75- by 1.25-cm rectangle bordering the vertical axis (thus representing only half of the sample, the symmetry being with respect to the vertical axis). Just below the Comp. B there is a 5-mm air gap represented as a 0.5- by 1.25-cm rectangle. The Plexiglas shell is shown as the rectangle to the right of the combined air gap and Comp. B rectangle, while the Plexiglas cover is seen as the 0.2- by 1.6-cm rectangle just below the air-gap rectangle. In each plot this assembly of rectangles is considered to be embedded in a larger 4.45- by 2.55-cm rectangle representing the aquarium water and the limits of the calculation.

In time sequence, the collection of two-dimensional plots comprising Fig. 20 gives an appreciation of how the shock waves progress through the water and penetrate the Plexiglas shell and the side of the Comp. B sample. While this side-shock event is taking place, the direct frontal shock has not yet traversed the air gap by the time of the last plot. By that time (15.98 μs) the side shock has indeed reached the center axis of the Comp. B according to the calculation.

It does seem that some small amount of the effects described for the #3221-#3222 series of experiments in Table II might be ascribed to side shocks.

3. Time-to-Explosion Calculations. Using standard engineering formulas derived from the Frank-Kamenetskii equation (Ref. 8, p. 139) and estimates for peak temperature, peak pressure, and the associated densities of the gases in the respective gas gaps derived from the foregoing computer runs, we calculated T_{exp}, the time to explosion, for the Comp. B/air, TNT/air, TNT/krypton, and TNT/methane sample configurations.

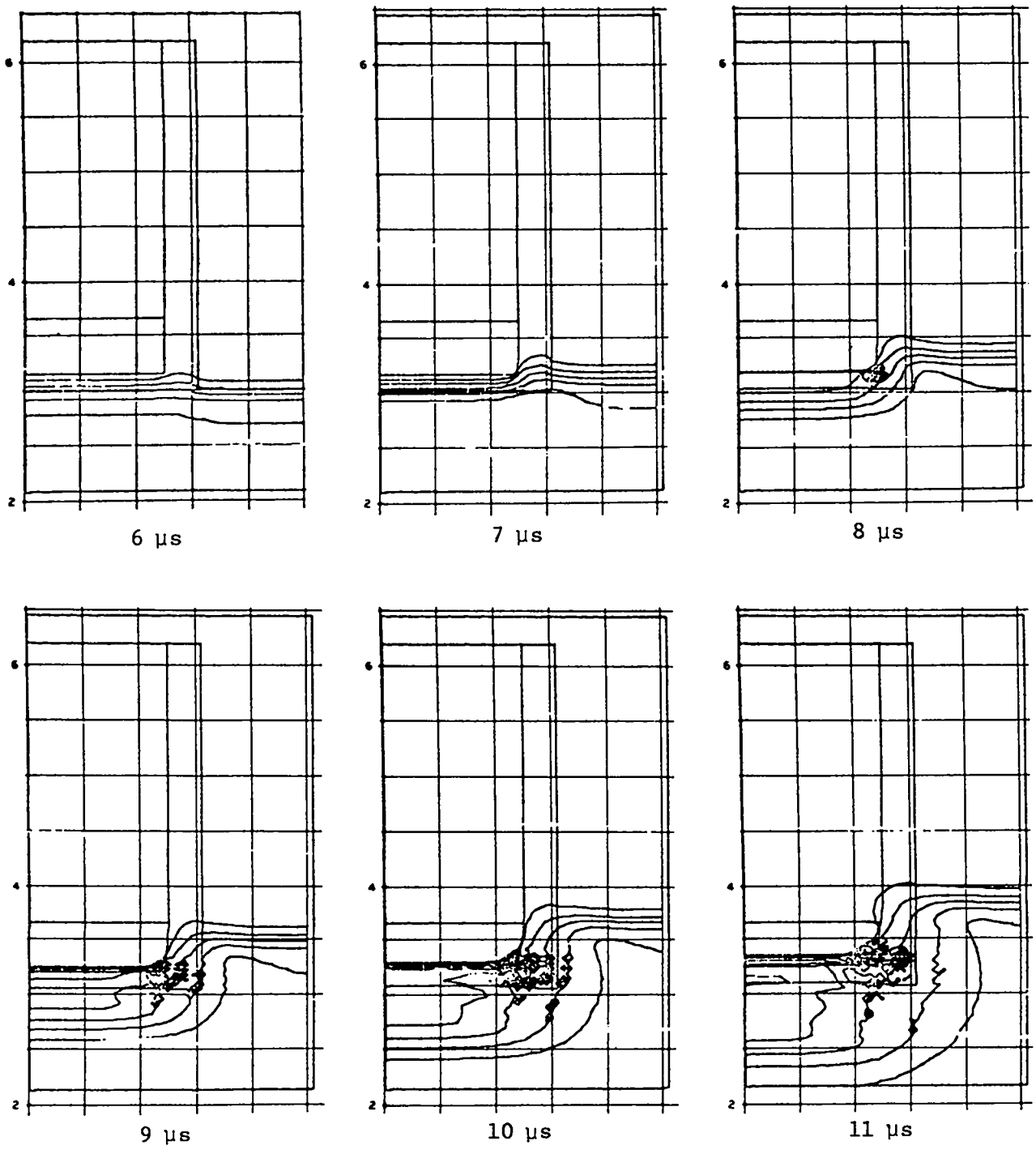

Fig. 20.
Secondary shock waves impinging on a sample; a Lagrangian calculation.

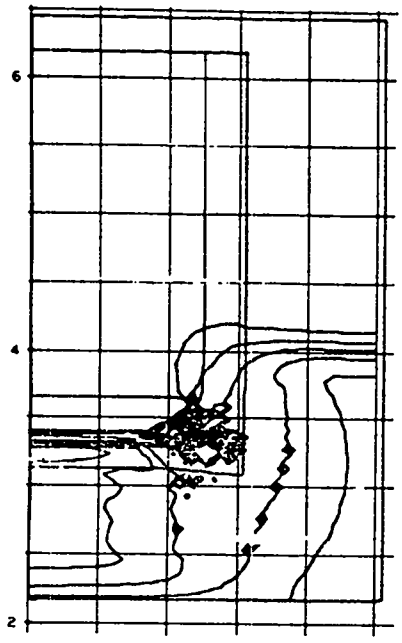

12 μs

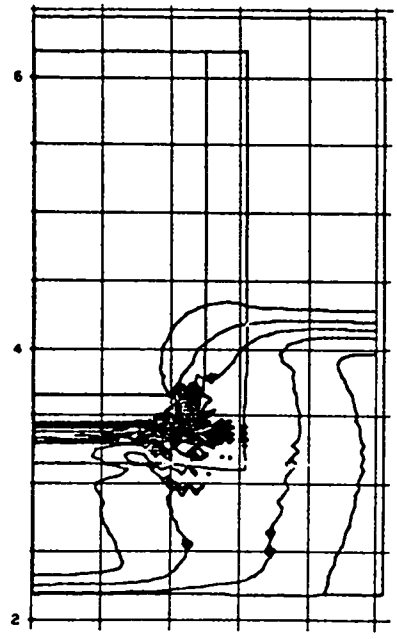

12.74 μs

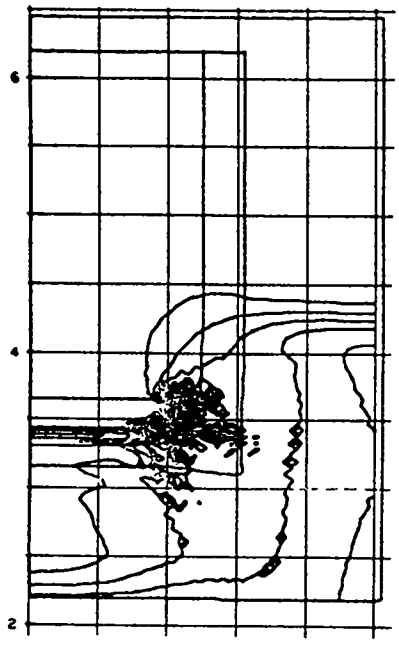

13.24 μs

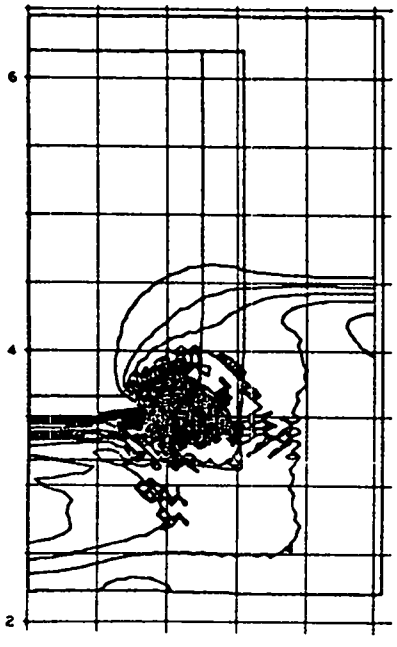

14.24 μs

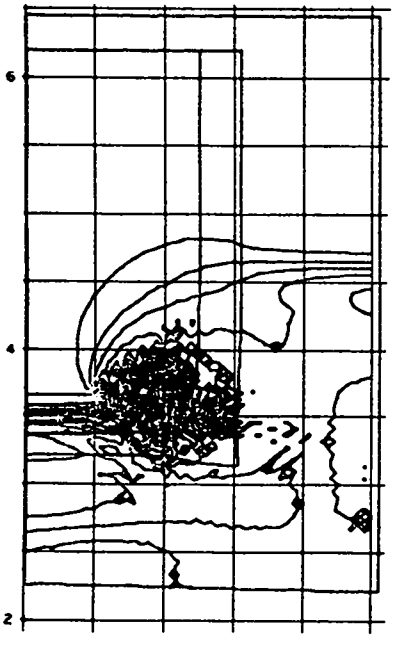

15.24 μs

15.49 μs

Fig. 20. (cont)

15.99 μs

Fig. 20. (cont)

The following chain of formulas was used in the calculation.

$$k_T = k_0\left(\frac{T}{T_0}\right)^{1/2} \quad , \tag{1}$$

where k_T is the coefficient of thermal conductivity of the gas relative to a reference level k_0 (cal/K/cm/s), and T is the peak temperature of the gas above a reference level T_0(K). T is taken from the foregoing calculation in this report which pertains to the particular gas present in the gap.

$$\alpha_T = \frac{k_T}{\rho_{gas}\, C_{V\,gas}} \quad , \tag{2}$$

where α_T is the thermal diffusivity (cm^2/s), ρ_{gas} is the density (g/cc), and C_V is the heat capacity of the gas (cal/K/g).

$$T_{HE} = \frac{T - 300}{1 + (k_{HE}/k_T)\ \ \alpha_T/\alpha_{HE}} \quad , \tag{3}$$

where k_{HE} is the given coefficient of thermal expansion (cal/K/cm/s) of the HE and α_{HE} is the given thermal diffusivity (cm^2/s) of the HE.

$$T_{exp} = \frac{C_{V_{HE}}\, RT^2}{QZE^*}\, e^{E^*/RT} \quad , \tag{4}$$

where T_{exp} is the time to explosion in μs, $C_{V_{HE}}$ is the given heat capacity (cal/K/g) of the HE, R is the universal gas constant, Q is the heat of decomposition in cal/g, Z is the frequency factor, and E* is the activation energy.

Thus, T_{exp} is computed using given quantities and quantities that are read from the computer calculations. The computation of T_{exp} is summarized in Table V. The considerably different times to explosion do not correlate with the experimentally observed amounts of decomposition in the respective explosive samples (see Tables I and II and Figs. 3-8 and 9-13).

4. Data for the Computations. The equation-of-state data for the components used in the foregoing SIN and 2DL calculations are listed in Appendix A.

TABLE V

COMPUTATION OF T_{exp}

	Comp. B/Air	TNT/Air	TNT/Krypton	TNT/Methane
T (read)	3500	3500	9250	1350
k_0 (given)	6.22×10^{-5}	6.22×10^{-5}	1.984×10^{-5}	8.18×10^{-5}
k_T	2.12×10^{-4}	2.21×10^{-4}	1.194×10^{-4}	1.735×10^{-4}
ρ_{gas} (read)	0.408	0.408	0.25	0.211
α_T	1.735×10^{-3}	1.735×10^{-3}	8.036×10^{-3}	1.545×10^{-3}
T_{HE}	1045	1062	975	523
p_{gas} (read)	4.25	4.25	4.6	5.8
k_{HE} (given)	6.3×10^{-4}	6.2×10^{-4}	6.2×10^{-4}	6.2×10^{-4}
α_{HE}	1.41×10^{-3}	1.44×10^{-3}	1.44×10^{-3}	1.44×10^{-3}
$C_{V\,HE}$	0.259	0.263	0.263	0.263
ρ_{HE}	1.714	1.64	1.64	1.64
$C_{V\,gas}$ (given)	0.30	0.30	0.0593	0.532
Q (given)	500	500	500	500
Z (given)	$2.0 \times 10^{+12}$	$1.0 \times 10^{+7}$	1.0×10^{7}	1.0×10^{7}
T_{exp} (in μs) (desired)	8.4×10^{-5}	0.93	4.59	1.0×10^{8}

The first listing is for explosive components, the next for inert components, and the last for the gaseous components. An explanation of some of these quantities follows.

There are two linear fits used for the shock velocity versus particle velocity relationship; these fits have the respective coefficients C,S and C_1,S_1. Which of these fits is to be used depends on the specific volume V. VSW is a value such that if V < VSW, the fit with C_1,S_1 is used, whereas if V > VSW, the fit with C,S is used. F, G, H, I, and J are polynomial coefficients used for fitting the relationship: Hugoniot temperature versus specific volume in the Walsh-Christian technique. γ_S is the value of $V(\partial P/\partial E)_V$, where in the equation of state we obtain the pressure derivative with respect to the energy at constant volume, and the energy dependence is assumed to be linear. V_0,T_0,P_0 are reference values of specific volume, pressure, and temperature. Finally, α is the linear coefficient for thermal expansion for the material.

The equation-of-state data for the gaseous components in Appendix A, Sec. 3, require some elucidation. There are three groups of data for, respectively, air, krypton, and methane. For each group there are two sets of data—one for an ambient pressure of 0.8 atm, such as we have in Los Alamos, and one pertaining to the sea-level environment of 1 atm.

At the top of each set of gaseous equation-of-state data there are three lines denoted as LN(P), LN(T), and LN(E). These are coefficients for the BKW isentrope polynomial fits, which are of the form (using natural logarithms):

$\ell n\ P = A + B\ \ell n\ V + C(\ell n\ V)^2 + D(\ell n\ V)^3 + E(\ell n\ V)^4$ with similar forms for $\ell n\ T$ and $\ell n\ E$ (Ref. 5, p. 15, Sec. XI).

There follows, in Appendix A, Sec. 3, for each set of gaseous equation-of-state data, a table of resulting numerical quantities which gives the particular equation of state for the gas and ambient pressure considered.

III. PIPE TESTS

A. Methodology

The pipe test for studying the process of hole closure in a sample of cast TNT or Comp. B explosive has been developed in M Division at LASL by B. G. Craig and E. F. Marshall. An internal spherical cavity is created in an explosive by making hemispherical impressions in the ends of each of two cylindrical test specimens of the explosive and then joining these specimens, as shown in Fig. 21, to form an air-filled spherical cavity. This double sample with cavity is then inserted into a thick steel pipe with a witness plug beneath it at the lower end. This cylindrical arrangement is then mounted vertically on a steel base block, with the witness plug resting on the base and the pair of explosive specimens above it. In the steel pipe, above the explosive specimens is a layer of HMX powder, which is separated from the former by a polyethylene flame barrier. Above the HMX powder there is a Plexiglas holder containing a shotgun primer. Next, in vertical order, there is a standard SE-1 detonator in its holder, with a detonator lead running through a channel in a confinement plug. The entire assembly is now topped with a thick steel block, a steel weight, and a lead brick.

Because any other type of record is likely to be obliterated in the explosion and shredding of the pipe, the results are interpreted by studying the deformation of the witness plug. With some explosives, however, there need not be complete destruction of the apparatus. For example, in pipe tests that have been conducted using PBX-9404 or FKM, the elastic limit of the tube was not exceeded by the peak pressure.

A variant on this experiment is to have a cylindrical gap between the two halves of the explosive, with a 6-mm shear ring as shown in Fig. 22.

B. Experimental Results

Results of the pipe tests are shown in Table VI. The first three columns list: (1) shot identification, (2) high explosive used as test specimen, and (3) type of air-filled cavity within the HE test specimen — whether a cylindrical cavity created by a shear ring (as described above) or a spherical cavity with radius in centimeters. The fourth column requires more explanation. Initially the witness plug is 2.54-cm-diam, 2.54-cm-high, stainless steel cylinder. After the shot the plug is splayed at the side and reduced in height. The amounts that the height of the witness plug has been reduced are given in this column. A certain amount of height reduction, or "set," results merely from the burning of the HMX powder, apart from what happens to the TNT or Comp. B. The flame barrier and test specimens were omitted in two experiments, and the HMX powder placed in direct contact with the witness plug. A set of 3.09 mm was observed when 8 g of HMX was used, and a set of 3.76 mm when 16 g was used. A somewhat greater amount of set results if the TNT or Comp. B burns rather than detonates. For example, none of the four TNT shots listed in Table VI were thought to have been accompanied by a detonation in the TNT. Sets of 1.60, 1.84, 1.98, and 1.94 mm were considered to indicate little or no reaction. On the other hand, sets

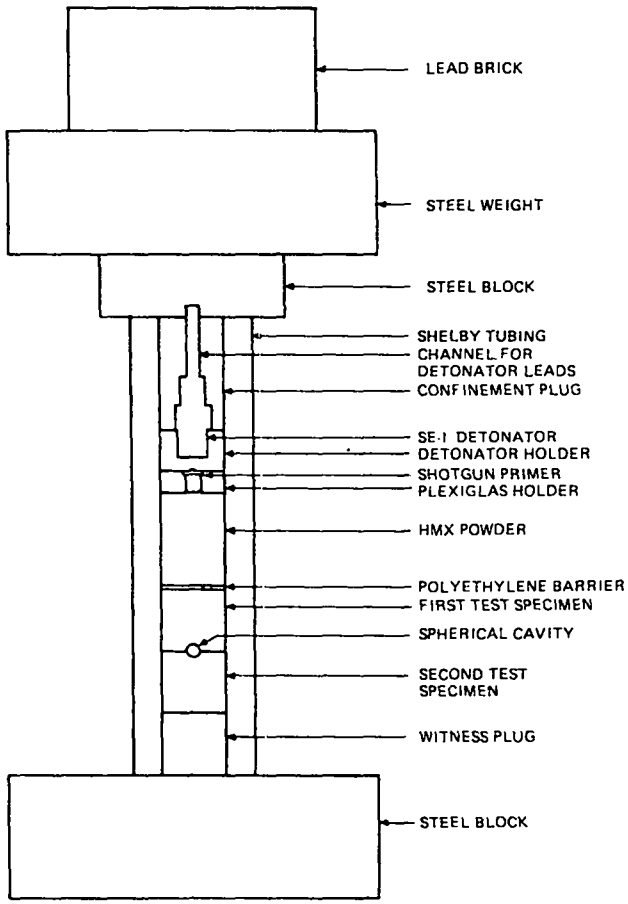

Fig. 21.
The pipe test with spherical cavity.

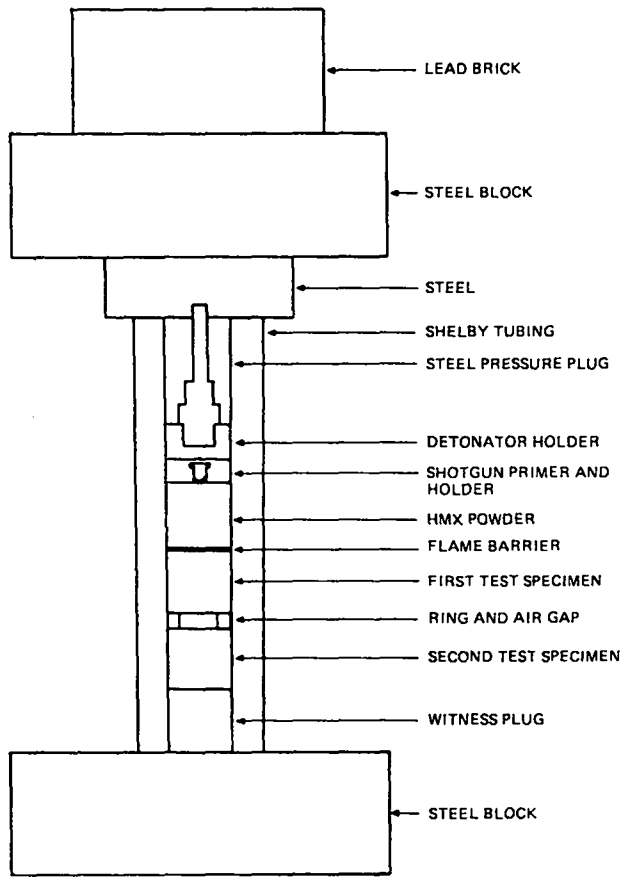

Fig. 22.
The pipe test with ring cavity.

of 8.31, 8.20, and 4.42 mm were indicative of a violent reaction in the explosive specimens. The set of 2.81 mm was regarded as indeterminate.

In Table VI, the four TNT shots are grouped together at the top. Listed next are the six Comp. B shots where the total mass of HMX powder (with flame barrier below) was 16 g. This was the same mass of HMX as in the four TNT shots. The four Comp. B shots at the bottom of the list were performed with only 8 g of HMX powder.

The general impression given in these tests is that detonation in TNT is difficult, that larger air cavities lead to a greater likelihood of detonation in Comp. B, and that the latter effect is more pronounced when a greater amount of HMX propellant is used.

C. Numerical Modeling of the Pipe Test

1. The Experience with Lagrangian Coordinates. In our initial attempt to model numerically the hole closure process in the pipe test, we used the LASL two-dimensional Lagrangian code and a cylindrical hole. Thus, in a plot of cylinder versus radius, the hole appeared as a rectangle. It was found that there

TABLE VI

PIPE SHOTS[a]

Shot No.	Test Material	Cavity	Set (mm)	Type Shrapnel
		16 g HMX		
C-11	HMX alone	None	3.76	Shattered
326-11 RS1722	TNT	6-mm shear ring	1.60	Big pieces[b]
326-37 RS1764	TNT	6-mm shear ring	1.84	Big pieces
326-20 RS1733	TNT	None	1.98	Big pieces
326-36 RS1763	TNT	None	1.94	Big pieces
326-24 RS1735	Comp. B	None	1.91	Big pieces
326-29 RS1753	Comp. B	¼"-diam spherical cavity	1.74	Big pieces
326-34 RS1761	Comp. B	¼"-diam spherical cavity	1.52	Big pieces
326-33 RS1760	Comp. B	½"-diam spherical cavity	8.31	Shattered[b]
326-35 RS1762	Comp. B	½"-diam spherical cavity	2.81	Big pieces[c]
326-25 RS1736	Comp. B	6-mm shear ring	8.20	Very shattered
		8 g HMX		
C-10	HMX alone	None	3.09	Split tube
326-18 RS1730	Comp. B	None	1.14	Big pieces
326-27 RS1751	Comp. B	¼"-diam spherical cavity	1.34	Big pieces
326-32 RS1759	Comp. B	½"-diam spherical cavity	1.98	Split tube
326-24 RS1732	Comp. B	6-mm shear ring	4.42	Shattered

[a]Standard setup, stainless steel witness plug (SS 304), 1.5-mm polyethylene barrier. All samples 25.4-mm diameter, 25.4 mm long.

[b]Big pieces indicate little or no reaction in the specimen. Shattered debris indicates a strong reaction in the specimen; that is, a detonation.

[c]Test 326-35 gave an indeterminate result.

were shock stability problems following the encounter of the pressure shock with the hole. Also, in the calculation, the lower right-hand corner of the hole, which was the point first reached by the incident shock, tended to remain stationary as the shock went by, giving a peculiar collapse of the hole. Beveling the corner of the hole did not remove these problems. It was decided that the difficulties were inherent in any attempt to model hole closure with Lagrangian coordinates and that an Eulerian coordinate system might be a better setting for the calculation.

2. Description of the Numerical Simulation Method Using the 2DE Code. The LASL 2DE reactive hydrodynamics code is described in LA-4846.[7] This code solves the difference analogs of the conservation equations of mass, momentum, and energy[7,8] with appropriate equations of state coupled with a reactive rate equation (Ref. 8, Chap. 4, Appendix C). The problem is solved with prescribed boundary and initial conditions in a two-dimensional geometry in terms of Eulerian coordinates. The basic geometry can be a plane geometry with Cartesian coordinates (which can describe a slab in three-space) or a finite configuration in three-space with cylindrical symmetry and cylindrical coordinates.

Boundary conditions may be chosen for the given configuration as follows: a driving piston, an axial boundary condition (on the axis or plane of symmetry), or a continuum boundary. The latter is a finite-difference type of boundary condition that allows the consideration of only a piece of a problem embedded in an infinite or large finite domain. The option for having elastic-plastic flow couples more equations into the parabolic system of differential equations. Artificial viscosity is used to "smear" the shocks normally expected with conservation laws and the code offers a choice of three of these viscosities. The interaction of different materials in a problem is handled with a clever system of mixed cells.

The 2DE code is a reliable, versatile, and significant investigative tool in reactive hydrodynamics and there has been much satisfactory experience in its use from an engineering viewpoint. The apparently satisfactory state of the computing art in this case contrasts considerably with the continued spotty state of our knowledge about conservation laws,[9,10] (see, however, the recent work of Nishida et al.[11]).

The 2DE code is basically a Cartesian coordinate code. When cylindrical geometry is being used, rectilinear radial and axial coordinates are employed. Naturally then, a cavity in a cylindrical block of Comp. B would itself conveniently be of cylindrical shape. Indeed, some cylindrical cavities were investigated numerically. In the 2DE code, however, provision is made for a circular interface between materials (Ref. 7, pp. 34,36). This is done by an overlay technique after the basic cylindrical coordinate information is entered as input. Hence, our main interest in spherical cavities was well accommodated by the 2DE code.

Figure 23 illustrates the configuration of our calculation. A radial slice through the cylinder is displayed and, because hydrodynamic events on this slice are expected to be symmetric with respect to the axis, we really show only half a slice. The abscissas of points are plotted horizontally along the radius and the ordinates are plotted vertically along the axis of the cylinder. The cylinder is 3 cm high and 3 cm in diameter. Except for the cavity, the cylinder is Comp. B, grade A. The cavity is air-filled. If the cavity is cylindrical, it is 1 cm high and 1 cm in diameter; if the cavity is spherical, its radius is either 0.5 or 0.25 cm. The cavity (either type) is centered at the exact midpoint of the larger 3-cm by 3-cm cylinder of Comp. B.

As shown at the bottom of Fig. 23, a piston boundary condition is prescribed. This does not correspond well with the intuitive notion of a piston. The boundary does not move up into the medium; rather, there is assumed to be a continuous flowing of material into the basic domain from the region beneath. One could conceive an actual piston moving upward if that piston were located, say, 3 cm below the lower boundary in Fig. 23, causing material to flow across that boundary. Then the material flowing into our domain could be calibrated in kilobars in terms of the pressure exerted by such a remote piston. The effect is that of a uniform shock traveling upward in the Comp. B region and interacting with the void.

Again, the axial boundary condition along the entire left margin in Fig. 23 implies that events to the left of the margin are the symmetric images of those within the domain, so that we are really treating this flow problem in a whole cylinder with a whole sphere (cylinder) as a void. The continuum condition at the top and right side implies that the Comp. B extends above and to the right and that any boundaries for the Comp. B in these directions are sufficiently remote to be ignored.

For problems assuming a cylindrical void (represented as a rectangle), the basic domain is divided into six initial regions as enumerated in Fig. 23. For each region the code requires specification of the material (Comp. B or air); the number of mesh cell widths in horizontal and vertical directions; initial values of density, pressure, mass fraction, horizontal and vertical components of velocity, energy and temperature; artificial viscosities; elastic-plastic constants as applicable; and whether the material is explosive or inert and, in the case of the latter, whether the material is being considered reactive. Equation-of-state constants for each material must also be specified. If a piston boundary condition is specified (as it is for the lower boundary in Fig. 23), values of applied pressure, energy, velocity, and mass that are consistent with the Hugoniot curve will be needed by the code.

When the void is to be spherical, rather than cylindrical as in the preceding paragraph, we set up the problem in the same way, specifying the input for region 3 of Fig. 23 as if it were cylindrical and Comp. B-filled rather than air-filled. In addition, the fact that the void is to be a sphere is initially specified by using the requisite input flag (Ref. 7, p. 36, Sec. C). Also to be specified are the center and radius of the corresponding half-circle centered on the z-axis, together with properties for the air filling. Routines incorporated in the code then perform the computation needed to produce an air-filled circular region, as shown in Fig. 23, with Comp. B in the complementary region. In fact, it is possible to have a configuration with more than one of these spherical voids.

3. Preparation of the 2DE Hole Closure Calculation. In Fig. 24 the fundamental rectangle is again divided into six regions. We overlay this rectangle with a grid such that the regional boundaries coincide with mesh lines. NRI is the number of rectangular intervals along the r-axis and NZJ is the number of rectangular intervals along the z-axis, obtained by projecting the six regions onto the respective axes. Each of these intervals is then divided into mesh cell widths, as shown in Fig. 24. The six regions are thus partitioned with mesh lines, creating cells whose sides have these widths. There are IMAX (respectively JMAX) mesh widths along the r- (respectively z-) axis. For these mesh widths we took DELR = DELZ = 0.05 cm.

Region 3 is the air-filled region, that is, the cavity. All the other regions have Comp. B, grade A (or other HE being tested). Thus, we start with a cylindrical void.

This is an initial value problem. Initial values of the dependent variables, constant over each of the six regions, are defined in the input file of the 2DE code as follows: The density RHO of the Comp. B is 1.715 g/cc, while RHO for the air is 0.00115577 g/cc; the pressure PO is 6×10^{-6} kbar for all regions; the mass fraction (fraction of unburned explosive) WO is unity for all regions except region 3, where it is zero; the components of initial velocity UO and VO are set to zero for all regions; the initial energy IO is zero in all regions except region 3, where it is 0.0024668 Mbar-cc/g; and the initial temperature TO is 300 K for all regions.

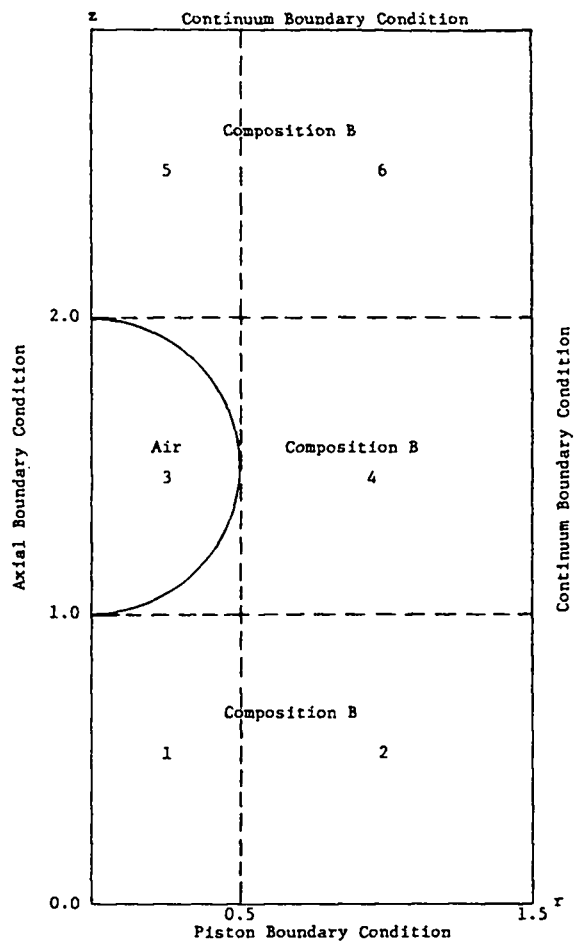

Fig. 23.
Configuration of the 2DE calculation.

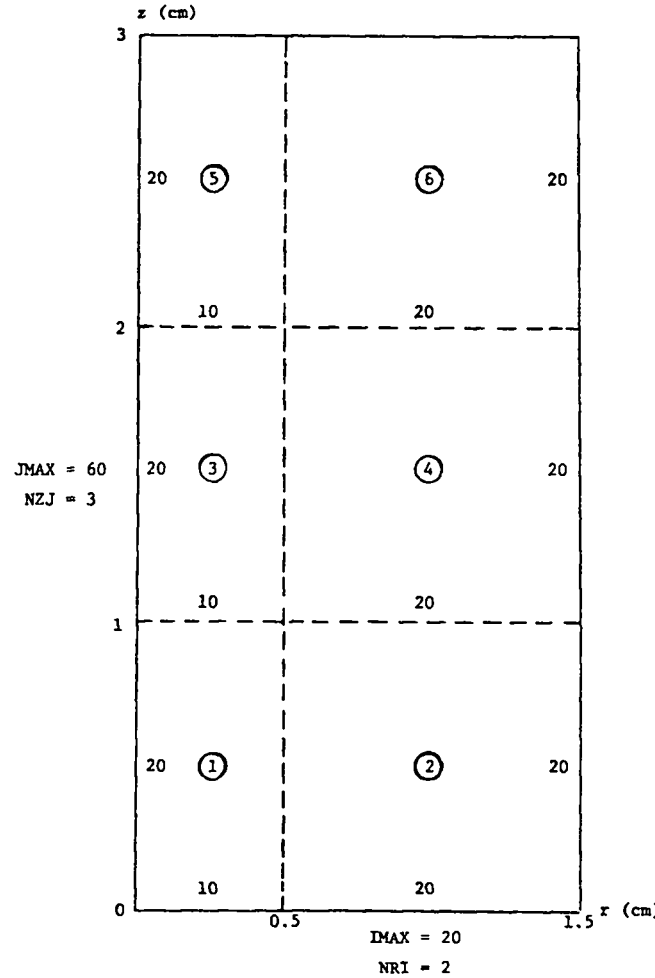

Fig. 24.
Mesh specifications.

The artificial viscosity VISC, used to enable computation in the presence of shocks, was 0.1 for Comp. B and 0.001 for air in region 3.

If circular input is to be used (that is, if the void is prescribed to be a sphere), we initially prescribe region 3 of Fig. 24 to contain Comp. B, as do the other regions. Then (Ref. 7, p. 36, Sec. C) the coordinates RO,ZO of the circle center (the void) are set, respectively, to 0, 1.5 cm (Fig. 23). We set RAD(1) = 0.5 and later set it to 0.25, where RAD(1) is the radius of the circle (L = 1 in our case). We set RHOOC(1) = 0.0011557, which is the density for air, while KCIR(1) = 2 because the material in the circle is prescribed to be air. Again IOC(1) = 0.0024668 (which was the initial internal energy for air) and the mass fraction WOC(1) = 0. The constants UOC(1) and VOC(1), which are the initial velocity components, have default values of zero (Ref. 7, p. 36, Sec. C).

The 2DE code accepts these constants and computes the circular void in region 3, originally assumed to contain nothing but Comp. B.

The S and G arrays consist of equation-of-state constants that are doubly indexed. The constants for Comp. B are denoted by S(L,1), L = 1,2,···,18,22,23 for the solid phase and by G(L,1), L = 1,···,17 for the gaseous phase (that is, detonation products). The constants for the air in the void are denoted,

respectively, by S(13,2), S(17,2), and S(18,2) (which, though air is not herein considered in its solid phase, are listed as such as an expedience), and by G(L,2), L = 1,···,17. The coefficients denoted by this indexing are listed below (see Ref. 7, p. 24). For the meaning of the abbreviations, see the 2DE handbook.[7]

S(1)	C	S(11)	γ_s	G(1)	A	G(11)	Q
S(2)	S	S(12)	C_V	G(2)	B	G(12)	R
S(3)	VSW	S(13)	V_0	G(3)	C	G(13)	S
S(4)	C1	S(14)	α	G(4)	D	G(14)	T
S(5)	S1	S(15)	SPA	G(5)	E	G(15)	U
S(6)	F	S(16)	USP	G(6)	K	G(16)	C_V'
S(7)	G	S(17)	T_0	G(7)	L	G(17)	Z
S(8)	H	S(18)	P_0	G(8)	M		
S(9)	I	S(22)	SPALL P	G(9)	N		
S(10)	J	S(23)	MINV	G(10)	O		

The actual values of these equation-of-state constants used in our calculations are given in Appendix B-1. When a line in Appendix B-1 starts with, say, G(1,1), the first number is G(1,1), the next is G(2,1), then G(3,1), etc. The first three rows of data begin with S(1,1), the next number is S(2,1) and so on for the entire three rows, as is often specified for FORTRAN namelist input.

The Forest Fire reaction constants C(I) are fed as input into the 2DE code in inverse order: C(15), C(14), ···, C(2), C(1). They are shown in Appendix B-2 in this inverse order. For help in the details of interpreting these constants, the reader should see LA-7245.[12]

To allow for elastic-plastic flow, the IEP=1 flag is set in the input file. With this option, the following constants must be specified for the Comp. B: MU(1) = 0.047, YO(1) = 0.0006, and PLAP = 0.15.

For the time increment in these calculations, we used DELT = 0.01 μs.

There are three significant references for the Forest Fire technique for modeling the events in the reaction zone behind the shock; namely, the book by Mader,[8] the report by Forest,[12] and the report by Mader and Forest.[13] The explicit step-by-step methodology for the reaction calculation is to be found in the latter two of these references (Ref. 12, Appendix B, Sec. IV, pp. 31-40; Ref. 13, Appendixes A and B, pp. 34-58). Using pressure as the independent variable, using the experimental reactive Hugoniot curve, solving the shock jump relations (for which a closed solvable system of equations is obtained by assuming the pressure wave to be square-topped if no better assumption can be made), and using the empirical Pop-plot rule, calculations are produced for the length of run to detonation, the time to detonation, and the explosive reaction rate. Associated quantities are the specific volume V, the particle velocity U_p behind the shock, the shock velocity U_S, the mass fraction of the remaining solid material W, and the temperature T. Tables presenting all these data for the Forest Fire calculation of sample problems or situations can be found in Ref. 12, Appendix B and Ref. 13, Appendix B.

Herewith, we present the same type of numerical tabulation of the above quantities for the present problem (see Appendix B, Secs. 3-5).

Appendix B-3 begins with the Pop-plot coefficients and the reactive Hugoniot curve coefficients appropriate for Comp. B, grade A, at a density of 1.715 g/cc. Next comes the Chapman-Jouguet pressure for this material and then the equation-of state constants for both the unreacted explosive and the detonation products. Note that these are the same constants previously given in Appendix B-1.

In Appendix B-4 (after a repetition of the Pop-plot and reactive Hugoniot curve constants) are the actual computed quantities determined by following the methodology mentioned in Refs. 13 and 14 for the Forest Fire calculation. The respective columns are: length of run in centimeters, pressure in millibars, specific volume in cubic centimeters per gram, particle velocity in centimeters per microsecond, shock velocity in centimeters per microsecond, mass fraction (dimensionless), reaction rate in microseconds^{-1}, temperature in degrees Kelvin, and time to detonation in microseconds.

Appendix B-5 gives first the Forest Fire coefficients already given in Appendix B-2 (in the inverse order acceptable to the 2DE code). These coefficients are those of a polynomial fit relating the data of columns 2 and 7 in Appendix B-4; namely, logarithm of reaction rate versus pressure. Appendix B-5 is a computation showing the accuracy of the polynomial fit.

4. LASL Calculation of Hole Closure in Comp. B. In presenting the two-dimensional time-distributed numerical results of this study, it is necessary to be selective because of the bulk of the data. There is a succession of two-dimensional plots for each dependent variable of interest, each plot representing a situation in two dimensions at a particular time. We present those plots which describe the most interesting events associated with the closing of the hole.

The first set of results presented is for a configuration such as that of Fig. 23, with a 0.5-cm-radius air-filled hole but with the Comp. B assumed to be inert. Thus, we turned off the reaction flag in running the calculation. The applied piston values were PAPP = 0.0163595, MAPP = 1.91, EAPP = 4.8694×10^{-4}, and VAPP = 0.0312071. These quantities are, respectively, applied pressure, applied mass, applied energy, and applied velocity at the piston (Ref. 7, p. 35).

We present plots for the pressure, density, mass fraction, and a one-dimensional plot of the pressure along the z-coordinate near the z-axis of Fig. 23. In Fig. 25a these variables are shown at 7 μs after the start of the run. There is one pressure isobar showing how far the shock wave has advanced. In the pressure plot the dots outlining an approximate half-circle represent the locations of mixed cells. The density plot has two contours representing drops in density of 0.1 g/cc. The heavy half-circle represents a very high density gradient at the boundary of the hole. Again, the heavy approximate circle in the mass fraction plot is due to abrupt mass fraction change at the hole boundary. The one-dimensional pressure plot shows the progress of the shock after 7 μs, near the axis of the cylinder.

In Fig. 25b the pressure wave has gone past the hole at 9 μs and, as shown in the density and mass fraction plots, the hole has been collapsed considerably. On the one-dimensional pressure plot we see the start of a pressure increase due to convergence in front of the hole, at least near the axis of the cylinder.

Figure 25c shows the collapsed hole completely enveloped by the pressure wave at 9.5 μs. The density plot shows the steep rise in density in the former location of the hole. In the mass fraction plot, six mixed cells are all that is left of the hole. The one-dimensional pressure plot shows that the high pressure area, in front of the former location of the hole, is feeding a second pressure increase just behind the former hole center.

At 10 μs (Fig. 25d) the reflected pressure wave, already seen at 9.5 μs, now dominates the picture and divergent flow will ensue from this time onward. The density plot shows contours of decreasing density going out from the point of compression. The mass fraction plot now shows only five mixed cells. A conservation-of-mass calculation showed only a 0.0018% loss of air mass during the entire calculation; those five mixed cells retain the air assumed to have been in the void at the start. The one-dimensional pressure plot in the z-direction near the axis of the cylinder now shows a bimodal distribution of pressure. The reflected wave on the left is now traveling toward the origin. From this time onward, both modes of the pressure plot will dissipate — one to the left, the other to the right.

Now we present some results from four runs performed with the reaction flag turned on. With the following phenomena there will be burning and we shall be looking for evidence of a detonation.

First, we continue with the 0.5-cm-radius spherical hole and with the same piston applied values: PAPP = 0.163595, MAPP = 1.91, EAPP = 4.8694×10^{-4}, and VAPP = 0.0312071. These values, as mentioned, were chosen to be consistent with the Hugoniot curve assumed for the problem. The sequence of plots presented in Fig. 26 is the same as that in Fig. 25.

At 7 μs the plots in Fig. 26a do not look markedly different than those in Fig. 25a at 7 μs for the unreacted case. The pressure wave in the isobar plot is a little more complicated, but its progress appears the same except that at 7 μs it is beginning to interact with the void. In the density plot the area of heavy density gradient appears to be slightly flattened. The mass fraction plot shows that collapse of the cavity has begun. The one-dimensional pressure plot is higher, steeper, and shows that the wave has gone slightly further.

At 8 μs, Fig. 26b, the pressure wave has enveloped the cavity and both the density and mass fraction plots show much squeezing and distortion of the void. The one-dimensional pressure plot near the axis of the cylinder shows a higher rise, a steep drop, and a place marked by two small x's where a second mode is developing. The small x's are mixed cells of the very distorted void boundary, so we are beginning to see the pressure mount in the void.

At 8.25 μs the isobar plot shows some steep gradients of pressure in the vicinity of the void and, likewise, the density plot shows steep gradients. The mass fraction plot shows the air that was in the void now confined to nine mixed cells. The one-dimensional pressure plot is definitely bimodal, with the maximum and minimum at two mixed cells (see Fig. 26c).

At 9 μs something apparently violent has happened at the former location of the void and the density plot confirms a generally divergent pattern of density contours. The mass fraction plot indicates heavy consumption of solids (modeled by Forest Fire), both at the former location of the void and in a concentric ring which has been blown away. The one-dimensional pressure plot near the axis of the cylinder again shows reflected and progressing waves, of a magnitude far exceeding anything observed in Fig. 25. This violent reaction shows that a detonation has occurred. The detonation evidently happened just before 8.5 μs (see Fig. 26d).

One might wonder what effect there would be with the same 0.5-cm spherical void situated within active Comp. B if we were to have a much weaker incident pressure wave. Therefore, we now report on a run with the same physical arrangement as the last run (Fig. 23), but with the following piston applied values: PAPP = 0.01, MAPP = 1.847, EAPP = 2.0869×10^{-4}, and VAPP = 0.0204300. A partial graphic portrayal of events is given in Fig. 27.

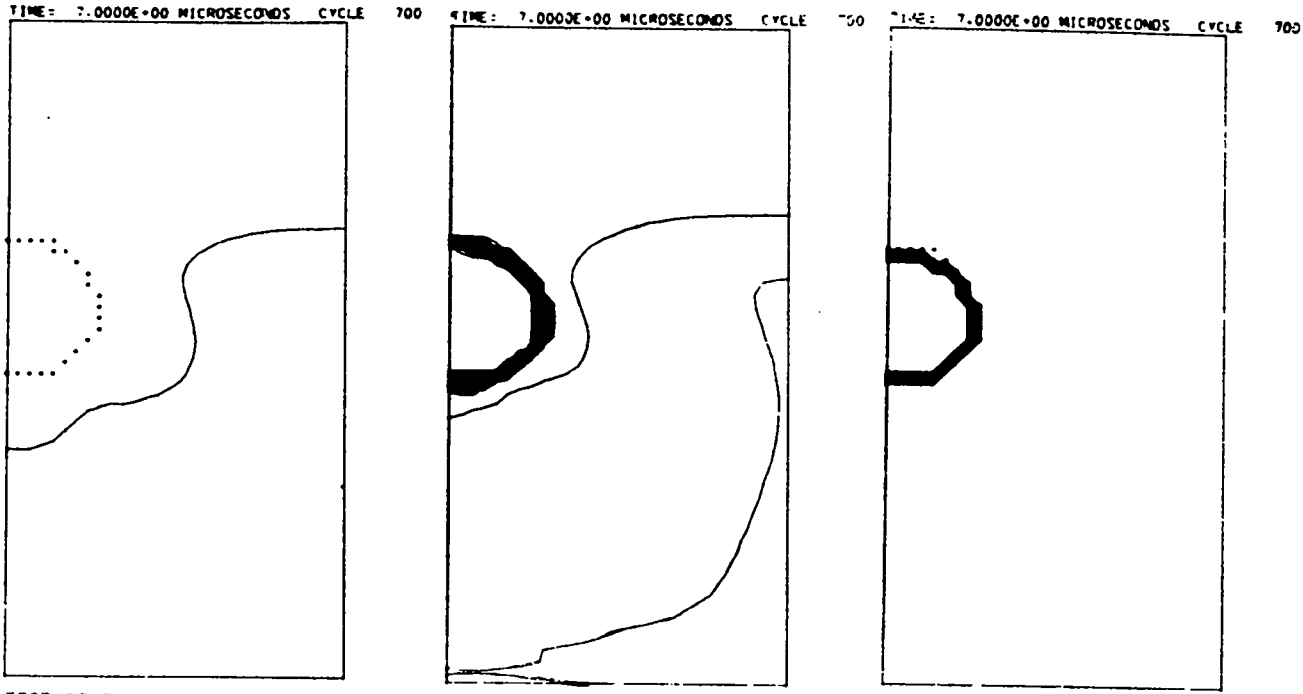

ISOBARS INTERVAL = 1.0000E-02

DENSITY INTERVAL = 1.0000E-01

MF MAT 1 INTERVAL = 5.0000E-02

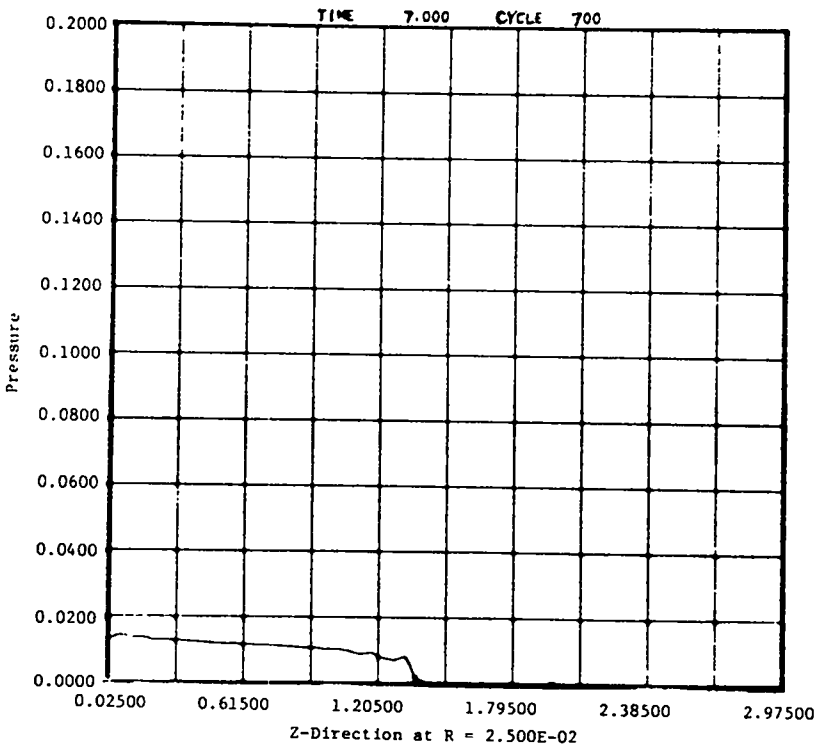

25a. Time = 7 μs

Fig. 25.
Closure of a 0.5-cm-radius hole in Comp. B by a 16-kbar shock wave. Reaction is not permitted.

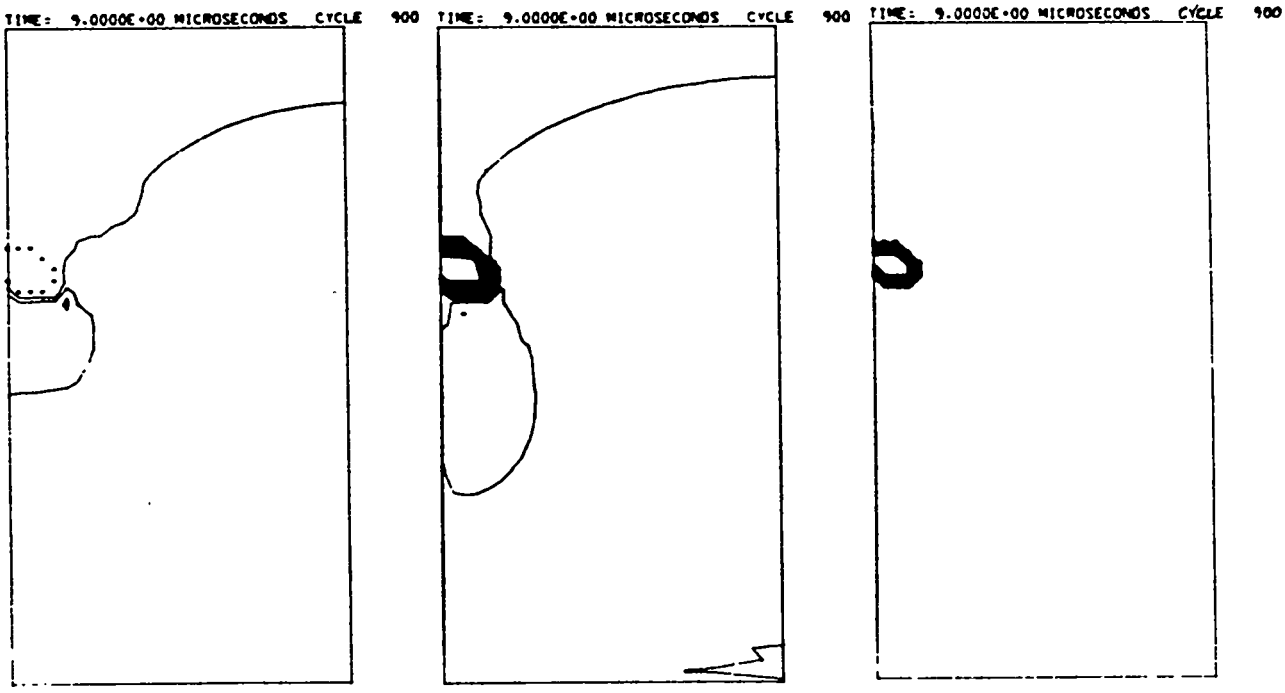

ISOBARS INTERVAL = 1.0000E-02 DENSITY INTERVAL = 1.0000E-01 MF MAT 1 INTERVAL = 5.0000E-02

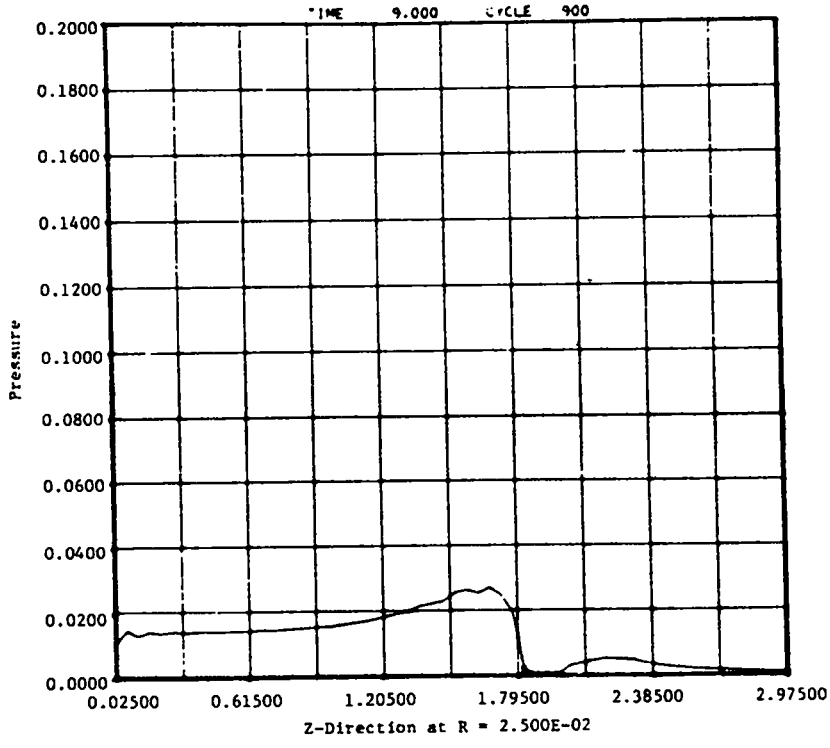

25b. Time = 9 μs

Fig. 25. (cont)

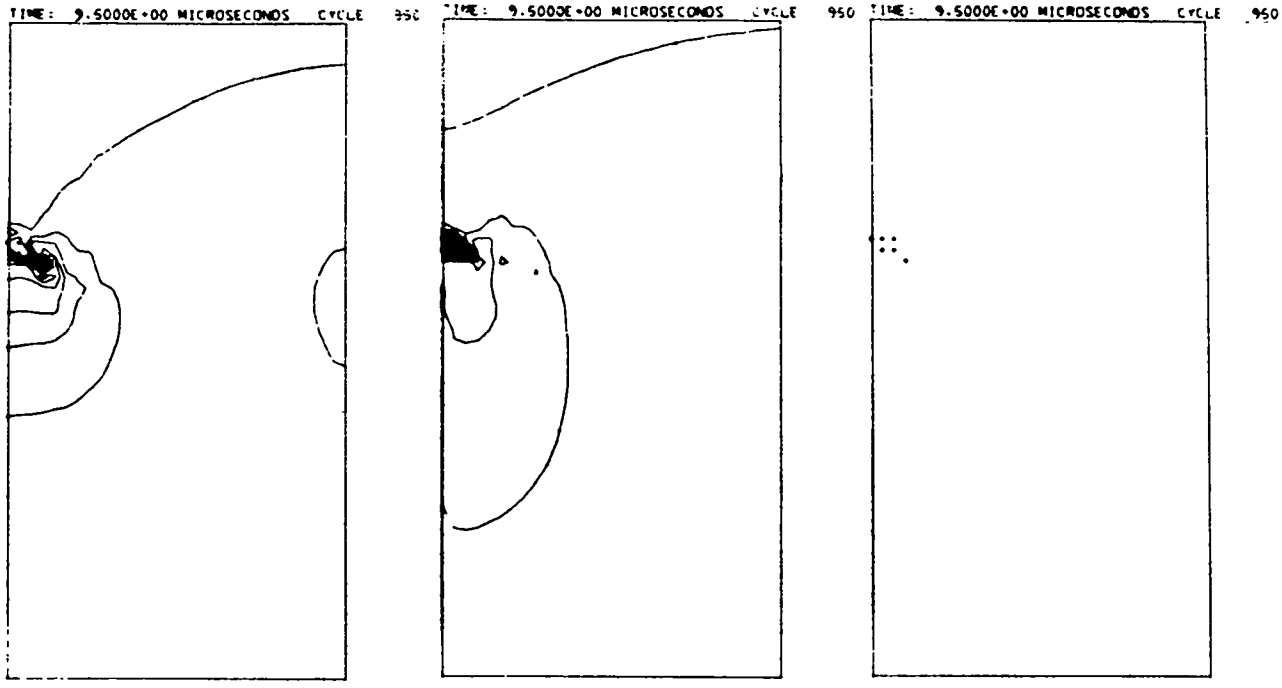

ISOBARS INTERVAL = 1.0000E-02 DENSITY INTERVAL = 1.0000E-01 MF MAT 1 INTERVAL = 5.0000E-02

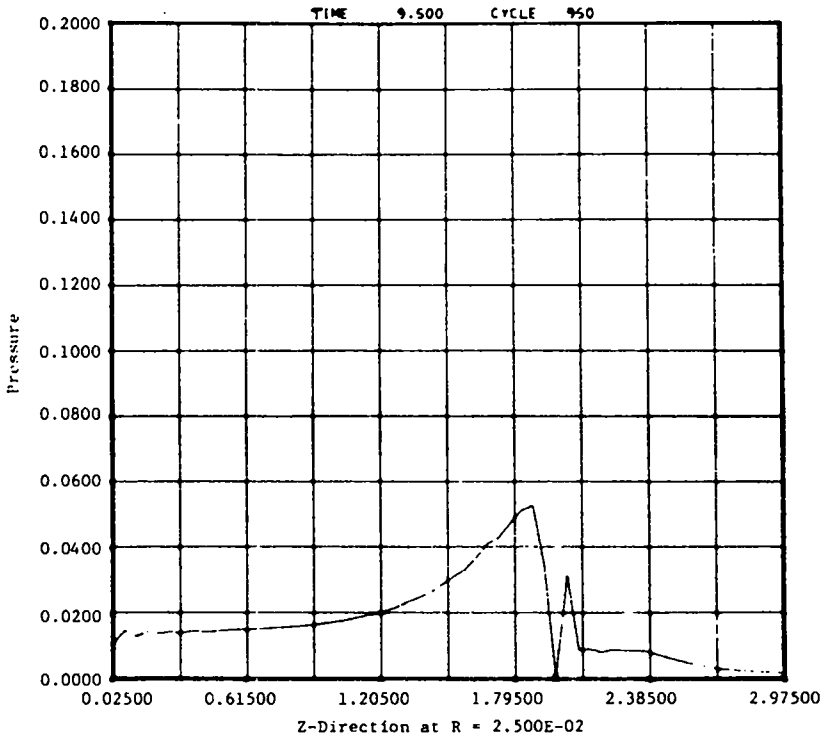

25c. Time = 9.5 μs

Fig. 25. (cont)

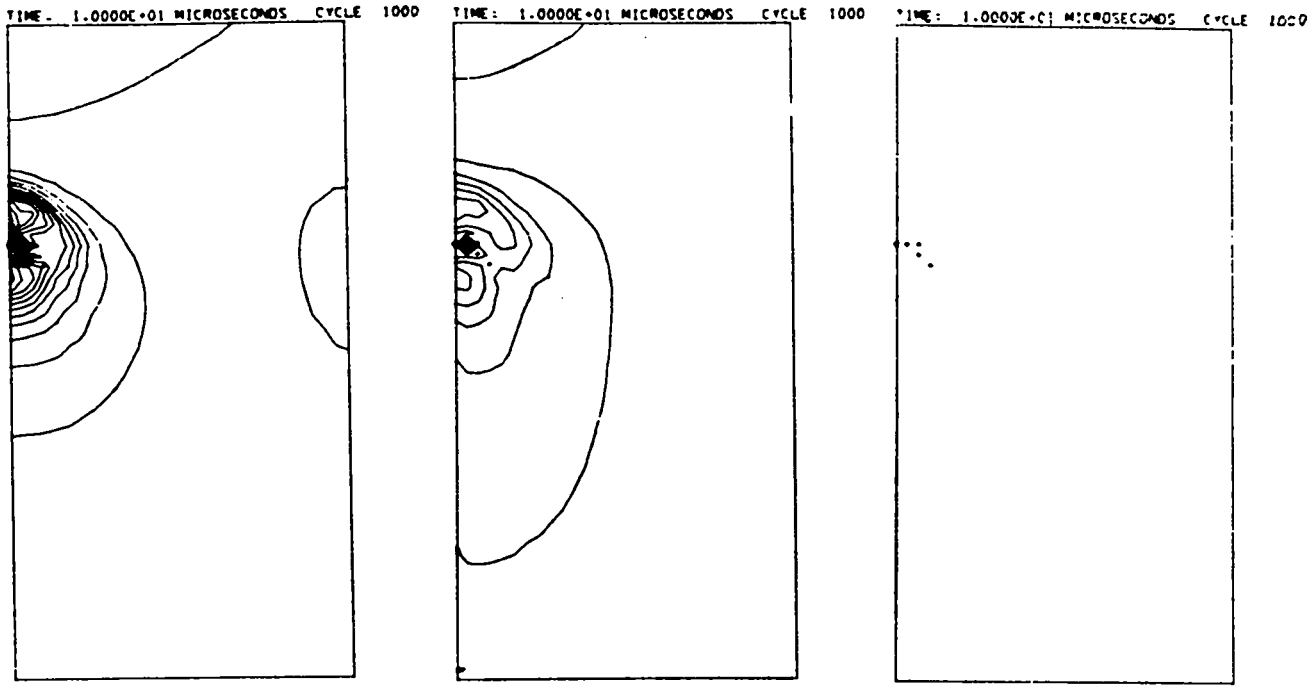

ISOBARS INTERVAL = 1.0000E-02 DENSITY INTERVAL = 1.0000E-01 MF MAT 1 INTERVAL = 5.0000E-02

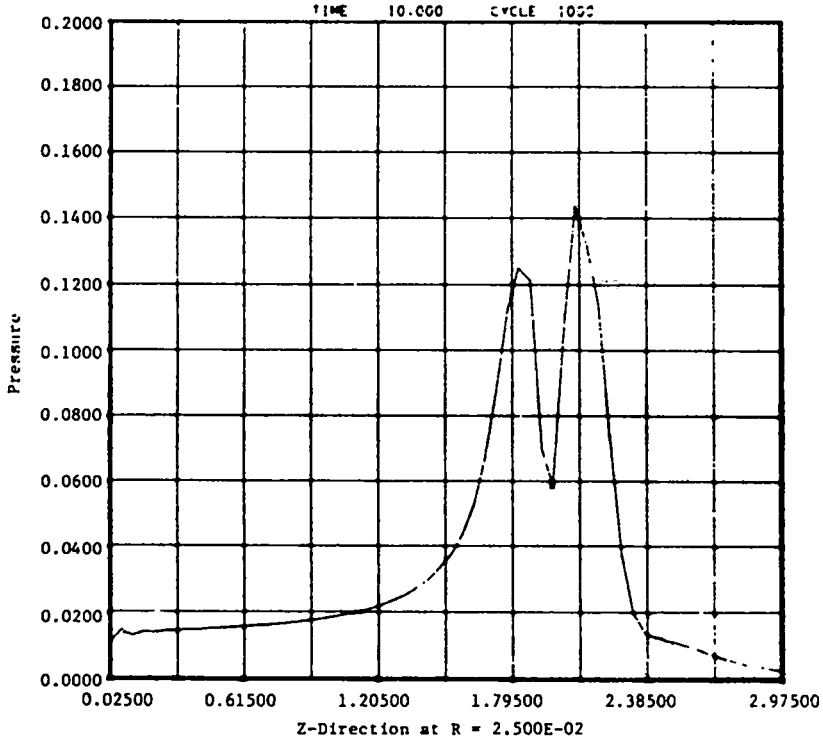

25d. Time = 10 μs

Fig. 25. (cont)

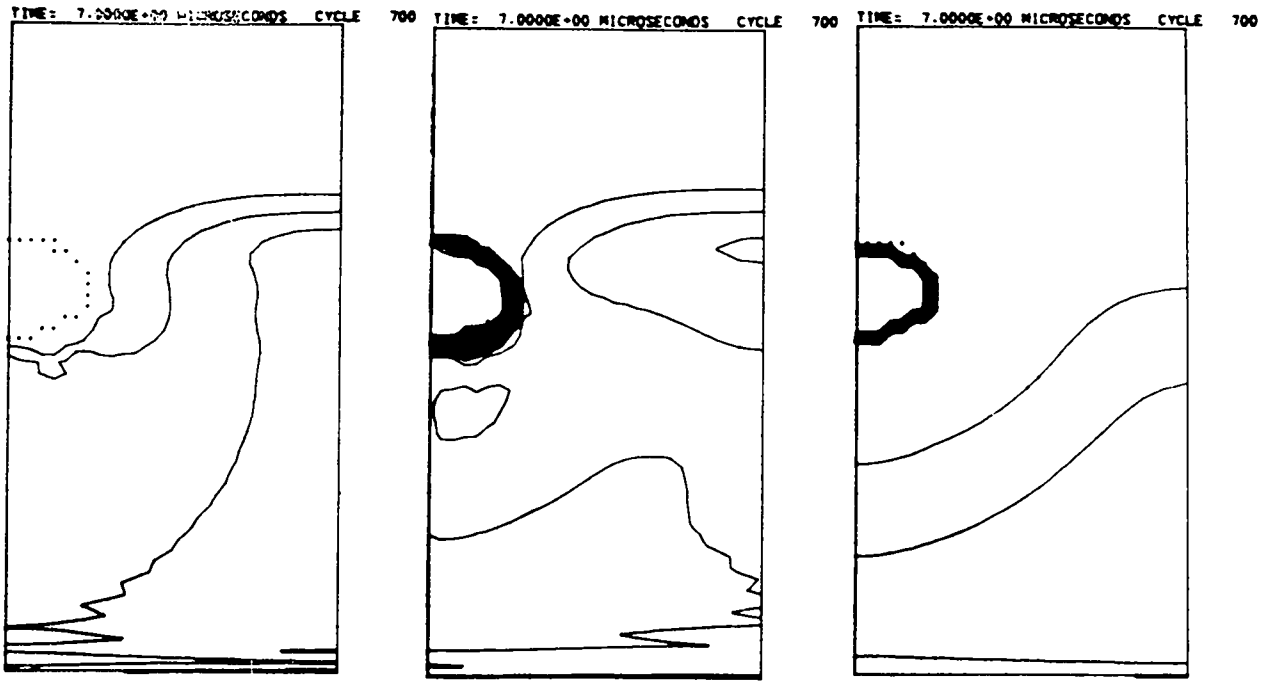

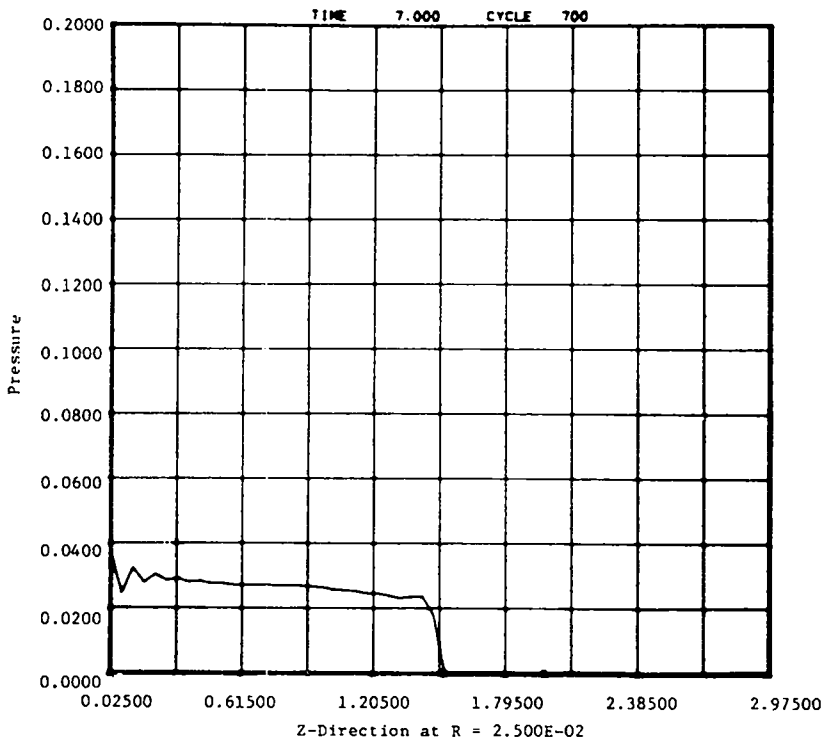

26a. 7 μs

Fig. 26.
Closure of a 0.5-cm-radius hole in Comp. B by a 16-kbar shock wave. Forest Fire is permitted.

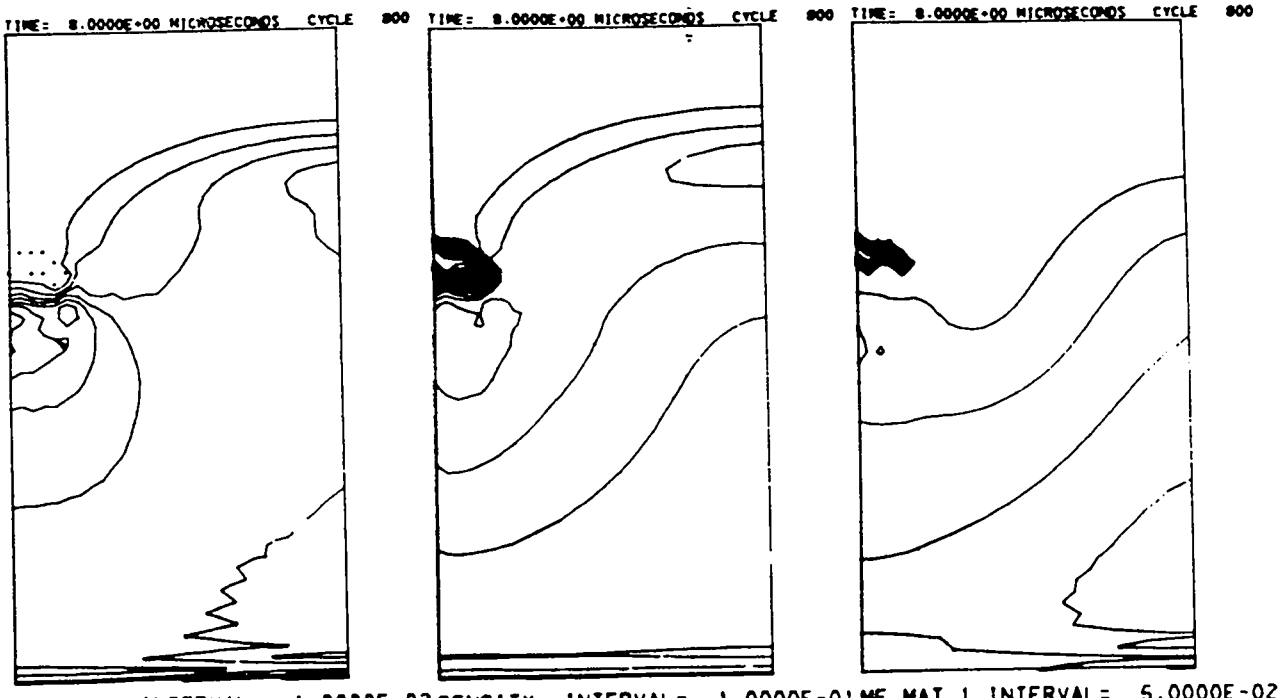

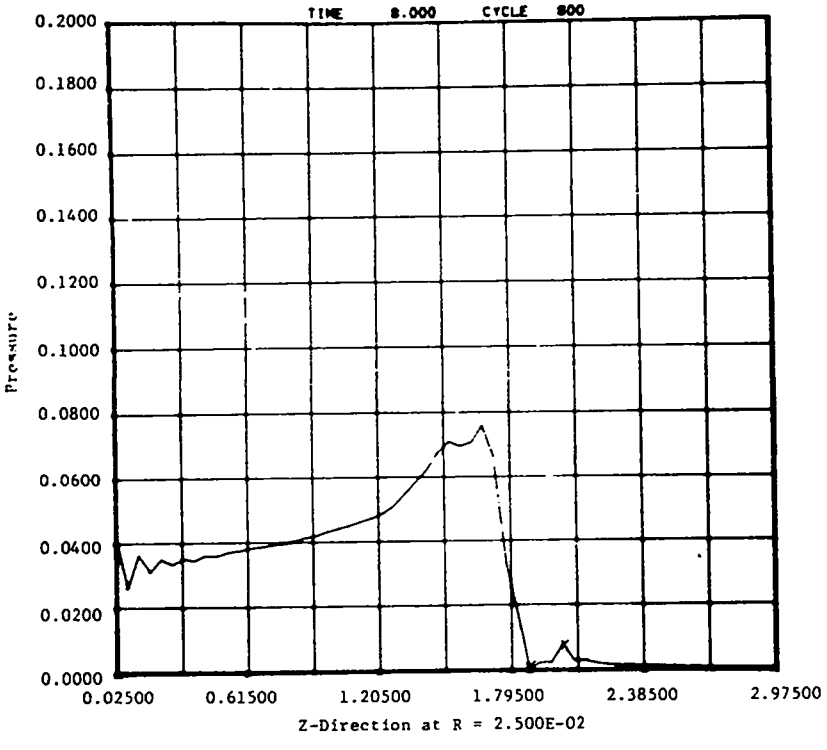

26b. 8 μs

Fig. 26. (cont)

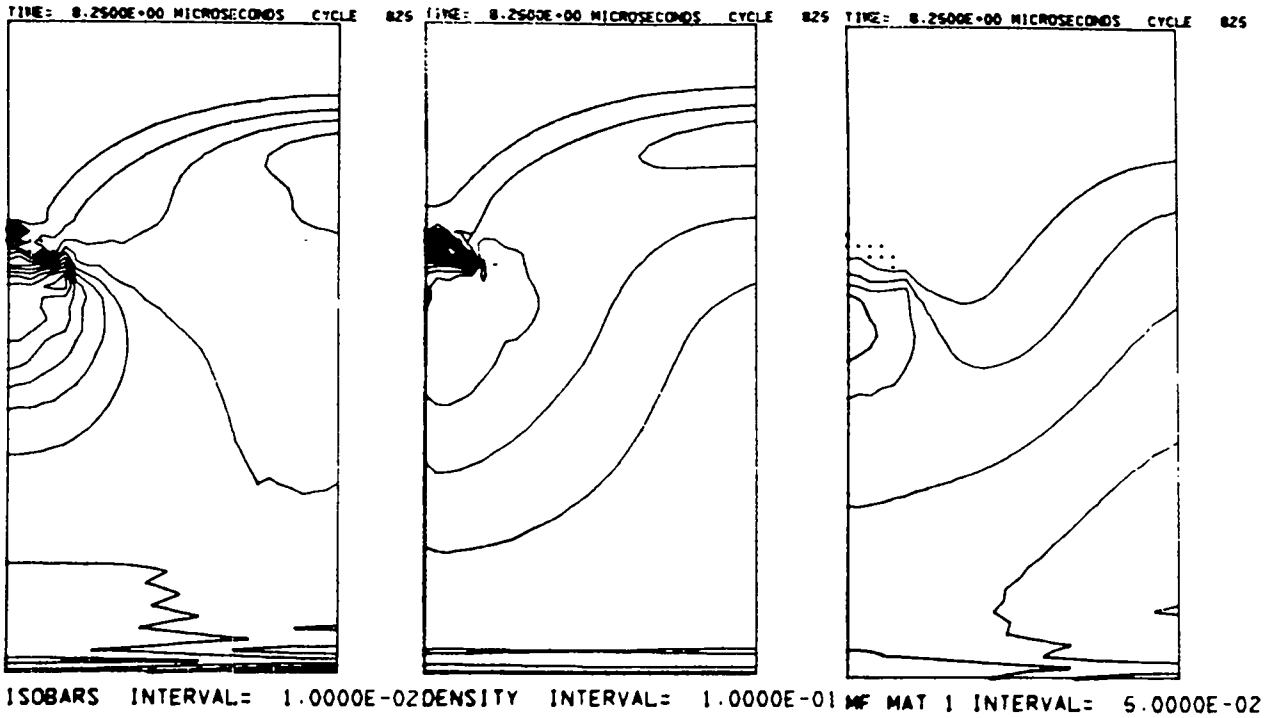

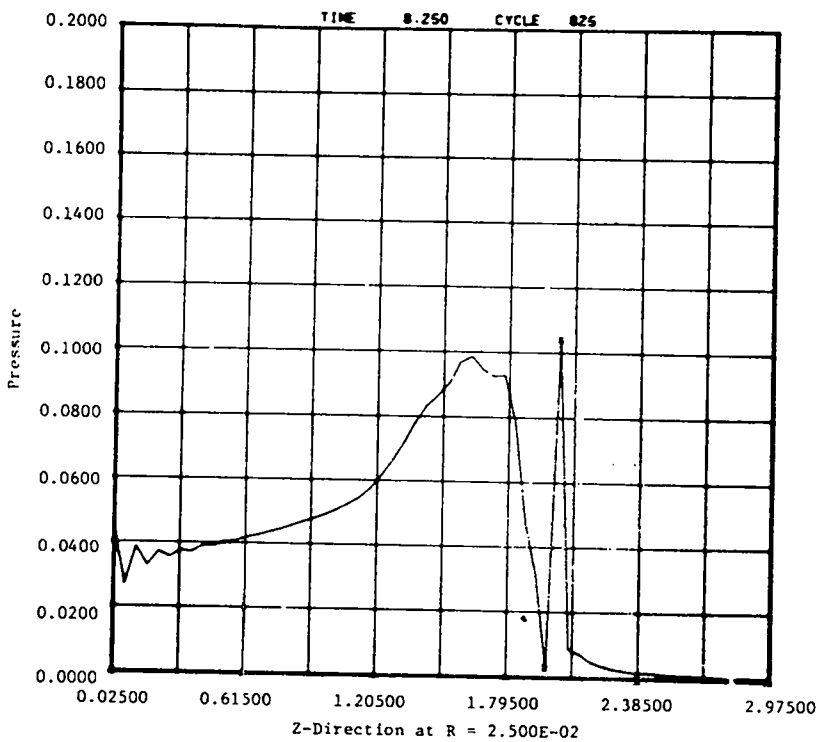

26c. 8.25 μs

Fig. 26. (cont)

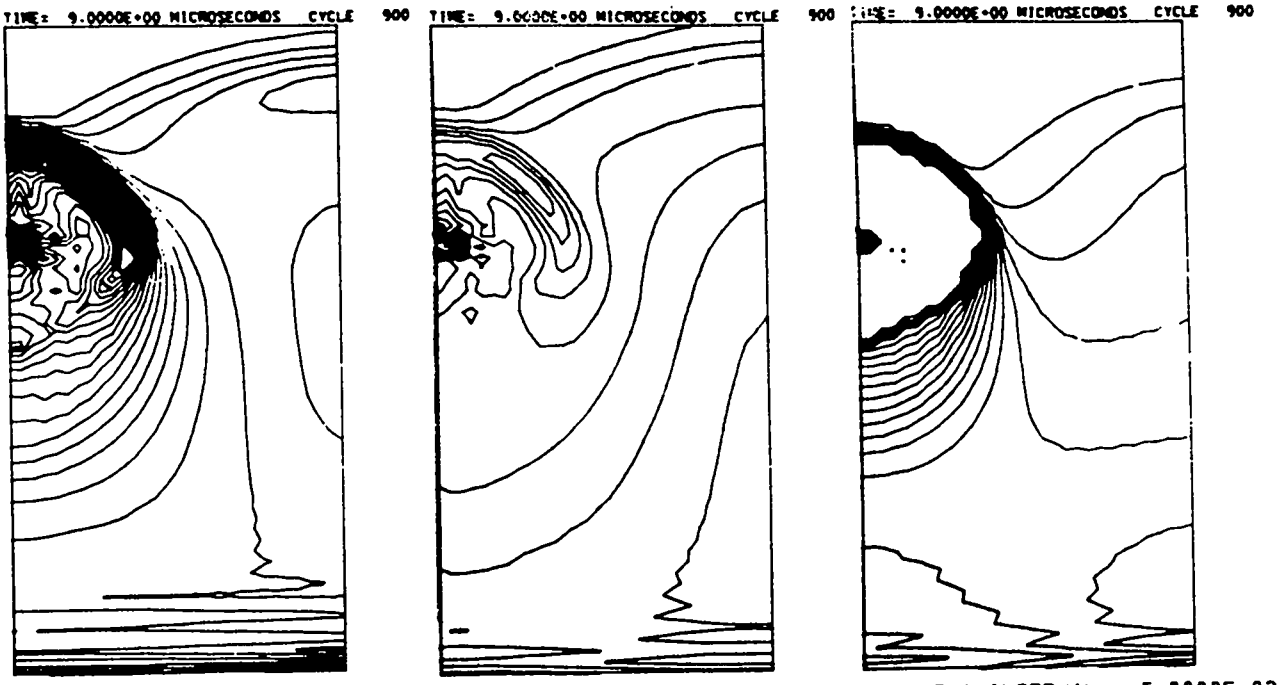

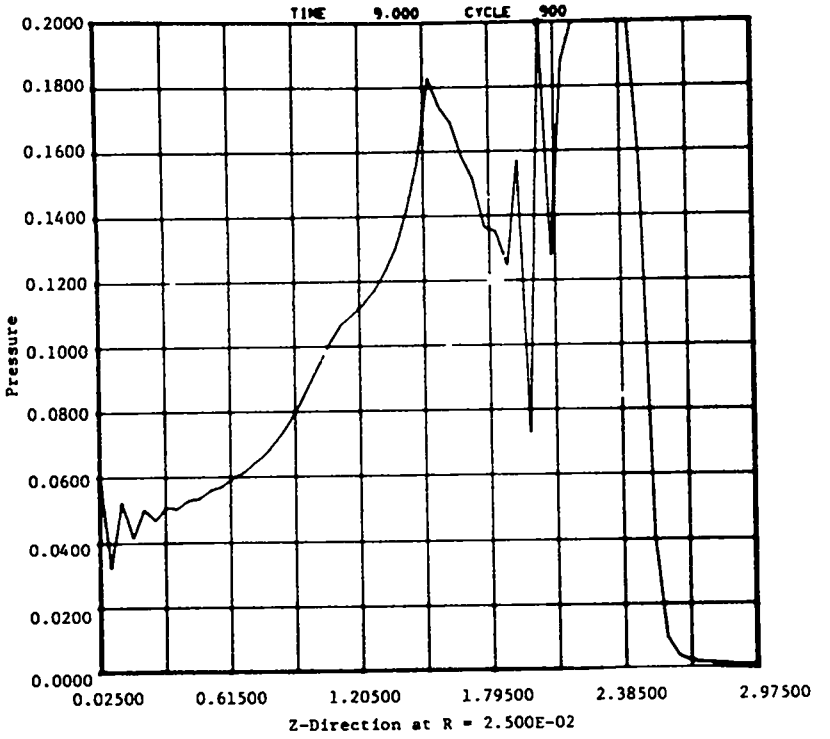

26d. 9 μs

Fig. 26. (cont)

The situation at 8 μs, under these weaker piston applied values, appears so similar to that represented in Fig. 26a that presentation of the plots is not warranted. The incident wave has not yet reached the void. At 10 μs, however, we note in Fig. 27a that the incident pressure wave has enveloped and interacted with the hole. In both the density and the mass fraction plots, partial collapse of the hole is noted. At 10 μs, in the one-dimensional pressure plot near the axis of the cylinder, there is a modest rise of pressure in front of the hole. The hole is marked here by two small x's denoting mixed cells on the boundary. There seems to be the beginning of a pressure rise beyond the hole.

At 10.75 μs, Fig. 27b, collapse of the void has taken place and we see in the isobar plot that a diverging pattern of pressure waves has formed. This again is indicated somewhat in the density contours. The steepness of the contours in the mass fraction plot shows that decomposition has begun. There is a peak in the one-dimensional pressure plot that is partially in front of, within, and behind what, if anything, is left of the hole (as adjudged by the small x's).

In Figs. 27c and d we see a striking picture of the diverging detonation wave in the isobar, density, and mass fraction plots. In Fig. 27d the decomposition is taking place on the diverging front. The one-dimensional pressure plot in Fig. 27c has become bimodal, with progressing and regressing waves. The right-moving progressive wave in Fig. 27d is evidently the detonation wave.

Next, we investigate the effect of having a smaller air-filled hole. With reference to Fig. 23, we study the case where the hole is only 0.25 cm in radius. This is easily done with the 2DE code, which we have already arranged to compute with circular input. One merely specifies as input that RAD(1) = 0.25 (Ref. 7, p. 36). We study this smaller hole with both strong and weak incident pressures as above.

Figure 28 shows the relevant graphical output for the computer run where the hole has a radius of 0.25 cm, with PAPP = 0.0163595, MAPP = 1.41, EAPP = 4.8694×10^{-4}, and VAPP = 0.0312071.

Prior to 6 μs, one sees only the incident wave which has not yet reached the hole or otherwise affected the air cavity, according to our calculations.

At 6 μs (Fig. 28a) the incident pressure wave has already enveloped the hole and collapse has begun. This is further evidenced in the density and mass fraction plots. In the one-dimensional plot the incident pressure wave, as it flows near the z-axis, has formed a steep front at the hole.

At 6.75 μs, the collapse is complete (Fig. 28b). There are some sharp pressure gradients at the collapse site, which observation is further reinforced by the density plot, and there are the beginnings of a divergent flow pattern. There are only five or six mixed cells in the mass fraction plot, into which, presumably, all the air has been forced. The one-dimensional pressure plot has formed a peak which is marked by small x's, which embrace what is left of the hole.

At 7.25 μs (Fig. 28c), in the isobar plot, divergence of flow from the location of the former hole is now the established pattern. This is also evidenced in the density and mass fraction plots. Moreover, decomposition has started; in fact, it started just before 7 μs. At 7.25 μs the detonation wave has separated completely from the hole location and the waves are diverging in a radial pattern. The one-dimensional pressure plot has become bimodal, with the preponderant pressure wave proceeding to the right. In the one-dimensional plot (Fig. 28d) we see how the detonation wave has grown. Pressure has dropped in the neighborhood of the collapsed hole.

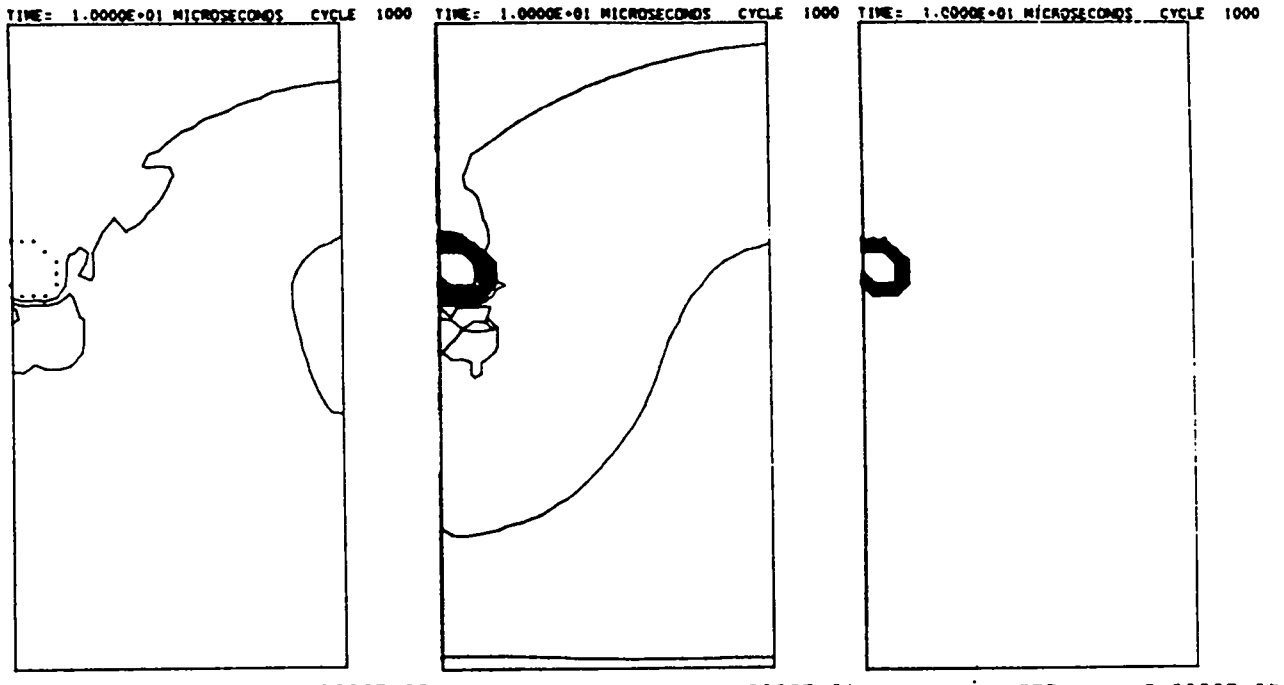

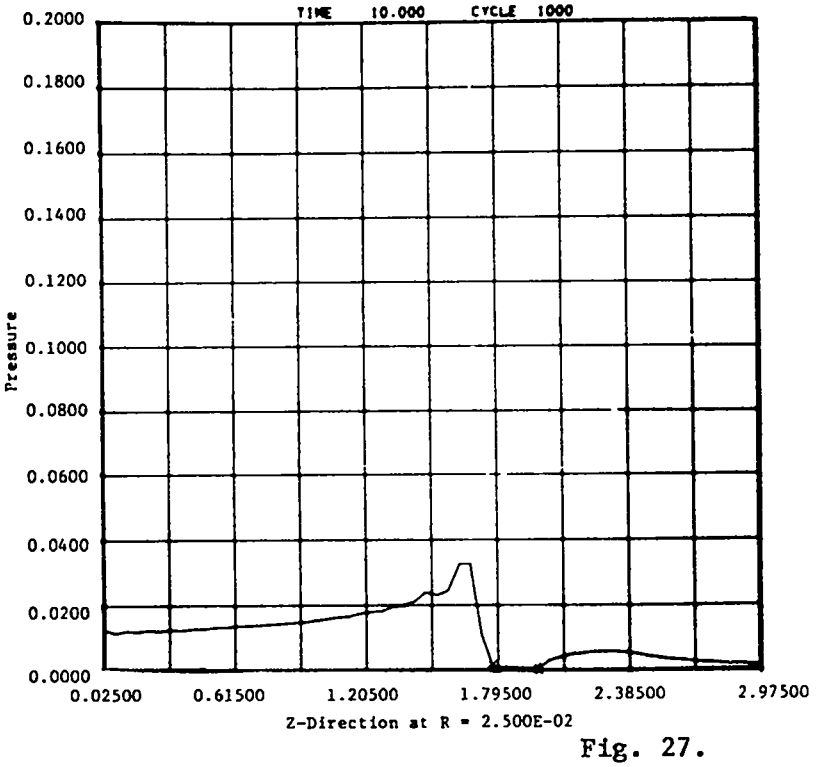

27a. 10 μs

Fig. 27.
Closure of a 0.5-cm-radius hole in Comp. B by a 10-kbar shock wave. Forest Fire reaction is permitted.

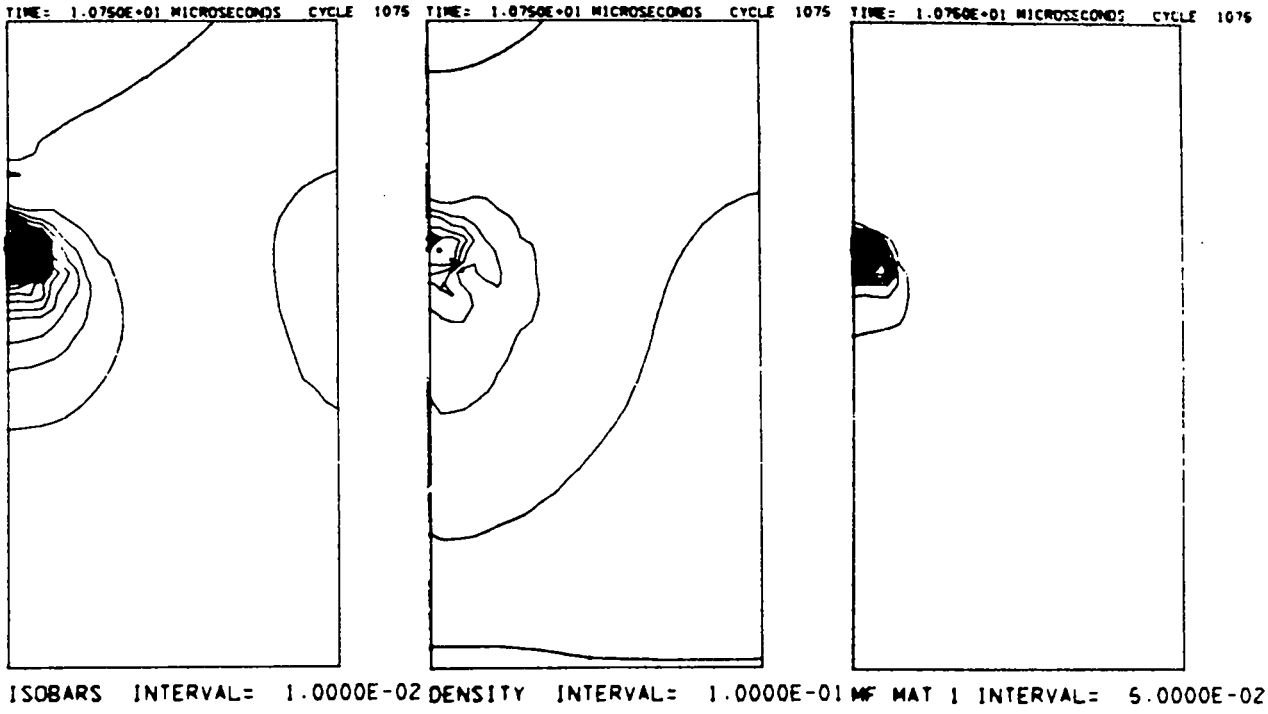

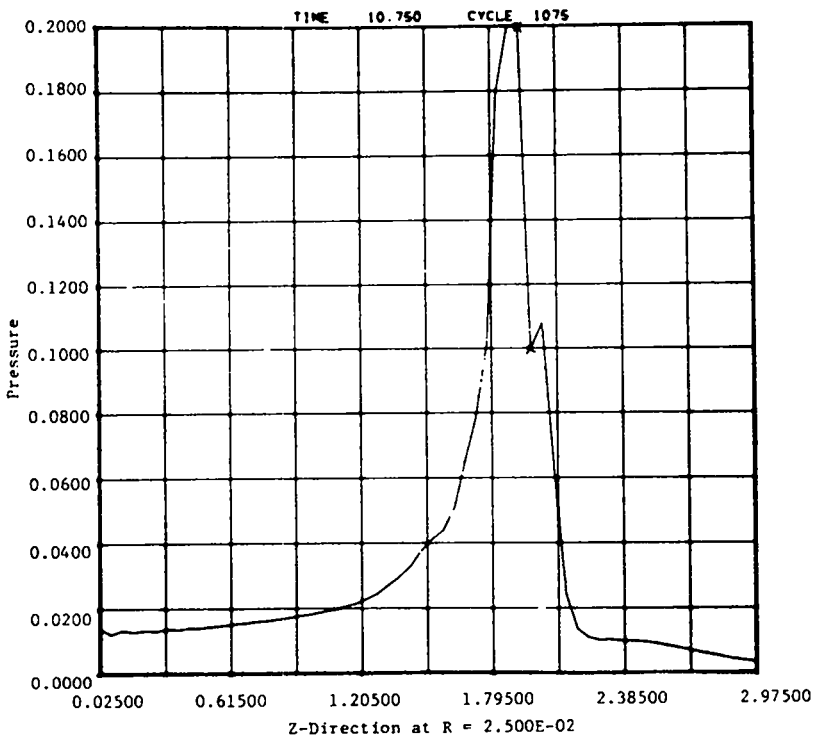

27b. 10.75 μs

Fig. 27. (cont)

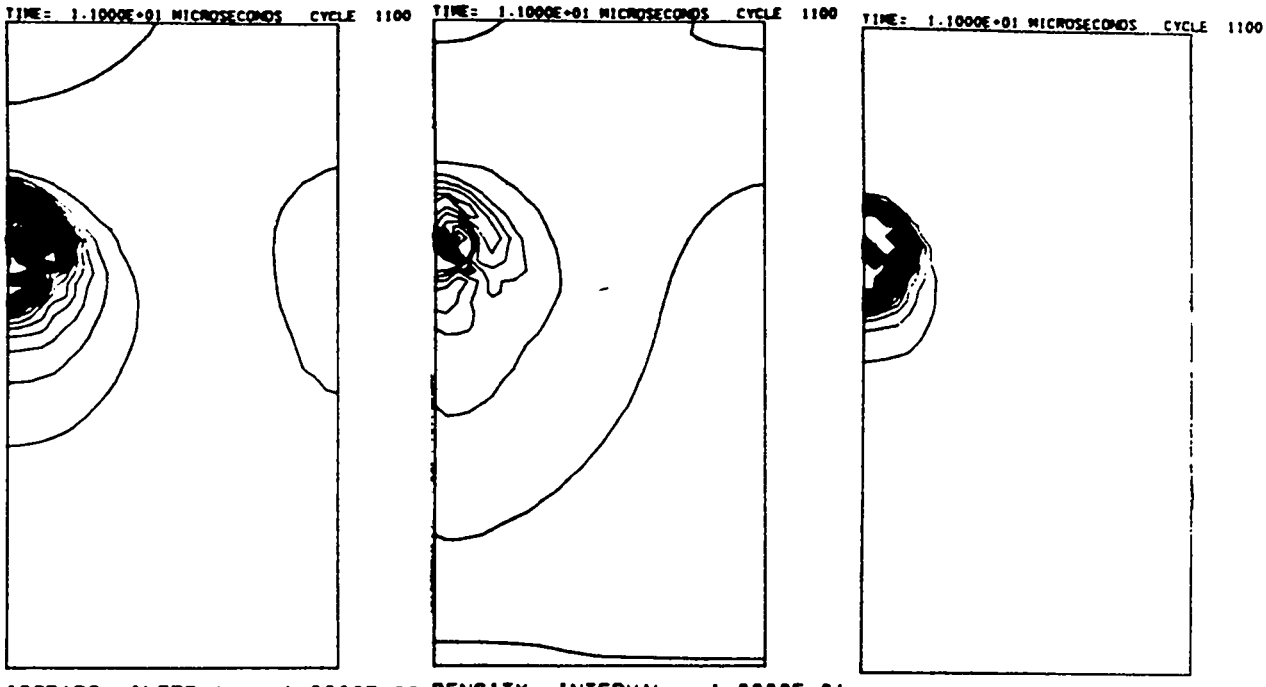

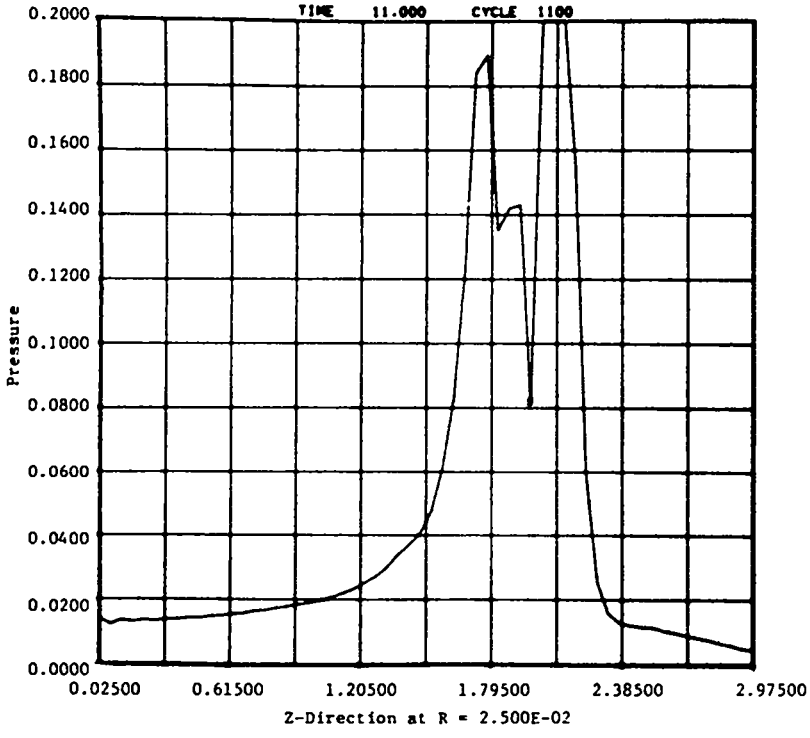

27c. 11 μs

Fig. 27. (cont)

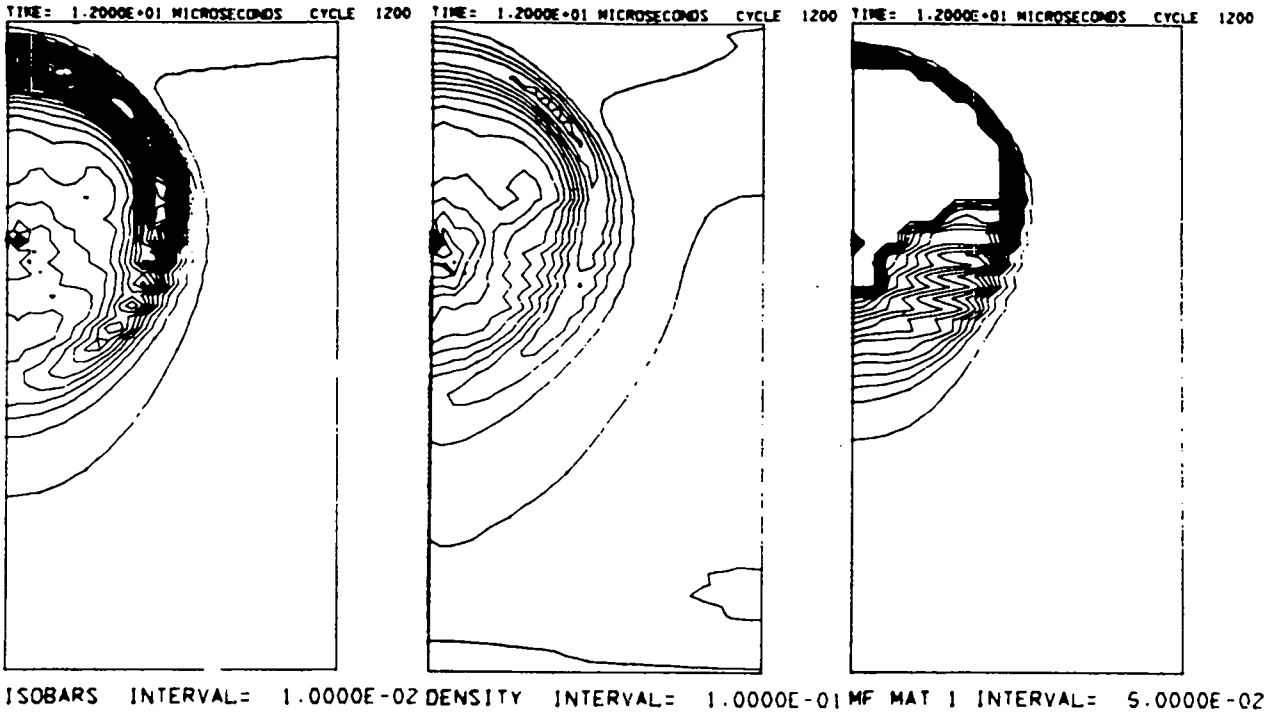

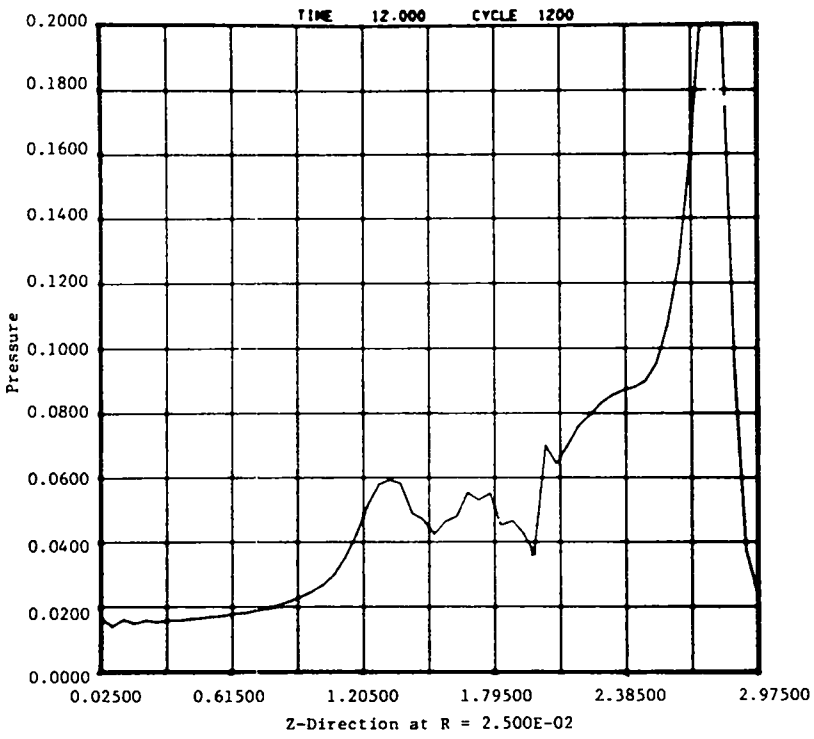

27d. 12 μs

Fig. 27. (cont)

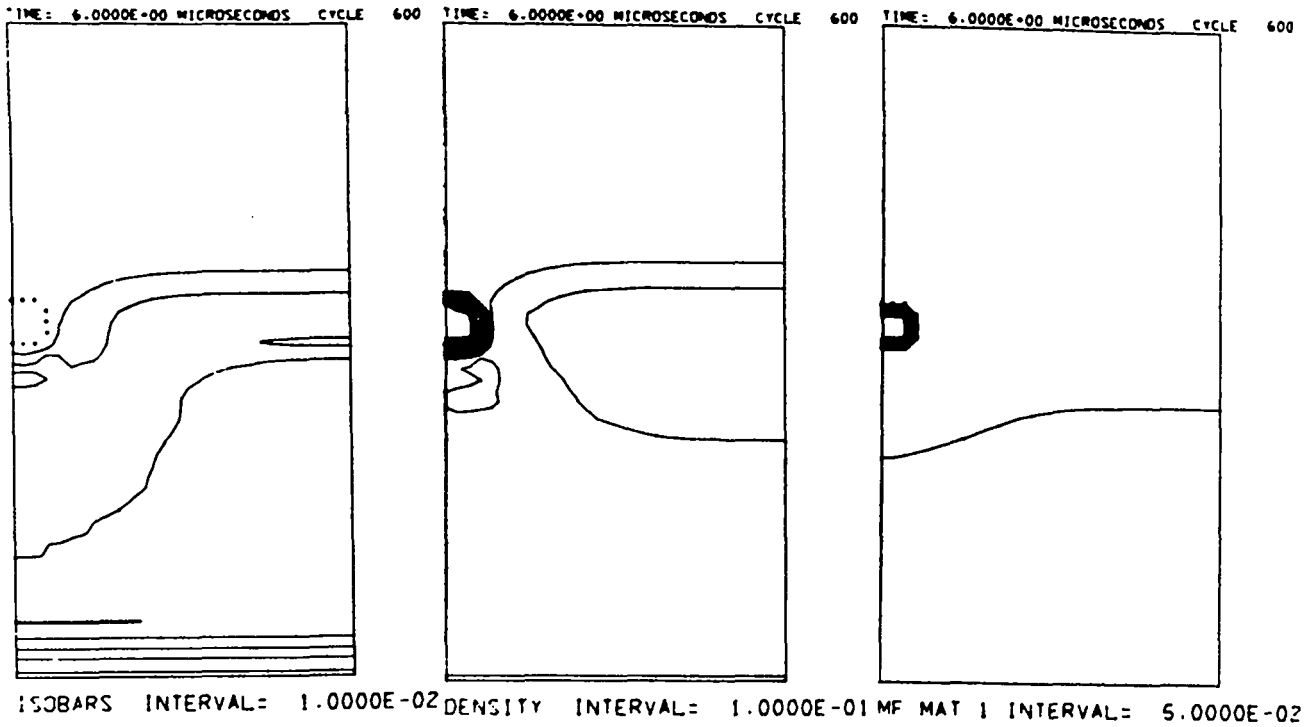

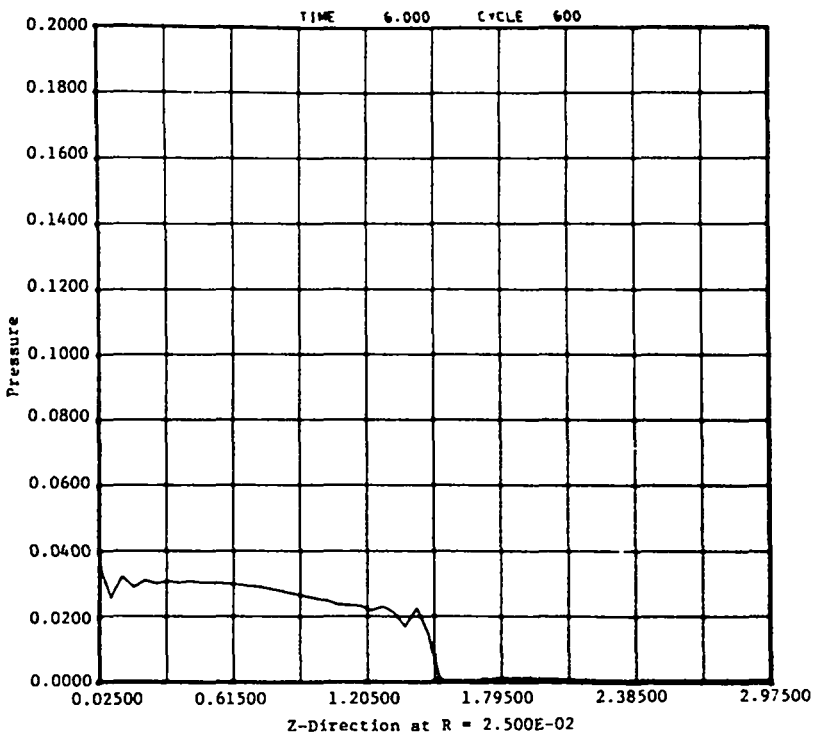

28a. 6 μs

Fig. 28.
Closure of a 0.25-cm-radius hole in Comp. B by a 16-kbar shock wave. Forest Fire reaction is permitted.

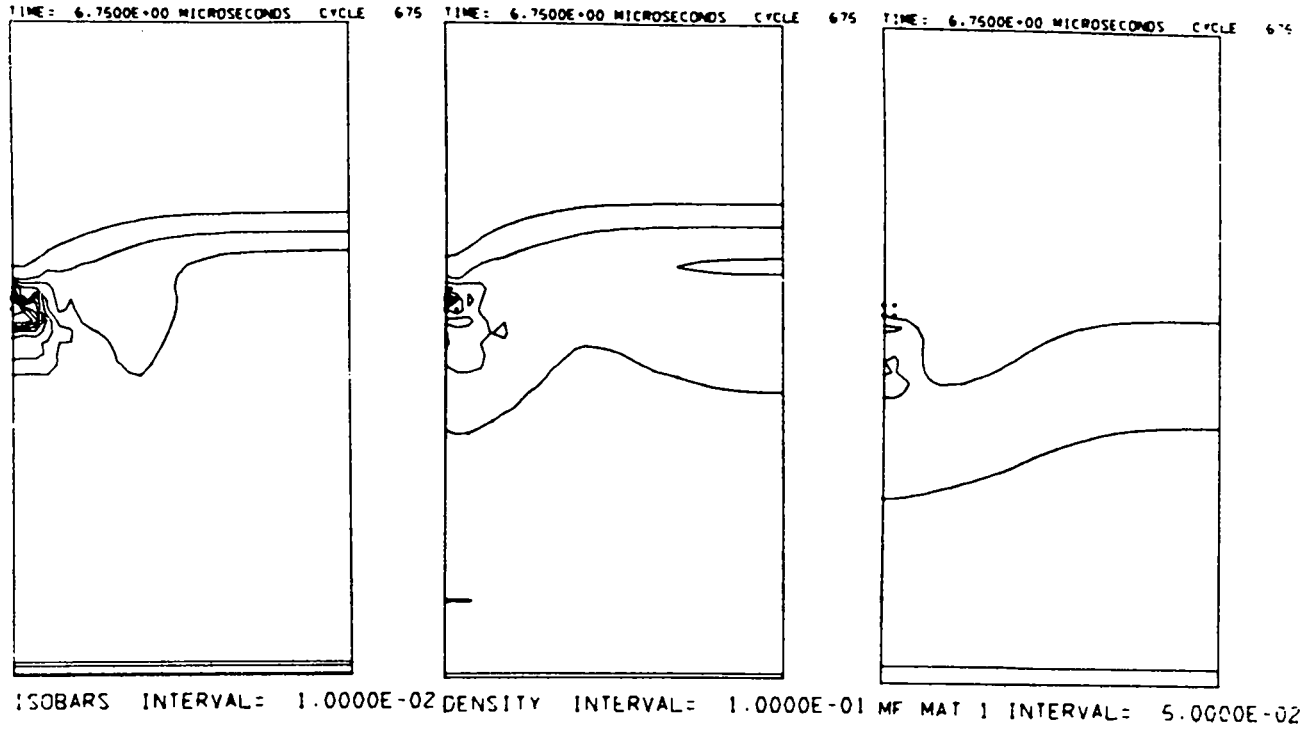

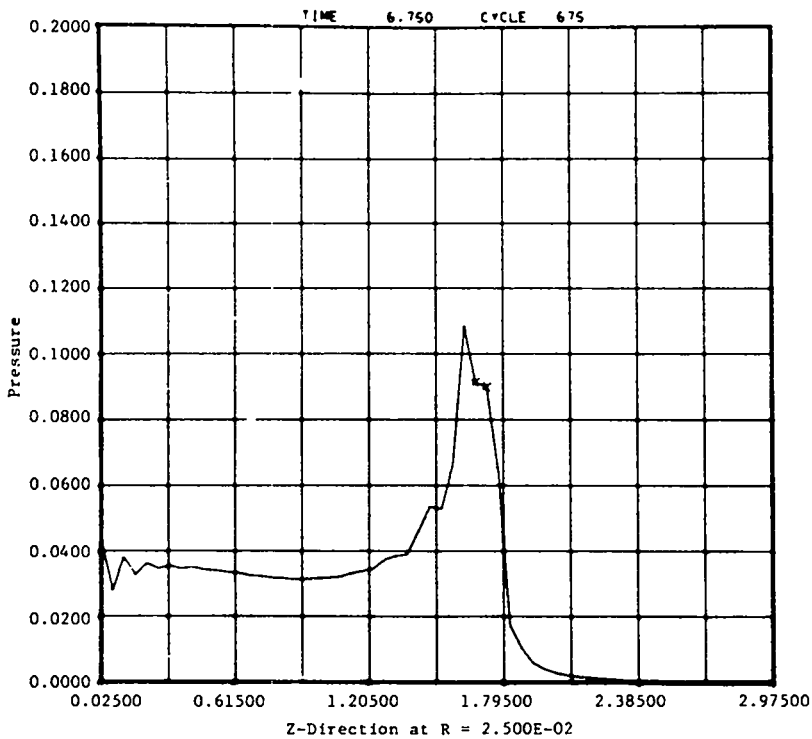

28b. 6.75 μs

Fig. 28. (cont)

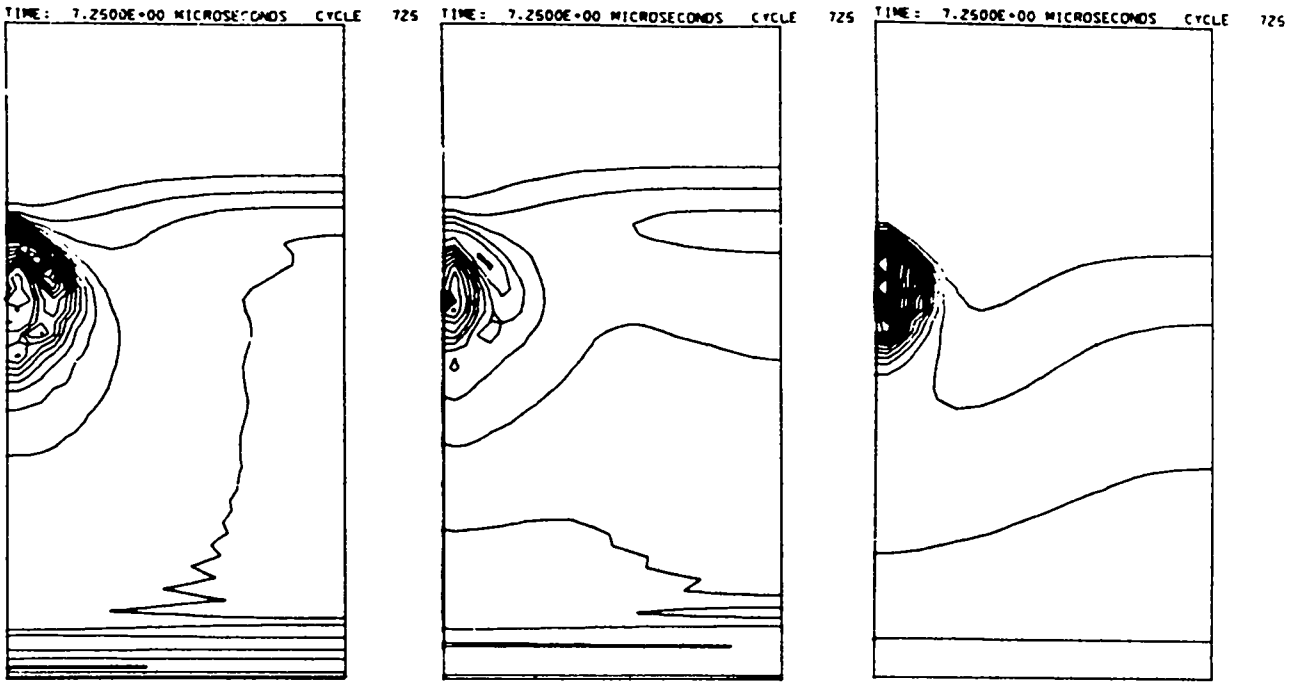

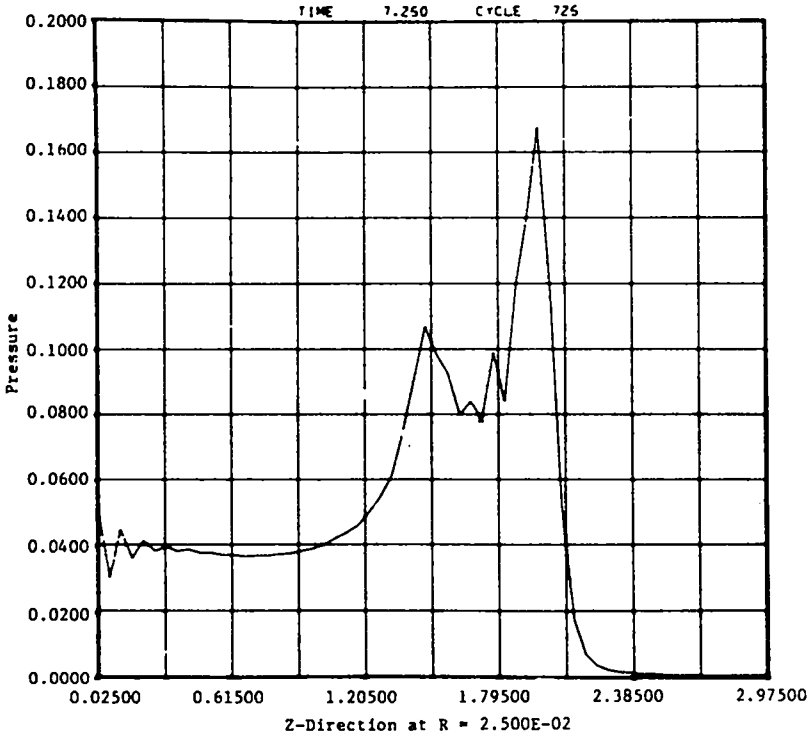

28c. 7.25 μs

Fig. 28. (cont)

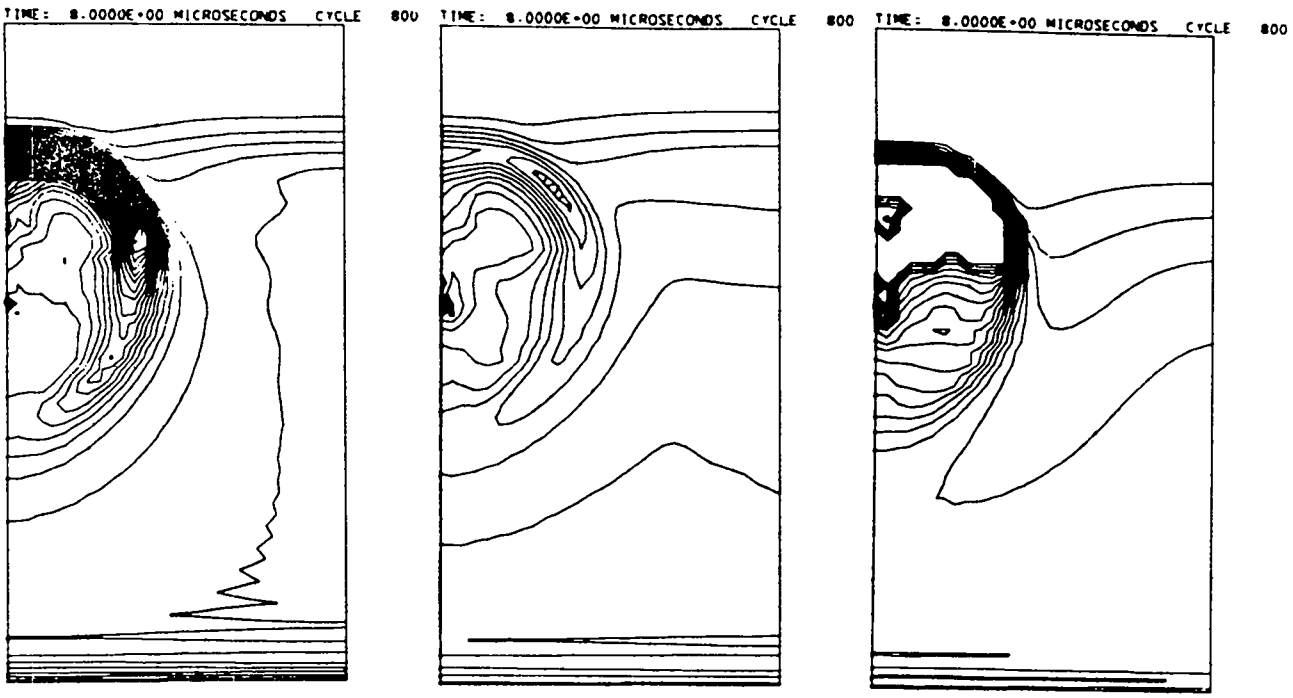

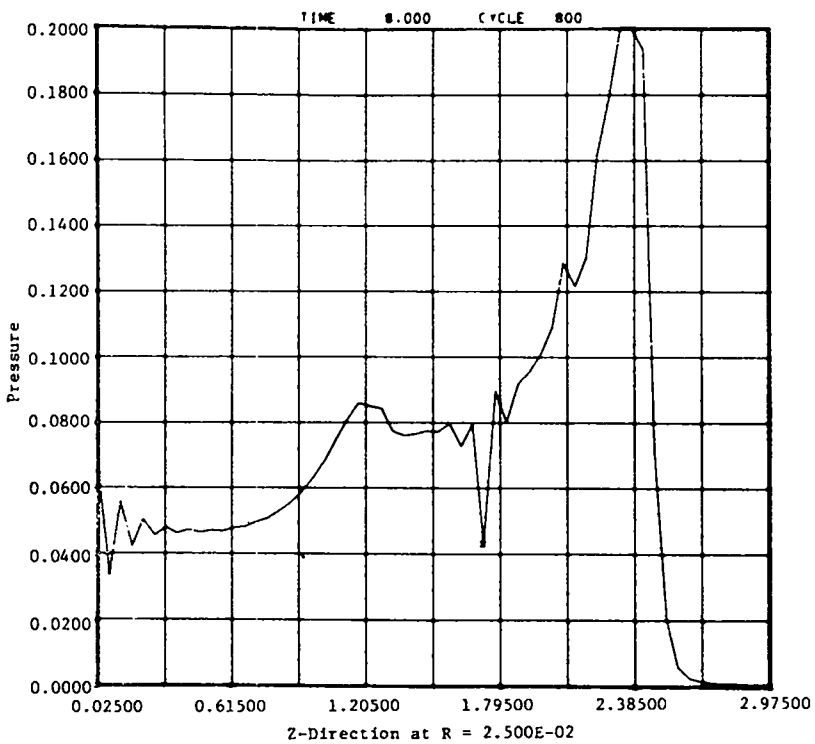

28d. 8 μs

Fig. 28. (cont)

For the 0.25-cm-radius hole and a weak pressure pulse (piston applied values PAPP = 0.01, MAPP = 1.84722776, EAPP = 2.08693×10^{-4}, and VAPP = 0.02043003), the rather lethargic chain of events is portrayed in Fig. 29. Prior to 7 μs we have only the incident pressure pulse before its arrival at the hole, the untouched 0.25-cm hole, and a one-dimensional plot showing a low wave of pressure with a front of rather gentle descent.

At 7 μs the incident wave, shown in Fig. 29a, is reacting weakly with the hole and there has been some collapse, as evidenced in the density and mass fraction plots. The one-dimensional pressure plot begins to form a small peak with some steepness of descent. At 8 μs (Fig. 29b) collapse of the hole is complete, with moderately steep pressure gradients and quite steep density gradients. The air that was in the hole is confined to five mixed cells. The pressure peak at collapse, as seen in the one-dimensional plot, is quite low. On the other side of the mixed cells, the pressure starts to rise.

Later, at 8.5 μs, a diverging flow pattern is well underway as seen in the isobar, density, and mass fraction plots of Fig. 29c. The peak in the one-dimensional plot is not impressive. There is no evidence of decomposition, much less detonation; likewise in Fig. 29d showing the situation at 9 μs. The one-dimensional pressure plot is bimodal, with approximately equal pulses moving in each direction. At 10 μs these two low pulses are yet more widely spread apart.

The interaction of a weak 10-kbar shock with a 0.25-cm-radius hole results in pressure pulses of a duration too short to result in propagating detonation. A larger hole of 0.5-cm radius with the same weak piston results in pulses of the same magnitude but of longer duration. The increased duration permits the buildup of the wave to propagating detonation.

IV. SUMMARY

A. Aquarium Experiments and Computations

It is still necessary to find the chief mechanism for the observed initiation of explosive charges resulting from the closure of base gaps in cavities. We have been unable to confirm the traditional explanation; namely, adiabatic compression of trapped air and thermal heating of the same. The object of our work has been to gain a better idea of the basic physical processes taking place in these collapsing voids.

The aquarium technique for studying the effect of a shocked base gap on pressed TNT and Comp. B has furnished information about the relative importance of possible base-gap mechanisms. The technique has been used to study the importance of

- the presence of gas-filled gaps,
- the presence of vacuum gaps,
- the presence of explosive powder in air-filled gaps and of gaps filled entirely with explosive powder, and
- the case of an air-filled gap where particles of explosive powder have been glued on the surface of the explosive in the gap.

Explosive samples have been given various protective coatings in the gaps, the effects of side gaps filled with air have been experimentally assessed, and grooved and ungrooved Plexiglas covers have been tested.

One-dimensional SIN calculations and two-dimensional 2DL calculations have been used to model the important features of various aquarium shots. The effects of heat conduction, shock initiation, and burning have been included in the numerical calculations to determine the importance of each effect.

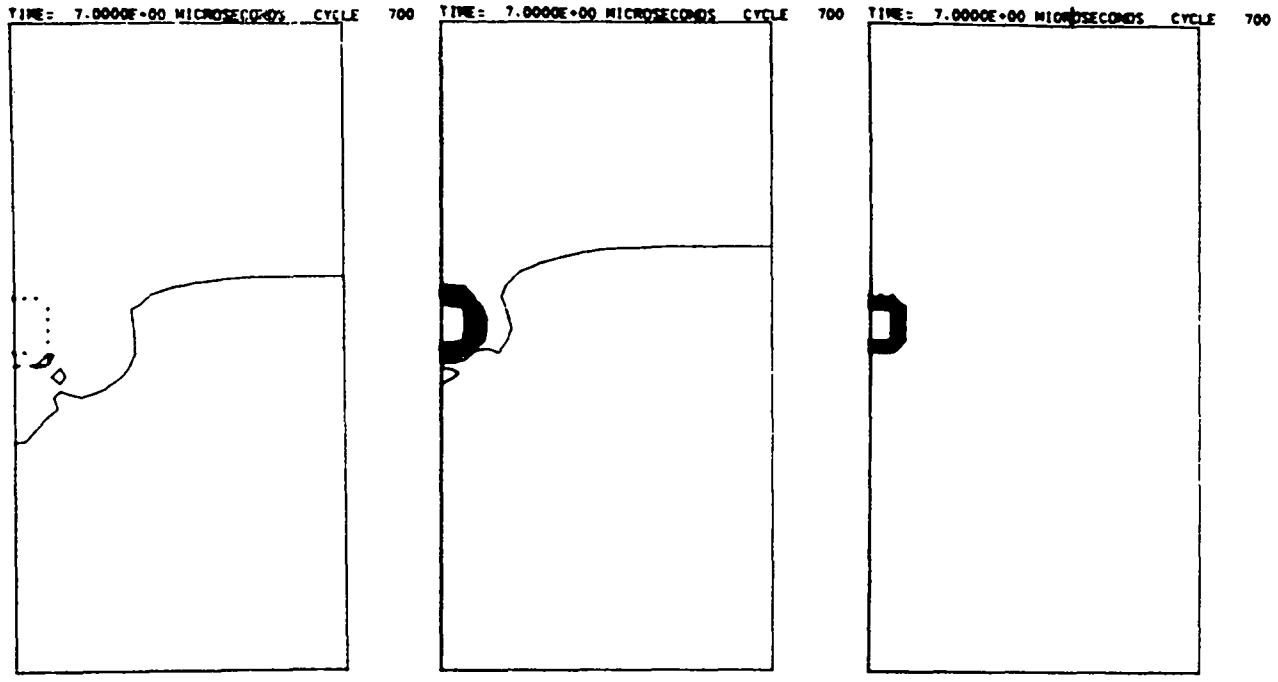

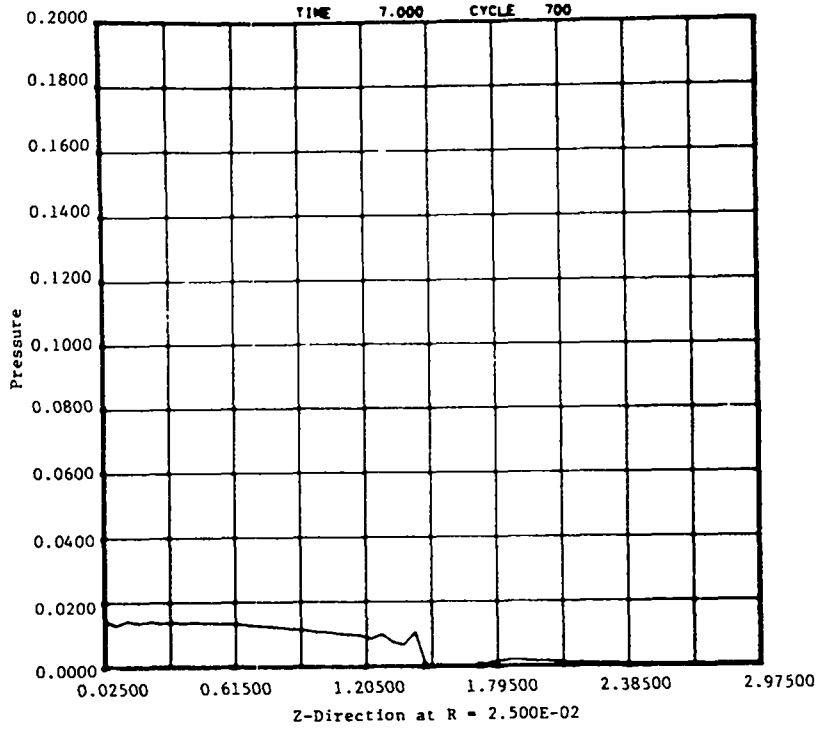

29a. 7 μs

Fig. 29.
Closure of a 0.25-cm-radius hole in Comp. b by a 10-kbar shock wave. Forest Fire reaction is permitted, and the interaction fails to result in propagating detonation.

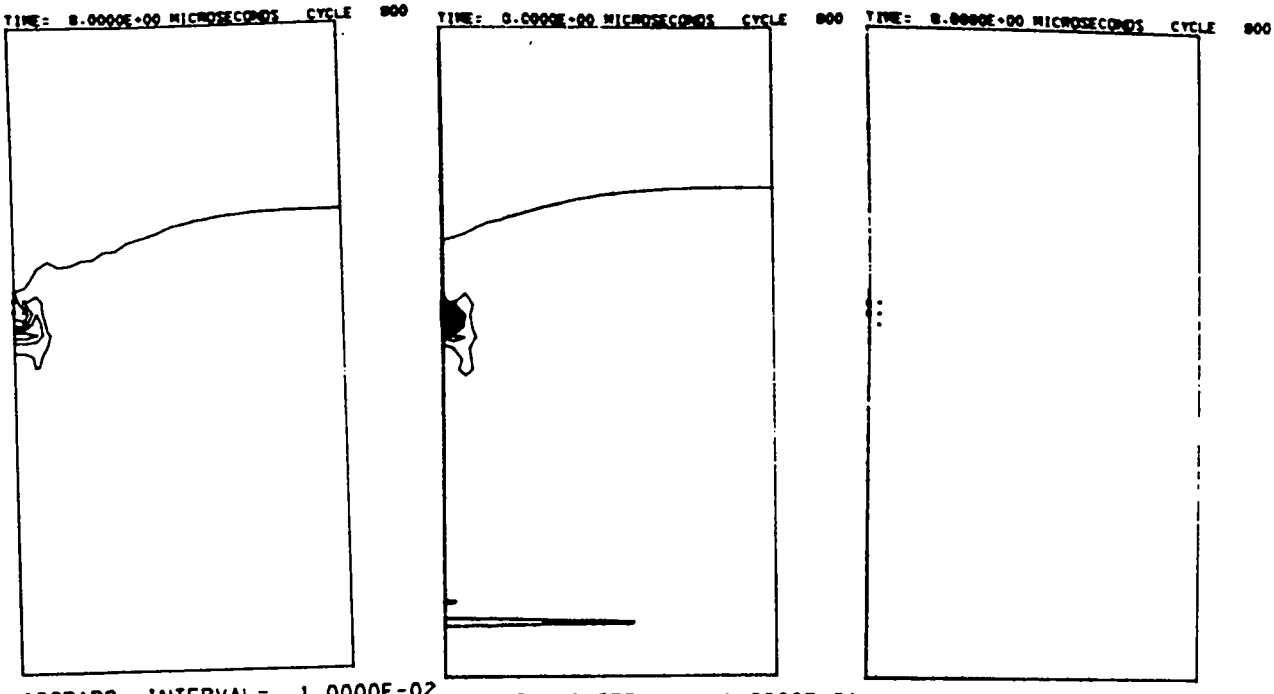

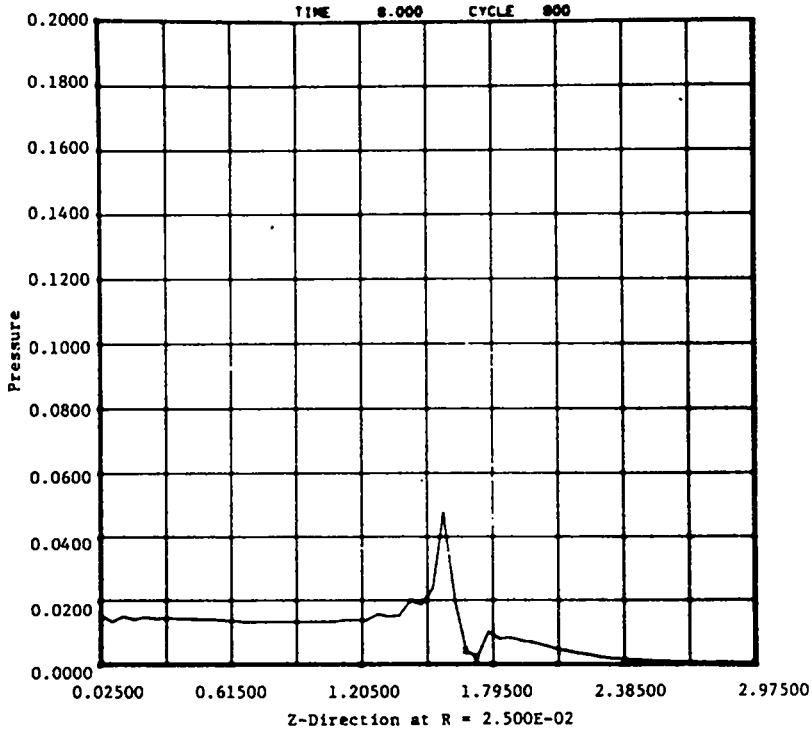

29b. 8 μs

Fig. 29. (cont)

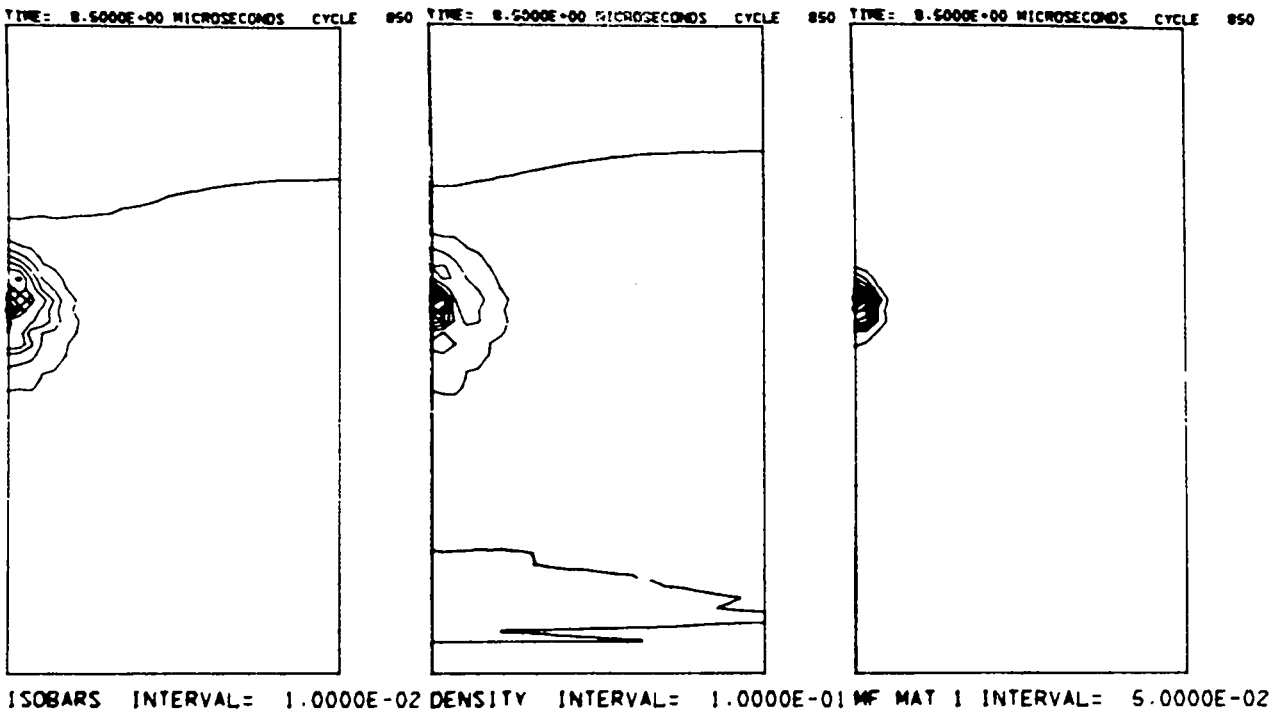

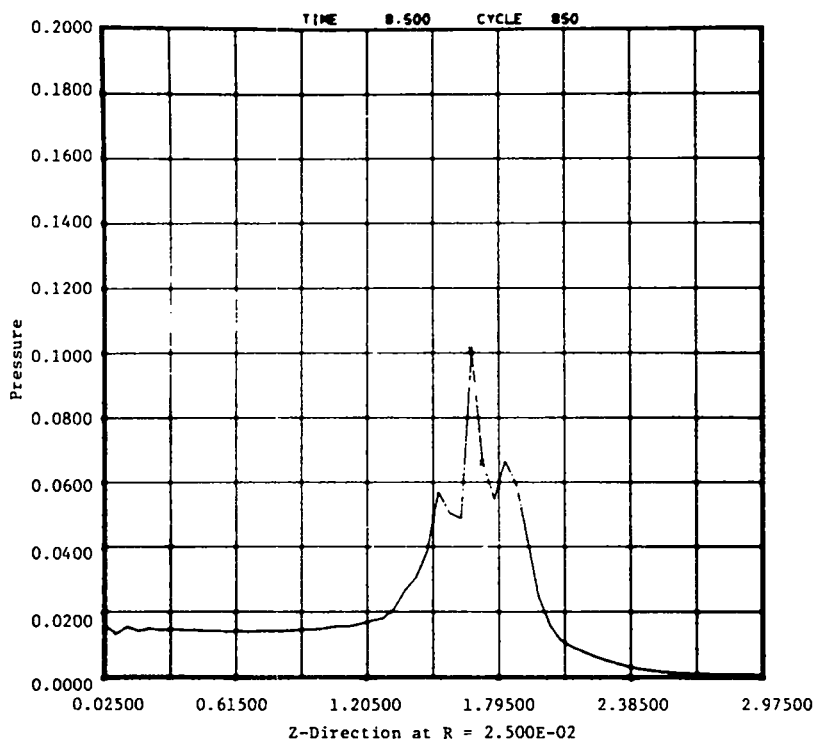

29c. 8.5 μs

Fig. 29. (cont)

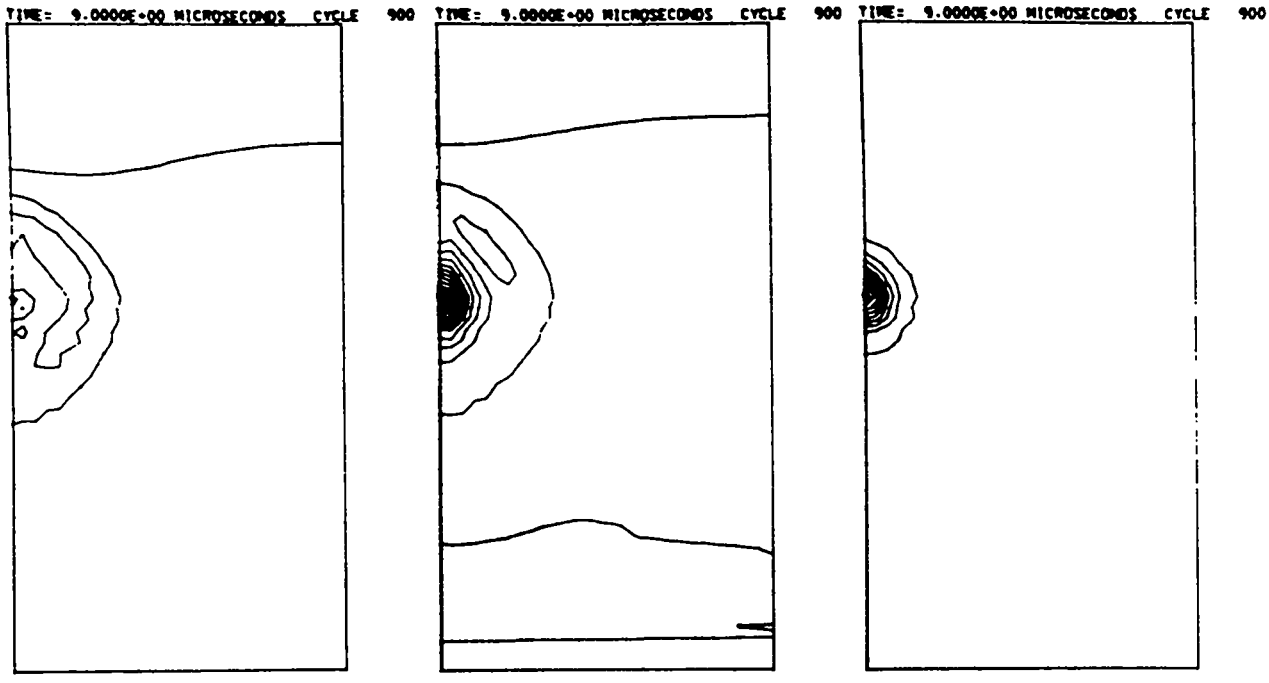

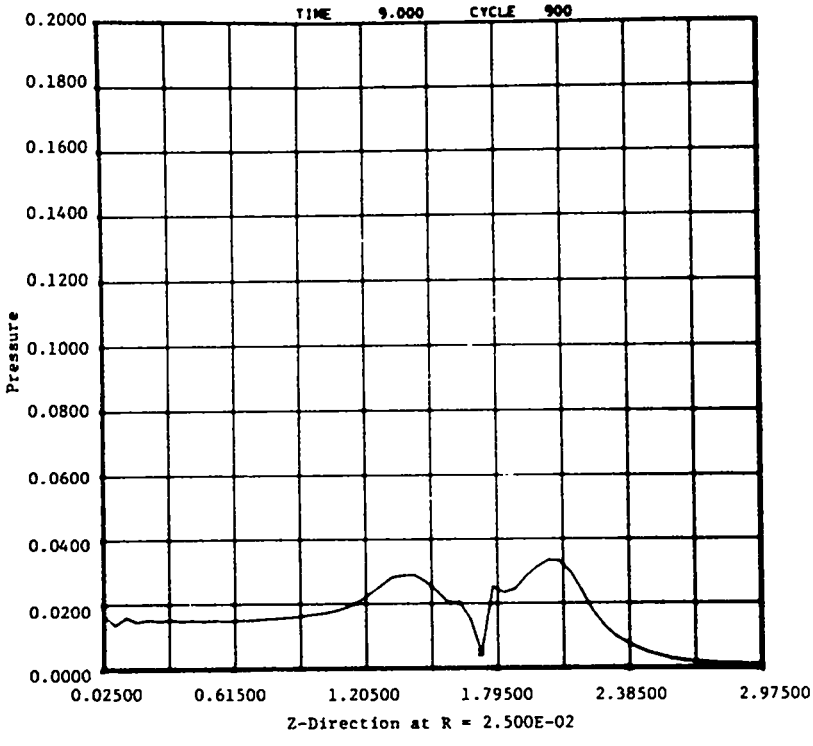

29d. 9 μs

Fig. 29. (cont)

The commonly accepted gas-compression, thermal ignition mechanism is not consistent with the following observations.

- TNT and Comp. B explosives give similar amounts of decomposition from air-filled gaps in the aquarium experiments, even though their Arrhenius kinetic rates differ by a factor of 10.[7]
- TNT and Comp. B give similar amounts of decomposition with vacuum gaps and with air-filled gaps.
- TNT has been observed to give similar amounts of decomposition with air gaps, krypton gaps, and methane gaps.
- The set-back simulator at AARADCOM, Dover, New Jersey, has been observed to give ignition of Comp. B at 1 kbar. At 1 kbar in an air gap, the accompanying temperature would be too low to result in ignition by the adiabatic mechanism.

We have made one very interesting observation in connection with aquarium experiment #3234-1 (see Table IV), wherein coarse Comp. B particles were glued on the surface of the explosive sample in the gap. In those experiments where explosive powder merely filled a gap, it seemed simply to be compressed into a cake by the shock, becoming in effect an extension of the Comp. B sample. Reactions were not impressive. When explosive particles were actually glued on the Comp. B surface as in experiment #3234-1, however, the decomposition was extensive and the sides of the sample were splayed. Our distinct impression is that rough, abrasive surfaces and grinding motions of the same (perhaps as the Plexiglas cover somes in contact with the explosive face) may have much to do with initiation in gaps and in base gaps of artillery shells.

Therefore, attempts should be made to investigate (both experimentally and by numerical modeling) heating that occurs because of frictional processes to determine if it may be the dominant mechanism of initiation of explosive charges resulting from the closure of gaps.

B. Pipe Tests and Computations

Experiments show that air-filled voids of small diameter in specimens of Comp. B driven by a strong charge of HMX powder in a pipe test fail to cause detonation. Only partial decomposition of the Comp. B is observed. When the Comp. B with a small void is driven by a weak charge of HMX powder (8 g of HMX instead of 16 g), there is less decomposition and this decomposition is possibly confined to the HMX powder alone.

Our small-hole computer runs (Figs. 28 and 29) did not show as much evidence of decomposition or detonation as did the runs with large holes (Figs. 26 and 27). Indeed in Fig. 29, with a weak piston, there was no evidence of decomposition. With a strong piston, as shown in Fig. 28, we did obtain a detonation wave computationally.

In contrast, the experimental data for the large air-filled hole shows clear evidence of a detonation in the sample of Comp. B, whether strongly driven or weakly driven (that is, with 16 g or with 8 g of HMX powder). Moreover, our computer modeling, as shown in Figs. 26 and 27, gives evidence of detonation with the large hole for both strong and weak pistons.

With a strong piston, hole closure occurs sooner with a smaller hole (as might be expected) and if detonation occurs, it comes at an earlier time. With a weak piston, collapse again occurs earlier with the smaller hole. Detonation is much more likely with the larger hole than with the smaller hole.

The numerical studies indicate that the essential features of the pipe test for Comp. B with a cavity can be reproduced by a hydrodynamic calculation with Forest Fire (the heterogeneous shock-initiation model), using independently

calibrated equations of state and burn rates. Assumed applied pressures in the range of 10 to 20 kbar will reproduce the observed sensitivity of the pipe-test experimental results to hole sizes of the order of 0.5- to 1.0-cm diameter.

The pipe test is primarily a shock initiation experiment. These calculations indicate that it is not examining the dominant mechanism of initiation associated either with premature initiation of shells or XDT (detonation induced by processes occurring after shock waves have dissipated). Shock initiation is not important for either process.

The pipe test is being supplanted by the "Popgun test," in which specimens are driven with small-arms-type gunpowder at less than pour density.

ACKNOWLEDGMENTS

The authors gratefully acknowledge the extensive contributions of B. G. Craig of M Division, LASL, and of Allen L. Bowman, Charles A. Forest, James D. Kershner, and Charles L. Mader, Group T-14, LASL. This work was partially supported by the AARADCOM in-bore premature study and the Joint Services Explosive Program.

REFERENCES

1. F. P. Bowden and A. D. Yoffe, Initiation and Growth of Explosions in Liquids and Solids (Cambridge University Press, London, 1952).

2. Arthur D. Little, Inc., "Development Standards for Cavities in Cast Loaded Artillery Projectiles," summary report for Picatinny Arsenal, Project WD5267-53, Task 4 (May 1955).

3. A. Popolato, "Quarterly Report for Joint Services Explosive Program, August 16 - November 30, 1973," Los Alamos Scientific Laboratory report LA-5521-PR (1974).

4. A. Popolato, "Quarterly Report for Joint Services Explosive Program, December 1973 - March 1974," Los Alamos Scientific Laboratory report LA-5616-PR (1974).

5. C. L. Mader and M. S. Shaw, "User's Manual for SIN," Los Alamos Scientific Laboratory report LA-7264-M (1978).

6. C. L. Mader, "The Two-Dimensional Hydrodynamic Hot Spot, Vol. III," Los Alamos Scientific Laboratory report LA-3450 (1966).

7. J. D. Kershner and C. L. Mader, "2DE: A Two-Dimensional Continuous Eulerian Hydrodynamic Code for Computing Multicomponent Reactive Hydrodynamic Problems," Los Alamos Scientific Laboratory report LA-4846 (1972).

8. C. L. Mader, Numerical Modeling of Detonations (University of California Press, Berkeley, 1979).

9. P. D. Lax, Hyperbolic Systems of Conservation Laws and the Mathematical Theory of Shock Waves, Regional Conference Series in Applied Mathematics, report No. 11 (NSF AND SIAM, 1975).

10. T. P. Liu, "Linear and Nonlinear Large-Time Behavior of Solutions of General Systems of Hyperbolic Conservation Laws," Comm. Pure & Appl. Math., Vol. XXX, 767-796 (1977).

11. A. Matsumura and T. Nishida, "The Initial Value Problem for the Equations of Motion of Compressible Viscous and Heat Conductive Fluids," to appear in Proc. Japanese Acad. Sci. (1980).

12. C. A. Forest, "Burning and Detonation," Los Alamos Scientific Laboratory report LA-7245 (1978).

13. C. L. Mader and C. A. Forest, "Two-Dimensional Homogeneous and Heterogeneous Detonation Wave Propagation," Los Alamos Scientific Laboratory report LA-6259 (1976).

APPENDIX A

MATERIAL CONSTANTS USED IN AQUARIUM COMPUTATIONS

1. High Explosives

PETN

C	2.33000000000E-01	J	-5.36251579151E+01
S	1.84200000000E+00	γ_s	7.70000000000E-01
F	-7.66189781324E+00	C_V	2.60000000000E-01
G	-7.95847702476E+01	V_0	6.45161290000E-01
H	-7.48636164900E+02	α	5.00000000000E-05
I	-1.65120245643E+02		

PBX-9404

C	2.42300000000E-01	J	-2.21893825727E+01
S	1.88300000000E+00	γ_s	6.75000000000E-01
F	-9.04187222042E+00	C_V	4.00000000000E-01
G	-7.13185252435E+01	V_0	5.42299349241E-01
H	-1.25204979360E+02	α	5.00000000000E-05
I	-9.20424177603E+01		

Comp. B, ρ = 1.20

C	3.77800000000E-03	H	3.33791363701E+02
S	2.87500000000E+00	I	4.25372330821E+02
VSW	5.49289043000E-01	J	2.07155716038E+02
C_1	6.00000000000E-02	γ_s	1.50000000000E+00
S_1	2.00000000000E+00	C_V	3.00000000000E-01
F	2.09371794800E+01	$V_\bullet$	8.33333333000E-01
G	1.16356102905E+02	α	5.00000000000E-05

Comp. B, ρ = 1.715

C	2.31000000000E-01	J	-3.91274655950E+01
S	1.83000000000E+00	γ_s	1.50000000000E+00
F	-8.86750780814E+00	C_V	2.59000000000E-01
G	-7.97357471516E+01	$V_\bullet$	5.83090379009E-01
H	-1.59428975952E+02	α	5.00000000000E-05
I	-1.35411036759E+02		

TNT

C	3.03300000000E-01	J	1.07753093582E+01
S	1.36600000000E+00	γ_s	1.73000000000E+00
F	1.14879244892E+01	C_V	2.93000000000E-01
G	2.94238153349E+01	$V_\bullet$	6.15763546798E-01
H	5.14078816020E+01	α	5.00000000000E-05
I	3.66668038080E+01		

2. Inert Component - Plexiglas

C	2.43200000000E-01	J	-1.46708193739E+01
S	1.57850000000E+00	γ_s	1.00000000000E+00
F	5.29380243506E+00	C_V	3.50000000000E-01
G	-4.24950371368E+00	$V_\bullet$	8.47457627000E-01
H	-1.55055576332E+01	α	1.00000000000E-04
I	-3.08638075572E+01		

3. Gaseous Components (tables and BKW EOS constants)

Air at 0.8 atm

A BKW ISENTROPE THRU BKW CJ PRESSURE FOR
AIR AT 300 DEG AND 0.8 ATMOS

LN(P)= -4.5525651463E+00 -9.1584491252E-01LNV -2.1288704554GE-01LNV*2 5.4146702954 7E-02LNV*3 -4.6651572500GE-03LNV*4

LN(T)= 6.1411219425E+00 1.0099419080 7E-01LNV -2.1837685705 4E-01LNV*2 5.4901424967 7E-02LNV*3 -4.7035249074 4F-03LNV*4

LN(E)= -1.6181507888E+00 8.5966902857 5E-02LNP 1.6688939090 5E-03LNP*2 -1.2702592247 2E-04LNP*3 -3.4388375401 0E-06LNP*4

THE CONSTANT ADDED TO ENERGIES WAS 1.00000000000E-01

PRESSURE (MBARS)	VOLUME (CC/GM)	TEMPERATURE (DEG K)	ENERGY+C (MB-CC/GM)	GAMMA (-DLNP/DLNV)	PARTICLE VELOCITY
8.00000000000E-07	1.0815173295 4E+03	3.00000000000E+02	1.02466882774E-01	2.32591914849E+00	0.
5.60000000000E-07	1.1290201562 5E+03	2.19223501685E+02	1.02430891041E-01	2.36452970559E+00	1.90897796072E-03
9.20000000000E-07	1.0449805095E+03	3.30000000000E+02	1.02499501554E-01	2.28588088991E+00	0.
1.05800000000E-06	9.8951909281 7E+02	3.63000000000E+02	1.02547327115E-01	2.24873831439E+00	0.
1.21670000000E-06	9.46497573210E+02	3.99300000000E+02	1.02613719229E-01	2.21147564728E+00	0.
1.39920500000E-06	8.85244045731E+02	4.29767728278E+02	1.02680435131E-01	2.15757892935E+00	0.
1.60908575000E-06	8.29913649874E+02	4.63026827840E+02	1.02764451190E-01	2.10636733569E+00	0.
1.85044861250E-06	7.74056618315E+02	4.96640930856E+02	1.02861002330E-01	2.05366475658E+00	0.
2.12801590437E-06	7.19130975066E+02	5.30608175595E+02	1.02970152435E-01	2.00020620725E+00	0.
2.44721628003E-06	6.65790726180E+02	5.64935981213E+02	1.03092031299E-01	1.94661948905E+00	0.
2.61430103354E-06	6.14510778130E+02	5.99635995324E+02	1.03226750680E-01	1.89342860904E+00	0.
3.23644618857E-06	5.65619603774E+02	6.34714379960E+02	1.03374468549E-01	1.84107132973E+00	0.
3.72191311685E-06	5.19329482298E+02	6.70181304868E+02	1.03535279719E-01	1.78991222854E+00	0.
4.28020008438E-06	4.75760937106E+02	7.06046470997E+02	1.03709328749E-01	1.74025420877E+00	0.
4.92223009704E-06	4.34962246450E+02	7.42319534779E+02	1.03896743615E-01	1.69234691395E+00	0.
5.66056461159E-06	3.96925987199E+02	7.79010791511E+02	1.04097678181E-01	1.64639421184E+00	0.
6.50964930333E-06	3.61602350786E+02	8.16130080185E+02	1.04312240392E-01	1.60256016044E+00	0.
7.48609569883E-06	3.28910010795E+02	8.53687730761E+02	1.04540605053E-01	1.56097403281E+00	0.
8.60901120385E-06	2.96744917064E+02	8.91694009580E+02	1.04782913506E-01	1.52173454962E+00	0.
9.90036288420E-06	2.70987367179E+02	9.30159165880E+02	1.05039315526E-01	1.48491347300E+00	0.
1.13854173168E-05	2.45507650367E+02	9.69093363518E+02	1.05309959179E-01	1.45055887437E+00	0.
1.30932299144E-05	2.22170511381E+02	1.00850874063E+03	1.05595035939E-01	1.41869577457E+00	0.
1.50572144015E-05	2.00838642150E+02	1.04840919000E+03	1.05894661770E-01	1.38933542117E+00	0.
1.73157965617E-05	1.81375375547E+02	1.08881049308E+03	1.06209077178E-01	1.36246525450E+00	0.
1.99131660460E-05	1.63646726871E+02	1.12972031838E+03	1.06538397193E-01	1.33806187679E+00	0.
2.29001409529E-05	1.47522905073E+02	1.17114615589E+03	1.06882821320E-01	1.31608625252E+00	0.
2.63351620958E-05	1.32879395320E+02	1.21310339762E+03	1.07242533435E-01	1.29648312095E+00	0.
3.02854364102E-05	1.19597697687E+02	1.25559537770E+03	1.07617721669E-01	1.27920509720E+00	0.
3.48262518717E-05	1.07565779221E+02	1.29863328410E+03	1.08008576871E-01	1.26416467628E+00	0.
4.00524896525E-05	9.66783838653E+01	1.34222668975E+03	1.08415298518E-01	1.25128498567E+00	0.
4.60603631004E-05	8.68359574264E+01	1.38638506551E+03	1.08838083742E-01	1.24047548262E+00	0.
5.29694175654E-05	7.79496188543E+01	1.43111796684E+03	1.09277133697E-01	1.23163770186E+00	0.
6.09148302002E-05	6.99318541610E+01	1.47643562828E+03	1.09732656053E-01	1.22466590334E+00	0.
7.00520547303E-05	6.27043335725E+01	1.52234908999E+03	1.10204864897E-01	1.21944756427E+00	0.
8.05598629398E-05	5.61946622576E+01	1.56886888029E+03	1.10693956439E-01	1.21586391872E+00	0.

9.26438423808E-05	5.33607192195E+01	1.61600699877E+03	1.11200177637E-01	1.21379340055E+00	0.
1.06540418738E-04	4.50672905623E+01	1.66377602865E+03	1.11723716123E-01	1.21309705622E+00	C
1.22521481549E-04	4.03322154515E+01	1.71218944971E+03	1.12264802169E-01	1.21364892424E+00	0.
1.40899703781E-04	3.60795729650E+01	1.76125175012E+03	1.12823658713E-01	1.21530538740E+00	0.
1.62034659348E-04	3.22625850320E+01	1.81100853767E+03	1.13400511434E-01	1.21792550232E+00	0.
1.86339856250E-04	2.88385488242E+01	1.86144665093E+03	1.13995588892E-01	1.22135631075E+00	0.
2.14290836988E-04	2.57690127176E+01	1.91259427061E+03	1.14609122718E-01	1.22545313616E+00	0.
2.46434462536E-04	2.30184858077E+01	1.96447103378E+03	1.15241347866E-01	1.23005486884E+00	0.
2.83399631916E-04	2.05551475332E+01	2.01709814827E+03	1.15892502920E-01	1.23530524232E+00	0.
3.25903957E704E-04	1.83500793127E+01	2.07049851562E+03	1.16562630455E-01	1.24014310359E+00	0.
3.74796013209E-04	1.63771116399E+01	2.12469698742E+03	1.17252577443E-01	1.24530467942E+00	0.
4.31015415191E-04	1.46125877051E+01	2.17971985133E+03	1.17981995711E-01	1.25032384098E+00	0.
4.95687727469E-04	1.30351433394E+01	2.23559627716E+03	1.18651342445E-01	1.25503236392E+00	0.
5.70017895590E-04	1.16255028635E+01	2.29235717543E+03	1.19440880729E-01	1.25926022016E+00	0.
6.55520569578E-04	1.03652902801E+01	2.35003602029E+03	1.20210880139E-01	1.26263580078E+00	0.
7.53848655015E-04	9.24185514959E+00	2.40865891264E+03	1.21001617408E-01	1.26558524325E+00	0.
8.66925953267E-04	6.23811205757E+00	2.46829469132E+03	1.21613375778E-01	1.26733769455E+00	0.
9.96954846257E-04	7.34235930819E+00	2.52894324899E+03	1.22645281407E-01	1.26791560920E+00	0.
1.14650957320E-03	6.54327979606E+00	2.59068068307E+03	1.23500921649E-01	1.26714499824E+00	0.
1.31848620918E-03	5.83061905895E+00	2.65354813744E+03	1.24377474738E-01	1.26485031448E+00	0.
1.51625891055E-03	5.19520291177E+00	2.71759232619E+03	1.25276269956E-01	1.26085958259E+00	0.
1.74368774713E-03	4.62880181744E+00	2.78287570762E+03	1.26197623788E-01	1.25499419480E+00	0.
2.00525240920E-03	4.12404015966E+00	2.84945806307E+03	1.27141891399E-01	1.24708451970E+00	0.
2.30604027059E-03	3.67430891388E+00	2.91740551988E+03	1.28109426742E-01	1.23695809039E+00	0.
2.65194631117E-03	3.27369053420E+00	2.98678965785E+03	1.29100601203E-01	1.22445262165E+00	0.
3.04973625785E-03	2.91688895909E+00	3.05768817691E+03	1.30115801575E-01	1.20837876335E+00	0.
3.50719899653E-03	2.59916663782E+00	3.13018493797E+03	1.31155431393E-01	1.19159420419E+00	0.
4.03327884600E-03	2.31628758280E+00	3.20437097172E+03	1.32219912287E-01	1.17093052245E+00	0.
4.63627067291E-03	2.06446593476E+00	3.28034492956E+03	1.33309685462E-01	1.14723106852E+00	0.
5.33401127384E-03	1.84031954978E+00	3.35821383521E+03	1.34425213319E-01	1.12034323163E+00	0.
6.13411296492E-03	1.64082815649E+00	3.43809388483E+03	1.35566981237E-01	1.09012011015E+00	0.
7.05422990965E-03	1.46329565022E+00	3.52011130746E+03	1.36735499529E-01	1.05642071939E+00	0.
8.11236439610E-03	1.30531622337E+00	3.60440332759E+03	1.37931305614E-01	1.01911086011E+00	0.
9.32921905552E-03	1.16474378170E+00	3.69111921469E+03	1.39154966428E-01	9.78063901469E-01	0.

Air at 1 atm

A BKW ISENTROPE THRU BKW CJ PRESSURE FOR
AIR AT 300 DEG AND 1.0 ATMOSPHERE

LN(P)= -4.50602542688E+00 -1.27546110628E+00_NV -3.74276600292E-03_NV*2 1.23929236747E-02_NV*3 -2.07694122929E-03_NV*4

LN(T)= 8.22644581441E+00 -2.51525130950E-01_NV -1.34446940047E-02_NV*2 1.40871016422E-02_NV*3 -2.16132189985E-03_NV*4

LN(E)= -1.62655447438E+00 9.05283146618E-02_NP 2.6900-997725E-03_NP*2 -5.43583122192E-05_NP*3 -1.58521895338E-06_NP*4

THE CONSTANT ADDED TO ENERGIES WAS 1.00000000000E-01

PRESSURE (MBARS)	VOLUME (CC/GM)	TEMPERATURE (DEG K)	ENERGY+C (MB-CC/GM)	GAMMA (-DLNP/DLNV)	PARTICLE VELOCITY
1.00000000000E-06	8.65224552363E+02	3.00000000000E+02	1.02456825065E-01	2.19540776989E+00	0.
1.15000000000E-06	8.27607307548E-02	3.30000000000E+02	1.02499504274E-01	2.16701624897E+00	0.
1.32250000000E-06	7.91625512157E+02	3.63000000000E+02	1.02547330335E-01	2.13913946424E+00	0.

1.52087500000E-06	7.57206061284E+02	3.99300000000E+02	1.02613723029E-01	2.11177309546E+00	0.
1.74900625000E-06	7.08684689338E+02	4.29767505734E+02	1.02680439055E-01	2.07193574851E+00	0.
2.01135718750E-06	6.63940115299E+02	4.63028530151E+02	1.02764465580E-01	2.03379379126E+00	0.
2.31306076562E-06	6.19254262585E+02	4.96640549020E+02	1.02851007218E-01	1.99421023513E+00	0.
2.66001988047E-06	5.75313293397E+02	5.30607699047E+02	1.02970157853E-01	1.95369706314E+00	0.
3.05902286254E-06	5.32641134784E+02	5.64936398126E+02	1.03092037264E-01	1.91268335454E+00	0.
3.51787629192E-06	4.91616990342E+02	5.99535290505E+02	1.03226767472E-01	1.87153263683E+00	0.
4.04555773571E-06	4.52503876949E+02	6.34713542268E+02	1.03374475794E-01	1.83055222115E+00	0.
4.65239139606E-06	4.15471616715E+02	6.70180315604E+02	1.03535267668E-01	1.79000198727E+00	0.
5.35025010547E-06	3.80616627258E+02	7.06045311259E+02	1.03709335459E-01	1.75010214890E+00	0.
6.15278762129E-06	3.47977530206E+02	7.42316283296E+02	1.03896753148E-01	1.71103904391E+00	0.
7.07570576449E-06	3.17546399192E+02	7.79009224336E+02	1.04097678247E-01	1.67296993300E+00	0.
8.13706162916E-06	2.89289347598E+02	8.16126270351E+02	1.04312251787E-01	1.63602702834E+00	0.
9.35762087354E-06	2.63135352612E+02	8.53625647913E+02	1.04540618524E-01	1.60032076194E+00	0.
1.07612640046E-05	2.39003160506E+02	8.91691619460E+02	1.04782927143E-01	1.56594253709E+00	0.
1.23754536053E-05	2.16797008817E+02	9.30156429955E+02	1.05039330443E-01	1.53296704939E+00	0.
1.42317716460E-05	1.96413128453E+02	9.69090259355E+02	1.05309985503E-01	1.50145425915E+00	0.
1.63665373929E-05	1.77743314798E+02	1.00250317728E+03	1.05595053812E-01	1.47145107822E+00	0.
1.88215180019E-05	1.60677721024E+02	1.04840512330E+03	1.05894701354E-01	1.44293262063E+00	0.
2.16447457022E-05	1.45107013094E+02	1.08880588082E+03	1.06209098653E-01	1.41610445623E+00	0.
2.48914575575E-05	1.30924002951E+02	1.12971508044E+03	1.06538420764E-01	1.39060169797E+00	0.
2.86251761911E-05	1.18024857491E+02	1.17114221324E+03	1.06882847216E-01	1.36709194804E+00	0.
3.29189526198E-05	1.06309964610E+02	1.21309666130E+03	1.07242561914E-01	1.34497512333E+00	0.
3.78567955128E-05	9.56845241457E+01	1.25556774664E+03	1.07617753021E-01	1.32444437762E+00	0.
4.35353148397E-05	8.60589105168E+01	1.29862465959E+03	1.08008611558E-01	1.30548671528E+00	0.
5.00656120656E-05	7.73489012682E+01	1.34221694157E+03	1.08415334896E-01	1.28806360491E+00	0.
5.75754538755E-05	6.94757007735E+01	1.38637405792E+03	1.08838125845E-01	1.27221138671E+00	0.
6.62117719568E-05	6.23659196663E+01	1.43110557645E+03	1.09277180474E-01	1.25784173768E+00	0.
7.61435377503E-05	5.59514786280E+01	1.47642188717E+03	1.09732709943E-01	1.24494209301E+00	0.
8.75650684128E-05	5.01693955119E+01	1.52233436465E+03	1.10204922562E-01	1.23347590318E+00	0.
1.00699828675E-04	4.49615949537E+01	1.56885134832E+03	1.10694030541E-01	1.22340298146E+00	0.
1.15804802976E-04	4.02746607252E+01	1.61598742261E+03	1.11200249250E-01	1.21467975874E+00	0.
1.33175523422E-04	3.60595769292E+01	1.66375425008E+03	1.11723796152E-01	1.20725952284E+00	0.
1.53151851936E-04	3.22714608784E+01	1.71216532667E+03	1.12264891770E-01	1.20109263469E+00	0.
1.76124629726E-04	2.88692936968E+01	1.76123516860E+03	1.12823759208E-01	1.19612672520E+00	0.
2.02543324185E-04	2.58156537171E+01	1.81097942414E+03	1.13400624332E-01	1.19230687567E+00	0.
2.32924822813E-04	2.30764562312E+01	1.86141498920E+03	1.13995715911E-01	1.18957578472E+00	0.
2.67863546235E-04	2.06207022463E+01	1.91256012036E+03	1.14609265808E-01	1.18787392381E+00	0.
3.08043078170E-04	1.84202380971E+01	1.96443455065E+03	1.15241509236E-01	1.18713968342E+00	0.
3.54249539895E-04	1.64495271428E+01	2.01705960814E+03	1.15892685054E-01	1.18730951169E+00	0.
4.07386970883E-04	1.46854342796E+01	2.07045633853E+03	1.16563038186E-01	1.18831804658E+00	0.
4.68495116512E-04	1.31070236209E+01	2.12465563451E+03	1.17252809931E-01	1.19009824498E+00	0.
5.38769268938E-04	1.16953594011E+01	2.17967837132E+03	1.17962252530E-01	1.19258150383E+00	0.
6.19584659337E-04	1.04333799402E+01	2.23555555426E+03	1.18691539525E-01	1.19569778434E+00	0.
7.12522356237E-04	9.30563433190E+00	2.29231847621E+03	1.19441215826E-01	1.19937573070E+00	0.
8.19400711973E-04	8.29883140738E+00	2.35000889715E+03	1.20211260314E-01	1.20354278937E+00	0.
9.42310818769E-04	7.39855043618E+00	2.40863919453E+03	1.21002047481E-01	1.20812532857E+00	0.
1.08365744158E-03	6.59552299409E+00	2.46627255104E+03	1.21813883725E-01	1.21304876058E+00	0.
1.24620605762E-03	5.87898871402E+00	2.52283210328E+03	1.22645594725E-01	1.21823767025E+00	0.
1.43313696549E-03	5.23969049191E+00	2.59058279187E+03	1.23501552015E-01	1.22361517448E+00	0.
1.64810751147E-03	4.66952605578E+00	2.65355460139E+03	1.24376203722E-01	1.22910712826E+00	0.
1.89532383519E-03	4.16115578848E+00	2.71763124576E+03	1.25277099555E-01	1.23463358252E+00	0.
2.17962218392E-03	3.70799551861E+00	2.78293900578E+03	1.26198570258E-01	1.24011805729E+00	0.
2.50655551151E-03	3.30414570469E+00	2.84955020250E+03	1.27142973345E-01	1.24548307216E+00	0.
2.88255033623E-03	2.94431762901E+00	2.91753130750E+03	1.28110664457E-01	1.25065092789E+00	0.
3.31493288297E-03	2.62377817460E+00	2.98695433895E+03	1.29102019295E-01	1.25554425077E+00	0.
3.81217262231E-03	2.33828993465E+00	3.05789718714E+03	1.30117428856E-01	1.26008602642E+00	0.
4.38399874566E-03	2.08406274284E+00	3.13044412527E+03	1.31157301654E-01	1.26419973181E+00	0.
5.04159855751E-03	1.85770810671E+00	3.20468639570E+03	1.32222065159E-01	1.26780964125E+00	0.

5.79783634113E-03	1.65619726525E+00	3.28072285253E+03	1.33312167434E-01	1.27084099704E+00	0.
6.66751409230E-03	1.47682453412E+00	3.35865057092E+03	1.34428178921E-01	1.27322025584E+00	0.
7.66764120615E-03	1.31717374709E+00	3.43981613014E+03	1.35570294423E-01	1.27467534152E+00	0.
8.81778738707E-03	1.17508207611E+00	3.52071547732E+03	1.36739335305E-01	1.27573591523E+00	0.
1.01404554951E-02	1.04864293793E+00	3.60509587876E+03	1.37935751935E-01	1.27573365233E+00	0.
1.16615238194E-02	9.36121520033E-01	3.69190646502E+03	1.39160126428E-01	1.27480259720E+00	0.
1.34107523923E-02	8.35932881582E-01	3.78130947457E+03	1.40413075725E-01	1.27267938334E+00	0.
1.54223652512E-02	7.46892243061E-01	3.87348149749E+03	1.41695255074E-01	1.26920356626E+00	0.
1.77357200389E-02	6.67603304340E-01	3.96861481662E+03	1.43007362002E-01	1.26591843003E+00	0.
2.03960780447E-02	5.97042384955E-01	4.06691883459E+03	1.44350140849E-01	1.26057033136E+00	0.
2.34554897513E-02	5.34244207214E-01	4.16862156537E+03	1.45724388024E-01	1.25411007574E+00	0.
2.69738132141E-02	4.78349159642E-01	4.27397114917E+03	1.47130956127E-01	1.24639275791E+00	0.
3.10198851962E-02	4.28591885520E-01	4.38323732492E+03	1.48570771167E-01	1.23737819875E+00	0.
3.56728679756E-02	3.84291082988E-01	4.49671275644E+03	1.50044621172E-01	1.22703125137E+00	0.
4.10237981719E-02	3.44840359626E-01	4.61471405536E+03	1.51554186600E-01	1.21532206203E+00	0.
4.71773678977E-02	3.09700067673E-01	4.73758227025E+03	1.53100043099E-01	1.20222526477E+00	0.
5.42539730824E-02	2.76389995137E-01	4.86566251101E+03	1.54683679357E-01	1.18772508355E+00	0.
6.23920690447E-02	2.50482837233E-01	4.99940224767E+03	1.56306517063E-01	1.17180530973E+00	0.
7.17508794014E-02	2.25598359916E-01	5.13914765993E+03	1.57970136288E-01	1.15445911595E+00	0.
8.25135113116E-02	2.03398190628E-01	5.28533721883E+03	1.59676307971E-01	1.13556356289E+00	0.
9.48905380084E-02	1.83581160559E-01	5.43839150027E+03	1.61427035580E-01	1.11548043647E+00	0.

Krypton at 0.8 atm

A BKW ISENTROPE THRU BKW CJ PRESSURE
KRYPTON

LN(P)= -3.92725236884E+00 -1.80380086133E+00LNV 3.10879484066E-02LNV*2 -3.22571683692E-03LNV*3 1.21868581087E-04LNV*4

LN(T)= 9.71007158008E+00 -6.92549922089E-01LNV 2.90442640168E-03LNV*2 2.75481541974E-04LNV*3 -5.22624844479E-05LNV*4

LN(E)= -1.49702754148E+00 2.28081098236E-01LNP 2.56870552217E-02LNP*2 1.34101905163E-03LNP*3 2.69963136745E-05LNP*4

THE CONSTANT ADDED TO ENERGIES WAS 1.00000000000E-01

PRESSURE (MBARS)	VOLUME (CC/GM)	TEMPERATURE (DEG K)	ENERGY+C (MB-CC/GM)	GAMMA (-DLNP/DLNV)	PARTICLE VELOCITY
8.00000000000E-07	3.73045946483E+02	3.00000000000E+02	1.00446648672E-01	1.67373221443E+00	0.
9.20000000000E-07	3.43472586358E+02	3.17589183957E+02	1.00472855379E-01	1.67364424847E+00	0.
1.05800000000E-06	3.15904926629E+02	3.35843302925E+02	1.00500057045E-01	1.67357097701E+00	0.
1.21670000000E-06	2.90550604146E+02	3.55143770074E+02	1.00528619620E-01	1.67351535057E+00	0.
1.39920500000E-06	2.67234432891E+02	3.75551702110E+02	1.00559237566E-01	1.67347908332E+00	0.
1.60908575000E-06	2.45792497030E+02	3.97131205544E+02	1.00591408334E-01	1.67345387862E+00	0.
1.85044861250E-06	2.26074046747E+02	4.19949363649E+02	1.00625426856E-01	1.67347143752E+00	0.
2.12801590437E-06	2.07940457130E+02	4.44077164358E+02	1.00661405911E-01	1.67350345860E+00	0.
2.44721829003E-06	1.91264261948E+02	4.69589516474E+02	1.00699456444E-01	1.67356163780E+00	0.
2.81430103354E-06	1.75926242950E+02	4.96565677690E+02	1.00739697945E-01	1.67364766917E+00	0.
3.23644618857E-06	1.61824613862E+02	5.25083395257E+02	1.00782256621E-01	1.67376323967E+00	0.
3.72191311685E-06	1.48854259579E+02	5.55249179967E+02	1.00827266805E-01	1.67391003887E+00	0.
4.28020008438E-06	1.36925038584E+02	5.87138574171E+02	1.00874859377E-01	1.67408974874E+00	0.
4.92223009704E-06	1.25956141472E+02	6.20856434580E+02	1.00925214223E-01	1.67430404830E+00	0.
5.66056461159E-06	1.15867501062E+02	6.56507230616E+02	1.00978459709E-01	1.67455461232E+00	0.

6.50964930333E-06	1.06589250060E+02	6.94201359148E+02	1.01034773395E-01	1.67484311101E+00	0.
7.48609659863E-06	9.80562220734E+01	7.34055476467E+02	1.01094332571E-01	1.67517120955E+00	0.
8.60931120365E-06	9.02084931344E+01	7.76192846390E+02	1.01157324825E-01	1.67554056616E+00	0.
9.90036288420E-06	8.29909598292E+01	8.20743719453E+02	1.01223948657E-01	1.67595284075E+00	0.
1.13854173168E-05	7.63529514741E+01	8.67845702153E+02	1.01294414106E-01	1.67640987542E+00	0.
1.30932299144E-05	7.02478734734E+01	9.17644187300E+02	1.01368934442E-01	1.67691271351E+00	0.
1.50572144015E-05	6.46328793704E+01	9.70292776532E+02	1.01447771862E-01	1.67746358919E+00	0.
1.73157965617E-05	5.94685692819E+01	1.02595373613E+03	1.01531148353E-01	1.67806392891E+00	0.
1.99131660460E-05	5.47187125956E+01	1.08479848734E+03	1.01619336307E-01	1.67871535083E+00	0.
2.29001409529E-05	5.03499929794E+01	1.14700809233E+03	1.01712614576E-01	1.67941946416E+00	0.
2.63351620958E-05	4.63317739058E+01	1.21277380729E+03	1.01811278285E-01	1.68017786855E+00	0.
3.02854364102E-05	4.26358830436E+01	1.28229763369E+03	1.01915639526E-01	1.68099215337E+00	0.
3.48262518717E-05	3.92364139975E+01	1.35579291149E+03	1.02026029876E-01	1.68186389695E+00	0.
4.00524896525E-05	3.61095440008E+01	1.43348494139E+03	1.02142798497E-01	1.68279465578E+00	0.
4.60603831004E-05	3.32333662775E+01	1.51561163995E+03	1.02266316286E-01	1.68378601371E+00	0.
5.29694175654E-05	3.05877358936E+01	1.60242422904E+03	1.02396975614E-01	1.68483948100E+00	0.
6.09148302002E-05	2.81541280119E+01	1.69418795125E+03	1.02535191925E-01	1.68595659343E+00	0.
7.00520547303E-05	2.59155075537E+01	1.79118289316E+03	1.02681405130E-01	1.68713886126E+00	0.
8.05598629398E-05	2.38562093473E+01	1.89370463617E+03	1.02836081082E-01	1.68839777823E+00	0.
9.26438423808E-05	2.19618279212E+01	2.00206531080E+03	1.02999713142E-01	1.68970482039E+00	0.
1.06540418738E-04	2.02191161653E+01	2.11659431454E+03	1.03172823855E-01	1.69109144497E+00	0.
1.22521481549E-04	1.86158921469E+01	2.23763932527E+03	1.03355966718E-01	1.69254906917E+00	0.
1.40899703781E-04	1.71409534238E+01	2.36556726246E+03	1.03549728077E-01	1.69407916885E+00	0.
1.62034659348E-04	1.57839962534E+01	2.50076532039E+03	1.03754729132E-01	1.69569307724E+00	0.
1.86339858250E-04	1.45355531406E+01	2.64364205189E+03	1.03971628085E-01	1.69736218344E+00	0.
2.14290836988E-04	1.33869062165E+01	2.79462850706E+03	1.04201122417E-01	1.69911783107E+00	0.
2.46434462536E-04	1.23300459765E+01	2.95417942964E+03	1.04443951324E-01	1.70095133672E+00	0.
2.83399631916E-04	1.13576049483E+01	3.12277451379E+03	1.04700898309E-01	1.70286398835E+00	0.
3.25909576704E-04	1.04628078922E+01	3.30091972436E+03	1.04972793943E-01	1.70485704369E+00	0.
3.74796013209E-04	9.63942416868E+00	3.48914868358E+03	1.05260518625E-01	1.70693172857E+00	0.
4.31015415191E-04	8.86172393866E+00	3.68802412769E+03	1.05565008723E-01	1.70908235166E+00	0.
4.95657727469E-04	8.18443788776E+00	3.89813943681E+03	1.05887247942E-01	1.71133072025E+00	0.
5.70017885905E-04	7.54272019009E+00	4.12012024183E+03	1.06226252916E-01	1.71365730339E+00	0.
6.55520569578E-04	6.95211445217E+00	4.35462611216E+03	1.06583256056E-01	1.71607005509E+00	0.
7.53848555015E-04	6.40852239335E+00	4.60235232677E+03	1.06971319851E-01	1.71857004495E+00	0.
8.66925953267E-04	5.90817504552E+00	4.86403173015E+03	1.07375739272E-01	1.72115623978E+00	0.
9.96964846257E-04	5.44760625878E+00	5.14043667424E+03	1.07803945484E-01	1.72383560185E+00	0.
1.14650957320E-03	5.02362832185E+00	5.43238101872E+03	1.08257055904E-01	1.72660303725E+00	0.
1.31848600918E-03	4.63330950750E+00	5.74072215645E+03	1.08735959563E-01	1.72946140475E+00	0.
1.51625891055E-03	4.27395335648E+00	6.06636294613E+03	1.09244883544E-01	1.73241151560E+00	0.
1.74369774713E-03	3.94307951078E+00	6.41025333975E+03	1.09762793581E-01	1.73545413546E+00	0.
2.00525240920E-03	3.63840590024E+00	6.77339121625E+03	1.10352403591E-01	1.73858999022E+00	0.
2.30604027056E-03	3.35783208290E+00	7.15682167784E+03	1.10955634209E-01	1.74181977910E+00	0.
2.65194631117E-03	3.09942354466E+00	7.56163336529E+03	1.11594534329E-01	1.74514419985E+00	0.
3.04973625785E-03	2.86139679054E+00	7.98894955069E+03	1.12271296424E-01	1.74856399351E+00	0.
3.50719899553E-03	2.64210511934E+00	8.43991146035E+03	1.12986277870E-01	1.75208001803E+00	0.
4.03327884600E-03	2.44002507238E+00	8.91564736295E+03	1.13748031113E-01	1.75569336228E+00	0.
4.63827067291E-03	2.25374370454E+00	9.41722549256E+03	1.14553345964E-01	1.75940551108E+00	0.
5.33401127384E-03	2.08194702062E+00	9.94558160362E+03	1.15407307024E-01	1.76321856855E+00	0.
6.13411296492E-03	1.92341015357E+00	1.05014186361E+04	1.16313367541E-01	1.76713553670E+00	0.
7.05422990965E-03	1.77699007172E+00	1.10850788635E+04	1.17275436922E-01	1.77116062805E+00	0.
8.11236439610E-03	1.64162169272E+00	1.16963923367E+04	1.18297372195E-01	1.77529956424E+00	0.
9.32921905552E-03	1.51631809033E+00	1.23345280695E+04	1.19386054254E-01	1.77955978169E+00	0.

Krypton at 1 atm

A BKW ISENTROPE THRU BKW CJ PRESSURE FOR
KRYPTON

LN(P)= -4.05257022050E+00 -1.8223300954SE+00LNV 3.755151017SSE-02LNV**2 -4.28688758021E-03LNV**3 1.8651299425SE-04LNV**4

LN(T)= 9.57198275156E+00 -7.0339456263SE-01LNV 7.351364872ISE-03LNV**2 -5.0607561254IE-04LNV**3 -4.3169500736ZE-06LNV**4

LN(E)= -1.55030603429E+00 2.14639300971E-01LNP 2.43869208430E-02LNP**2 1.28563060752E-03LNP**3 2.61585496917E-05LNP**4

THE CONSTANT ADDED TO ENERGIES WAS 1.000000000000E-01

PRESSURE (MBARS)	VOLUME (CC/GM)	TEMPERATURE (DEG K)	ENERGY+C (MB-CC/GM)	GAMMA (-DLNP/DLNV)	PARTICLE VELOCITY
1.000000000000E-06	2.988326073896E+02	3.000000000000E+02	1.004466908396E-01	1.673923158465E+00	0.
1.150000000000E-06	2.749698053205E+02	3.175872815736E+02	1.004729011770E-01	1.674021256316E+00	0.
1.322500000000E-06	2.529116620226E+02	3.358396909026E+02	1.005001083816E-01	1.674130435916E+00	0.
1.520875000000E-06	2.326242587016E+02	3.551367636606E+02	1.005286765496E-01	1.674243407606E+00	0.
1.749006250000E-06	2.139674432316E+02	3.755413480946E+02	1.005593008196E-01	1.674365641096E+00	0.
2.011357187506E-06	1.968100765326E+02	3.971168633386E+02	1.005914767476E-01	1.674495744626E+00	0.
2.313060765626E-06	1.810315553726E+02	4.199303132086E+02	1.006255053816E-01	1.674648322946E+00	0.
2.660019880476E-06	1.665209788056E+02	4.440525125566E+02	1.006614936246E-01	1.674813976936E+00	0.
3.059022862546E-06	1.531763682796E+02	4.695563018106E+02	1.006995545776E-01	1.674999303306E+00	0.
3.517876291926E-06	1.409039486956E+02	4.965267731416E+02	1.007398078946E-01	1.675206894186E+00	0.
4.045557735716E-06	1.296174896926E+02	5.250415090616E+02	1.007823801766E-01	1.675439336806E+00	0.
4.652338396056E-06	1.192376963146E+02	5.551908341266E+02	1.008274053666E-01	1.675699821996E+00	0.
5.350250105476E-06	1.096916604766E+02	5.870680804196E+02	1.008750251906E-01	1.675989098806E+00	0.
6.152876821296E-06	1.009123281446E+02	6.207718675326E+02	1.009253895086E-01	1.676311564046E+00	0.
7.075705764496E-06	9.283804729056E+01	6.564063978216E+02	1.009785572966E-01	1.676669171686E+00	0.
8.137061629166E-06	8.541212391606E+01	6.940817676936E+02	1.010349961636E-01	1.677064477396E+00	0.
9.357620673546E-06	7.856242497826E+01	7.339142957806E+02	1.010945838946E-01	1.677500028916E+00	0.
1.076126430466E-05	7.230101142466E+01	7.760268686396E+02	1.011576085236E-01	1.677978365426E+00	0.
1.237545360536E-05	6.652380074566E+01	8.205493063036E+02	1.012242690466E-01	1.678502016876E+00	0.
1.423177164606E-05	6.121025667476E+01	8.676187444146E+02	1.012947760706E-01	1.679073503256E+00	0.
1.636653739296E-05	5.632310385296E+01	9.173800409196E+02	1.013693529886E-01	1.679695333836E+00	0.
1.882151800196E-05	5.182806545016E+01	9.699862013826E+02	1.014482346266E-01	1.680370006316E+00	0.
2.164474570226E-05	4.769362189616E+01	1.025598628166E+03	1.015316710946E-01	1.681100005956E+00	0.
2.489145755756E-05	4.389078902436E+01	1.084388593196E+03	1.016199273486E-01	1.681867804626E+00	0.
2.862517619116E-05	4.039291406756E+01	1.146535735756E+03	1.017132828746E-01	1.682735859636E+00	0.
3.291895261986E-05	3.717548806726E+01	1.212230586416E+03	1.018120339406E-01	1.683646613616E+00	0.
3.785679551286E-05	3.421597338006E+01	1.281674118516E+03	1.019164942206E-01	1.684622495396E+00	0.
4.353531483976E-05	3.149364506266E+01	1.355078528386E+03	1.020269956396E-01	1.685665900846E+00	0.
5.006561206566E-05	2.898944502186E+01	1.432667845826E+03	1.021438904776E-01	1.686779230536E+00	0.
5.757545387556E-05	2.668584790126E+01	1.514678576296E+03	1.022675505566E-01	1.687969484866E+00	0.
6.621177195686E-05	2.456673776056E+01	1.601360376226E+03	1.023983704946E-01	1.689225101416E+00	0.
7.614353775036E-05	2.261729467886E+01	1.692976763146E+03	1.025367680336E-01	1.690562311866E+00	0.
8.756506841286E-05	2.082389048406E+01	1.789805862336E+03	1.026831856676E-01	1.691978777986E+00	0.
1.006996286756E-04	1.917399287296E+01	1.892141191596E+03	1.028380921476E-01	1.693476771186E+00	0.
1.158048029766E-04	1.765607724726E+01	2.000292486076E+03	1.030019840936E-01	1.695058534496E+00	0.
1.331755234226E-04	1.625954564546E+01	2.114586555126E+03	1.031753677016E-01	1.696726280756E+00	0.
1.531518519366E-04	1.497465219746E+01	2.235368243066E+03	1.033589605766E-01	1.698482190706E+00	0.
1.761246297266E-04	1.379243457916E+01	2.363001286046E+03	1.035529936876E-01	1.700328410956E+00	0.

2.025433241 85E-04	1.27046509820E+01	2.497869417 30E+03	1.037584133 47E-01	1.702267051 92E+00	0.
2.329248228 13E-04	1.17037221559E+01	2.640377373 06E+03	1.039757836 18E-01	1.704300185 66E+00	0.
2.678635462 35E-04	1.07826781149E+01	2.790952011 69E+03	1.042058084 78E-01	1.706429843 63E+00	0.
3.080430761 70E-04	9.93510913169E+00	2.950043478 62E+03	1.044492344 28E-01	1.708658014 36E+00	0.
3.542495390 95E-04	9.15512067585E+00	3.118126430 00E+03	1.047068531 73E-01	1.710986641 09E+00	0.
4.073869708 80E-04	8.43729197734E+00	3.295701317 91E+03	1.049795044 86E-01	1.713417619 29E+00	0.
4.684950165 25E-04	7.77663792480E+00	3.483295740 87E+03	1.052683792 68E-01	1.715952794 19E+00	0.
5.387692689 89E-04	7.16857402786E+00	3.681465850 52E+03	1.055735229 18E-01	1.718593959 19E+00	0.
6.195846593 77E-04	6.60888420147E+00	3.890797894 59E+03	1.058968386 73E-01	1.721342846 29E+00	0.
7.125223582 37E-04	6.09368139333E+00	4.111909680 32E+03	1.062390915 49E-01	1.724201143 44E+00	0.
8.194007119 73E-04	5.61942907180E+00	4.345452321 04E+03	1.066014122 80E-01	1.727170481 89E+00	0.
9.423108187 69E-04	5.18281671429E+00	4.592111914 62E+03	1.069950016 61E-01	1.730252358 56E+00	0.
1.083657441 58E-03	4.78084422067E+00	4.852611367 39E+03	1.073511351 75E-01	1.733448322 52E+00	0.
1.246206057 82E-03	4.41073203073E+00	5.127712290 44E+03	1.076211679 76E-01	1.736759774 27E+00	0.
1.433136966 49E-03	4.06993129190E+00	5.418216963 44E+03	1.082765402 35E-01	1.740188063 75E+00	0.
1.648107511 47E-03	3.75609597632E+00	5.724970323 17E+03	1.087567629 31E-01	1.743734468 53E+00	0.
1.895323638 19E-03	3.46706628643E+00	6.048851874 64E+03	1.092695241 02E-01	1.747400193 41E+00	0.
2.179622183 92E-03	3.20086332073E+00	6.390827307 33E+03	1.098104959 12E-01	1.751186372 48E+00	0.
2.506565511 51E-03	2.95565486240E+00	6.751843935 55E+03	1.103835429 51E-01	1.755094075 86E+00	0.
2.882550336 23E-03	2.72976206990E+00	7.132957389 58E+03	1.109906294 03E-01	1.759124325 14E+00	0.
3.314932888 97E-03	2.52163695560E+00	7.535223626 31E+03	1.116338551 5E-01	1.763276123 8E+00	0.
3.812172622 31E-03	2.32985252420E+00	7.959755531 01E+03	1.123154580 40E-01	1.767555507 24E+00	0.
4.383996745 65E-03	2.15305145071E+00	8.407677698 65E+03	1.130378848 66E-01	1.771960636 50E+00	0.
5.041598557 51E-03	1.99013532080E+00	8.880106579 32E+03	1.138037234 06E-01	1.776495192 67E+00	0.
5.797836341 13E-03	1.83985451537E+00	9.378101257 98E+03	1.146158426 40E-01	1.781152254 17E+00	0.
6.667514092 30E-03	1.70119899962E+00	9.902595963 23E+03	1.154773992 7E-01	1.785944208 67E+00	0.
7.667641206 5E-03	1.57319044390E+00	1.045430311 41E+04	1.163919197 52E-01	1.790871443 62E+00	0.
8.817787387 07E-03	1.45491626697E+00	1.103358845 91E+04	1.173633868 94E-01	1.795939048 07E+00	0.

Methane at 0.8 atm

A BKW ISENTROPE THRU BKW CJ PRESSURE FOR METHANE

LN(P = -1.353291312 97E+00 -3.089145246 89E+00LNV 3.862245299 64E-01LNV**2 -3.251269624 74E-02LNV**3 8.173336651 37E-04LNV**4

LN(T)= 7.554961056 56E+00 -3.701180323 68E-01LNV 3.226335085 28E-02LNV**2 9.474419952 79E-04LNV**3 -3.975230783 78E-04LNV**4

LN(E = -1.032328623 38E+00 3.277135853 18E-01LNP 3.861672864 46E-02LNP**2 2.255015397 60E-03LNP**3 5.138445974 43E-05LNP**4

THE CONSTANT ADDED TO ENERGIES WAS 1.000000000000E-01

PRESSURE (MBARS)	VOLUME (CC/GM)	TEMPERATURE (DEG K)	ENERGY+C (MB-CC/GM)	GAMMA (-DLNP/DLNV)	PARTICLE VELOCITY
6.000000000000E-07	1.957230523 02E+03	3.000000000000E+02	1.037741230 94E-01	1.414207870 75E+00	0.
9.200000000000E-07	1.775627557 11E+03	3.127726590 25E+02	1.039294559 62E-01	1.400538884 11E+00	0.
1.058000000000E-06	1.680831294 648E+03	3.255380604 47E+02	1.040940941 15E-01	1.387115970 80E+00	0.
1.216700000000E-06	1.454556638 48E+03	3.382715309 23E+02	1.042679816 42E-01	1.373991054 84E+00	0.
1.399205000000E-06	1.313634132 59E+03	3.509573440 2E+02	1.044511585 20E-01	1.361219413 36E+00	0.
1.609085750000E-06	1.184794231 67E+03	3.635800277 500E+02	1.046436560 18E-01	1.348855938 11E+00	0.
1.850448612 50E-06	1.067276370 79E+03	3.762737301 66E+02	1.048549454 1E-01	1.336955274 54E+00	0.
2.128015904 37E-06	9.603230365 98E+02	3.885890304 42E+02	1.050566821 69E-01	1.325571764 24E+00	0.

2.447218290036-06	8.631889365456+02	4.009580265626+02	1.052772142066-01	1.314759254196+00	0.
2.814301037546-06	7.751476499186+02	4.132306526736+02	1.055507073086-01	1.304570812096+00	0.
3.236446188576-06	6.954971696946+02	4.254065997086+02	1.057462336246-01	1.295058402146+00	0.
3.721931116856-06	6.235637184276+02	4.374862765716+02	1.059946582376-01	1.286272560546+00	0.
4.280200083866-06	5.587051146386+02	4.494806259806+02	1.062523071456-01	1.278262057226+00	0.
4.922302097046-06	5.003131695356+02	4.613914557876+02	1.065191380016-01	1.271073836906+00	0.
5.660564611596-06	4.478153676946+02	4.732290159266+02	1.067951098536-01	1.264752401896+00	0.
6.509549303336-06	4.006758399556+02	4.850035549416+02	1.070801862056-01	1.259340031596+00	0.
7.486096698836-06	3.583956857236+02	4.967259254346+02	1.073743377926-01	1.254876430116+00	0.
8.603013203656-06	3.205126992706+02	5.084074481776+02	1.076775450006-01	1.251398632096+00	0.
9.900362884206-06	2.866005979646+02	5.200596373186+02	1.079897999656-01	1.248940877566+00	0.
1.138546173168E-05	2.562678363586+02	5.316939938246+02	1.083111083766-01	1.247534488406+00	0.
1.309322951446-05	2.291561050546+02	5.433217914166+02	1.086411491056-01	1.247207741236+00	0.
1.505721442156-05	2.049385868316+02	5.549540580506+02	1.089803985426-01	1.247985733926+00	0.
1.731579656176-05	1.833180861056+02	5.666013959326+02	1.093296468776-01	1.249890245536+00	0.
1.991316604606-05	1.640250529516+02	5.782739836836+02	1.096875502026-01	1.252939590926+00	0.
2.290014095296-05	1.468155912686+02	5.899815459016+02	1.100547911376-01	1.257148477056+00	0.
2.633516209586-05	1.314694828686+02	6.017333499186+02	1.104314880626-01	1.262527845376+00	0.
3.028546361026-05	1.177882635386+02	6.135383312226+02	1.108177839456-01	1.269067699956+00	0.
3.482625187176-05	1.055933759416+02	6.254046295806+02	1.112138485816-01	1.276822314116+00	0.
4.005248965256-05	9.472445202886+01	6.373408539666+02	1.116198903246-01	1.285739426226+00	0.
4.606036310046-05	8.503716567396+01	6.493543292956+02	1.120361265246-01	1.295831426106+00	0.
5.296941756546-05	7.640328125456+01	6.614527838906+02	1.124628304776-01	1.307088337976+00	0.
6.091483020026-05	6.870710486096+01	6.736436541956+02	1.129003094216-01	1.319497062976+00	0.
7.005205473036-05	6.184547750396+01	6.859343142436+02	1.133489139646-01	1.333040223086+00	0.
8.055986293986-05	5.572626437346+01	6.983321715146+02	1.138090428856-01	1.347696603616+00	0.
9.264384238086-05	5.026725195656+01	7.108447622196+02	1.142811480796-01	1.363441374656+00	0.
1.065404187386-04	4.539514379006+01	7.234798485996+02	1.147657398676-01	1.380246370316+00	0.
1.225214815496-04	4.104467557746+01	7.362455164446+02	1.152633926496-01	1.398080421546+00	0.
1.408997037816-04	3.715764713206+01	7.491502708456+02	1.157747508666-01	1.416909734866+00	0.
1.620346593486-04	3.368245299496+01	7.622032818866+02	1.163005352666-01	1.436698306836+00	0.
1.863398582506-04	3.057306968466+01	7.754121350116+02	1.168414757786-01	1.457408758056+00	0.
2.142908369886-04	2.778679566046+01	7.887902232566+02	1.173985886966-01	1.479001334136+00	0.
3.259095767046-04	2.104417260076+01	8.300463168796+02	1.191770578626-01	1.548672084126+00	0.
3.747960132096-04	1.823667326826+01	8.442145622566+02	1.198096134356-01	1.573398277766+00	0.
4.310154151916-04	1.760979054946+01	8.586143065556+02	1.204643513096-01	1.598794584596+00	0.
4.956677274696-04	1.614371475306+01	8.732509800256+02	1.211428532746-01	1.624840564336+00	0.
5.700178865906-04	1.482093353866+01	8.881709565956+02	1.218468542886-01	1.651492988596+00	0.
6.555205695786-04	1.362568373526+01	9.033615488766+02	1.225783141856-01	1.678716027176+00	0.
7.538486550156-04	1.254472497146+01	9.188514548456+02	1.233392420356-01	1.706475239946+00	0.
8.669259532676-04	1.156541774926+01	9.346590377816+02	1.241316776776-01	1.734736381246+00	0.
9.969648462576-04	1.067708615336+01	9.508046350786+02	1.249586809636-01	1.763475219386+00	0.
1.146509573226-03	9.870822930556+00	9.673089656356+02	1.258223159796-01	1.792655121116+00	0.
1.318486009186-03	9.136320304796+00	9.841936962066+02	1.267255678536-01	1.822251466246+00	0.
1.516258910556-03	8.467859140046+00	1.001481369736+03	1.276716722356-01	1.852238696316+00	0.
1.743697747136-03	7.858162832936+00	1.019194312156+03	1.286563332486-01	1.882592978546+00	0.
2.005252409206-03	7.301300125376+00	1.037356018816+03	1.296867474656-01	1.913292176436+00	0.
2.306040270586-03	6.791957474276+00	1.055950116336+03	1.307631286356-01	1.944315789146+00	0.
2.651946311176-03	6.325561878816+00	1.075126395006+03	1.318957837636-01	1.975644895816+00	0.
3.049738257856-03	5.897612952716+00	1.094770606086+03	1.331756017086-01	2.007262074326+00	0.
3.507198996536-03	5.505017295806+00	1.114961721706+03	1.344614376456-01	2.039151836306+00	0.
4.033278846006-03	5.143859085016+00	1.135721095096+03	1.356211761866-01	2.071298647726+00	0.
4.638270672916-03	4.811359927276+00	1.157068653746+03	1.372507923156-01	2.103689524326+00	0.
5.334011273946-03	4.504860505986+00	1.179025014976+03	1.387868914496-01	2.136312878536+00	0.
6.134112964926-03	4.221979557016+00	1.201608967836+03	1.404066665956-01	2.169155742486+00	0.
7.054229909656-03	3.960582570916+00	1.224836902646+03	1.421279394546-01	2.202209878326+00	0.
8.112364396106-03	3.718755078136+00	1.248722846556+03	1.439592557756-01	2.235464513126+00	0.
9.329219055526-03	3.494775387926+00	1.273275055306+03	1.459097934176-01	2.268911599866+00	0.

Methane at 1 atm

A BKW ISENTROPE THRU BKW CJ PRESSURE FOR
METHANE

LN(P)= -1.3480475027E+00 -3.1086245934IE+00LNV 3.89987909030E-01LNV*2 -3.26767046710E-02LNV*3 7.87663653538E-04LNV*4

LN(T)= 7.5444859773TE+00 -3.8027168664E-01LNV 3.49428361021E-02LNV*2 7.40392155830E-04LNV*3 -4.19446909634E-04LNV*4

LN(E)= -1.03910951791E+00 3.46100212142E-01LNP 4.10998577720E-02LNP*2 2.41893084613E-03LNP*3 5.56277645329E-05LNP*4

THE CONSTANT ADDED TO ENERGIES WAS 1.00000000000E-01

PRESSURE (MBARS)	VOLUME (CC/GM)	TEMPERATURE (DEG K)	ENERGY+C (MB-CC/GM)	GAMMA (-DLNP/DLNV)	PARTICLE VELOCITY
1.00000000000E-06	1.56845071364E+03	3.00000000000E+02	9.74886529222E-02	1.42179066013E+00	0.
1.15000000000E-06	1.42321096034E+03	3.12789686434E+02	9.76440569013E-02	1.40739994785E+00	0.
1.32250000000E-06	1.28939003283E+03	3.25574640005E+02	9.78087075540E-02	1.39334512054E+00	0.
1.52087500000E-06	1.16642113193E+03	3.38335249688E+02	9.79626021735E-02	1.37968432107E+00	0.
1.74900625000E-06	1.05372268912E+03	3.51057040188E+02	9.81657845272E-02	1.36647685574E+00	0.
2.01135718750E-06	9.50690463249E+02	3.63726154567E+02	9.83592881623E-02	1.35378091814E+00	0.
2.31306076562E-06	8.56712752565E+02	3.76330400753E+02	9.85501371580E-02	1.34165385572E+00	0.
2.66001988047E-06	7.71180643517E+02	3.88859914984E+02	9.87713447508E-02	1.33015213588E+00	0.
3.05902286254E-06	6.93495577092E+02	4.01307606145E+02	9.89919128449E-02	1.31933118076E+00	0.
3.51787629192E-06	6.23074918561E+02	4.13669360682E+02	9.92218324932E-02	1.30924510290E+00	0.
4.04555773571E-06	5.59356171129E+02	4.25944025161E+02	9.94610853057E-02	1.29994639595E+00	0.
4.65239139606E-06	5.01800199141E+02	4.38133209332E+02	9.97096456272E-02	1.29148561833E+00	0.
5.35025010547E-06	4.49893677769E+02	4.50240964509E+02	9.99674832628E-02	1.28391109642E+00	0.
6.15276762129E-06	4.03150884028E+02	4.62273392002E+02	1.00234566508E-01	1.27726866119E+00	0.
7.07570576449E-06	3.61114893882E+02	4.74238228483E+02	1.00510865262E-01	1.27160142193E+00	0.
8.13706162916E-06	3.23356231947E+02	4.86144443489E+02	1.00796354049E-01	1.26694957367E+00	0.
9.35762087354E-06	2.89463021988E+02	4.98001672345E+02	1.01091014848E-01	1.26335023116E+00	0.
1.07612640046E-05	2.59120694842E+02	5.09820837455E+02	1.01394839554E-01	1.26083728097E+00	0.
1.23754536053E-05	2.31931318817E+02	5.21612162985E+02	1.01707832805E-01	1.25944124403E+00	0.
1.42317716460E-05	2.07602625078E+02	5.33386462592E+02	1.02030013073E-01	1.25918314282E+00	0.
1.63665373929E-05	1.85848782181E+02	5.45154376638E+02	1.02361415611E-01	1.26010436952E+00	0.
1.86215180019E-05	1.66409023345E+02	5.56926353605E+02	1.02702093807E-01	1.26220655472E+00	0.
2.16447457022E-05	1.49046136234E+02	5.68712530040E+02	1.03052121146E-01	1.26551143719E+00	0.
2.489.4575575E-05	1.33544914713E+02	5.80522703427E+02	1.03411593134E-01	1.27003073933E+00	0.
2.86251761911E-05	1.19710559928E+02	5.92366312988E+02	1.03780629380E-01	1.27577205348E+00	0.
3.29189526198E-05	1.07367136732E+02	6.04252444058E+02	1.04159375885E-01	1.28273874605E+00	0.
3.78567955128E-05	9.63560414581E+01	6.16189852290E+02	1.04548007598E-01	1.29092988765E+00	0.
4.35353148397E-05	8.65345739606E+01	6.28187235594E+02	1.04946740006E-01	1.30034018305E+00	0.
5.00656120656E-05	7.77744300369E+01	6.40252461511E+02	1.05355801346E-01	1.31096009625E+00	0.
5.75754538755E-05	6.99602066758E+01	6.52393757793E+02	1.05775478114E-01	1.32277635140E+00	0.
6.62117719568E-05	6.29894468145E+01	6.64619114862E+02	1.06206093675E-01	1.33576999217E+00	0.
7.61435377503E-05	5.67695622816E+01	6.76935514807E+02	1.06648018494E-01	1.34991944945E+00	0.
8.75650684128E-05	5.12180505036E+01	6.89354025597E+02	1.07101674671E-01	1.36519899174E+00	0.
1.00699828575E-04	4.62612320482E+01	7.01879894355E+02	1.07567541102E-01	1.38157942634E+00	0.
1.15804802976E-04	4.18333721434E+01	7.14522641634E+02	1.08046158885E-01	1.39902844335E+00	0.
1.33175523422E-04	3.78758788593E+01	7.27291154654E+02	1.08538137039E-01	1.41751100607E+00	0.
1.53151851936E-04	3.43365731325E+01	7.40194777405E+02	1.09044158505E-01	1.43698977784E+00	0.
1.76124629726E-04	3.11690256372E+01	7.53243395650E+02	1.09564986424E-01	1.45742557360E+00	0.

2.02543324185E-04	2.83319083769E+01	7.66446021862E+02	1.10101402831E-01	1.47877820594E+00	0.
2.32924822813E-04	2.57886319230E+01	7.79816370404E+02	1.10654464564E-01	1.50100554310E+00	0.
2.67863546235E-04	2.35065922649E+01	7.93365280080E+02	1.11225165987E-01	1.52406589535E+00	0.
3.08043078170E-04	2.14568925872E+01	8.07105452627E+02	1.11814657091E-01	1.54791725407E+00	0.
3.54249539895E-04	1.96139051439E+01	8.21050451663E+02	1.12424204898E-01	1.57251794155E+00	0.
4.07386970860E-04	1.79549105647E+01	8.35214707800E+02	1.13055200480E-01	1.59782696394E+00	0.
4.68493116512E-04	1.64597745039E+01	8.49613538092E+02	1.13709167874E-01	1.62360431194E+00	0.
5.38759268988E-04	1.51106576590E+01	8.64263143586E+02	1.14387773567E-01	1.65041121273E+00	0.
6.19584659337E-04	1.38917561465E+01	8.79180628510E+02	1.15092939766E-01	1.67761033320E+00	0.
7.12522356237E-04	1.27890594649E+01	8.94363957410E+02	1.15626340587E-01	1.70536593549E+00	0.
8.19400771973E-04	1.17901973833E+01	9.09892417421E+02	1.16590467069E-01	1.73364387790E+00	0.
9.42310618769E-04	1.08841406222E+01	9.25724893293E+02	1.17387527116E-01	1.76241211121E+00	0.
1.08365744156E-03	1.00611584177E+01	9.41902137526E+02	1.18220090824E-01	1.79164012731E+00	0.
1.24620625762E-03	9.31259419463E+00	9.58445311278E+02	1.19090927901E-01	1.82130039202E+00	0.
1.43313696649E-03	8.63079797787E+00	9.75376210198E+02	1.20003059033E-01	1.85136427500E+00	0.
1.64810751147E-03	8.00895928408E+00	9.92717197657E+02	1.20959752569E-01	1.88180764977E+00	0.
1.89532363819E-03	7.44104903924E+00	1.01049109743E+03	1.21964560972E-01	1.91260728976E+00	0.
2.17962218352E-03	6.92165810511E+00	1.02672106716E+03	1.23021341839E-01	1.94374165778E+00	0.
2.50656551151E-03	6.44600888115E+00	1.04743044509E+03	1.24134284777E-01	1.97519084184E+00	0.
2.88255033623E-03	6.00983813447E+00	1.06664258506E+03	1.25307941006E-01	2.00693648458E+00	0.
3.31493288897E-03	5.60933640983E+00	1.08638053355E+03	1.26547255911E-01	2.03896170786E+00	0.
3.81217262231E-03	5.24111436043E+00	1.10666696217E+03	1.27857504721E-01	2.07125103043E+00	0.
4.38399874566E-03	4.90213058503E+00	1.12752089740E+03	1.29244682686E-01	2.10379080857E+00	0.
5.04159855751E-03	4.58968104763E+00	1.14896792553E+03	1.30715113853E-01	2.13658710643E+00	0.
5.79783834113E-03	4.30133009798E+00	1.17102473063E+03	1.32275688253E-01	2.16956852346E+00	0.
6.66751409230E-03	4.03489868477E+00	1.19370813223E+03	1.33933926476E-01	2.20278418879E+00	0.
7.66764120615E-03	3.78843136261E+00	1.21703220011E+03	1.35698009743E-01	2.23620407658E+00	0.
8.81778738707E-03	3.56017162408E+00	1.24100758125E+03	1.37576837004E-01	2.26981884596E+00	0.

APPENDIX B

MATERIAL CONSTANTS USED IN PIPE TEST COMPUTATIONS

1. EOS Constants

Equation of State for Composition B

S(1,1) = .247, +1.88, +0., +0., +0., -6.67122275062E+00, -6.54470724004E+01,
-1.26689986425E+02, -1.03958493089E+02, -2.82360096898E+01, +1.325, +0.33,
0.583090379009, 0.0001, 0., 0., 300., 0.000001

G(1,1) = 3.52584878974, -2.33429189056, 0.597267325606, 3.04510424546E-3,

G(5,1) = -0.1752264031, -1.56087684485, 0.533121475935, 0.0806310874142,

G(9,1) = -3.33816891056E-3, -6.84399991171E-4, 7.5027805855, -.441209000835,

G(13,1) = 0.151292636188, 0.0677883292739, -0.0242403364371, 0.5, 0.1,

Equation of State for Air

S(13,2) = 865.224, S(17,2) = 300., 1.E-6,

G(1,2) = -4.50602542688, -1.27546110628, -.00374276600292, .0123929236747,

G(5,2) = -.00207694122929, -1.62655447438, .0905283146618, .00269004997726,

G(9,3) = -5.43583122192E-5, -1.58521895338E-6, 8.22644581441, -.25152513095,

G(13,2) = -.0134446940047, .0140871016422, -.00218132189985, 0.5, 0.1,

2. Forest Fire Reaction Constants

DWDT(1) = -3.90837771109E+13, 8.42165393554E+13, -8.15921576697E+13,
4.70008155979E+13, -1.79360385684E+13, 4.78196646064E+12,
-9.15443709404E+11, 1.27369703194E+11, -1.28969829135E+10,
9.43237549612E+08, -4.90557557768E+07, 1.77389261289E+06,
-4.35851265884E+04, 7.54066950304+02, -1.05480898447E+01

3. Pop Plot and Reactive Hugoniot Coefficients for Comp. B, Grade A; CJ Pressure; Detonation Products EOS Constants

```
 comp b, grade a, trott and jung pop plot and hugoniot            4oct79     rho = 1.71500

pop plot, ln(run) = a1 + a2*ln(p-a3),  a1 = -3.429950e+00  a2 = -1.133880e+00  a3 =  0.

reaction hugoniot,  us = c + s*up,      c =  2.470000e-01   s =  2.736500e+00

cj detonation pressure =  2.844000e-01

 hom equation of state constants
 compb, trott + jung, june 1971                                                t+j c-b
unreacted explosive
 2.47000000000e-01 1.88000000000e+00 0.                 0.
 0.               -6.67122275062e+00-6.54470724004e+01-1.26689986425e+02
-1.03958493089e+02-2.82360096898e+01 1.32500000000e+00 3.30000000000e-01
 5.83090379009e-01 1.00000000000e-04 0.                 0.
 3.00000000000e+02 1.00000000000e-06 0.                 0.
 0.                0.                0.
detonation products
-3.52584878974e+00-2.33429189056e+00 5.97267325606e-01 3.04510424546e-03
-1.75226403100e-01-1.56087684485e+00 5.33121475935e-01 8.06310874142e-02
 3.33816891056e-03-6.84399991171e-04 7.50278058550e+00-4.41209000835e-01
 1.51292636188e-01 6.77883292739e-02-2.42403364371e-02 5.00000000000e-01
 1.00000000000e-01
```

4. Forest Fire Calculation

comp b, grade a, trott and jung pop plot and hugoniot 4oct79 rho = 1.71500
pop plot, ln(run) = a1 + a2*ln(p-a3), a1 = -3.429950e+00 a2 = -1.133880e+00 a3 = 0.
reaction hugoniot, us = c + s*up, c = 2.470000e-01 s = 2.736500e+00

run	p	v	up	us	w	rate	temperature	time
8.99067	.00700	.55400	.01427	.28605	.99855	9.9190e-04	329.65222	27.03327
7.72745	.00800	.55094	.01604	.29088	.99801	1.4218e-03	334.72379	22.65250
6.76138	.00900	.54807	.01775	.29558	.99740	1.9416e-03	339.94025	19.35691
6.00001	.01000	.54535	.01943	.30016	.99674	2.4165e-03	345.29881	16.80017
2.73413	.02000	.52450	.03423	.34067	.98774	1.4607e-02	406.13670	6.45791
1.72645	.03000	.51046	.04668	.37474	.97565	4.0786e-02	477.49551	3.62262
1.24591	.04000	.50006	.05763	.40471	.96145	8.5224e-02	555.95029	2.38504
.96739	.05000	.49190	.06752	.43178	.94556	1.5261e-01	639.23232	1.71749
.78672	.06000	.48526	.07661	.45665	.92823	2.4826e-01	725.87758	1.31007
.66056	.07000	.47971	.08507	.47980	.90955	3.7850e-01	814.87267	1.04028
.56775	.08000	.47495	.09301	.50152	.88958	5.5074e-01	905.55649	.85093
.49677	.09000	.47082	.10052	.52207	.86832	7.7393e-01	997.43526	.71214
.44083	.10000	.46719	.10766	.54161	.84574	1.0590e+00	1090.14313	.60689
.39567	.11000	.46395	.11448	.56027	.82178	1.4193e+00	1183.41471	.52488
.35850	.12000	.46104	.12102	.57817	.79640	1.8723e+00	1276.99371	.45954
.32740	.13000	.45841	.12731	.59539	.76948	2.4389e+00	1370.73051	.40651
.30101	.14000	.45601	.13338	.61201	.74092	3.1469e+00	1464.47434	.36279
.27836	.15000	.45381	.13926	.62808	.71059	4.0292e+00	1558.12576	.32625
.25872	.16000	.45178	.14495	.64365	.67837	5.1419e+00	1651.49351	.29535
.24153	.17000	.44990	.15047	.65877	.64406	6.5439e+00	1744.55602	.26895
.22637	.18000	.44816	.15584	.67347	.60747	8.3256e+00	1837.20254	.24619
.21291	.19000	.44653	.16108	.68779	.56838	1.0619e+01	1929.34503	.22641
.20088	.20000	.44501	.16618	.70175	.52650	1.3627e+01	2020.92414	.20909
.19007	.21000	.44358	.17116	.71539	.48161	1.7604e+01	2111.78655	.19383
.18030	.22000	.44223	.17603	.72872	.43328	2.3071e+01	2201.92488	.18030
.17144	.23000	.44096	.18080	.74176	.38115	3.0838e+01	2291.22732	.16825
.16336	.24000	.43976	.18547	.75453	.32475	4.2459e+01	2379.59743	.15745
.15598	.25000	.43863	.19004	.76705	.26345	6.1412e+01	2467.01831	.14774
.14919	.26000	.43754	.19453	.77933	.19671	9.6355e+01	2553.30799	.13896
.14294	.27000	.43652	.19894	.79139	.12370	1.7950e+02	2638.39987	.13100
.13717	.28000	.43554	.20326	.80323	.04349	5.9851e+02	2722.19200	.12376

5. Polynomial Fit for Forest Fire Calculation

```
 comp b, grade a, trott and jung pop plot and hugoniot              4oct79     rho = 1.71500
ln(rate) = c(1) + c(2)*p + ... + c(m+1)*(p**m)
c(i=1,15) =  -1.0548089845e+01  7.5406695030e+02 -4.3585126588e+04  1.7738926129e+06 -4.9055755777e+07
              9.4323754961e+08 -1.2896982914e+10  1.2736970319e+11 -9.1544370940e+11  4.7819664606e+12
             -1.7936038568e+13  4.7000815598e+13 -8.1592157670e+13  8.4216539355e+13 -3.9083777111e+13
```

pressure	rate	fit	rel. error
7.000000e-03	9.919009e-04	1.007589e-03	-.015817
8.000000e-03	1.421773e-03	1.401907e-03	.013973
9.000000e-03	1.941615e-03	1.890045e-03	.026561
1.000000e-02	2.416511e-03	2.478791e-03	-.025773
2.000000e-02	1.460745e-02	1.464353e-02	-.002470
3.000000e-02	4.078595e-02	4.057070e-02	.005278
4.000000e-02	8.522415e-02	8.534549e-02	-.001424
5.000000e-02	1.526065e-01	1.531670e-01	-.003673
6.000000e-02	2.482640e-01	2.480946e-01	.000682
7.000000e-02	3.785028e-01	3.772960e-01	.003188
8.000000e-02	5.507358e-01	5.502233e-01	.000931
9.000000e-02	7.739284e-01	7.755965e-01	-.002155
1.000000e-01	1.059023e+00	1.061413e+00	-.002256
1.100000e-01	1.419306e+00	1.419164e+00	.000100
1.200000e-01	1.872254e+00	1.868044e+00	.002248
1.300000e-01	2.438933e+00	2.434569e+00	.001790
1.400000e-01	3.146907e+00	3.148300e+00	-.000443
1.500000e-01	4.029180e+00	4.039831e+00	-.002644
1.600000e-01	5.141871e+00	5.147901e+00	-.001173
1.700000e-01	6.543861e+00	6.535911e+00	.001215
1.800000e-01	8.325550e+00	8.308095e+00	.002097
1.900000e-01	1.061910e+01	1.061369e+01	.000509
2.000000e-01	1.362651e+01	1.364248e+01	-.001172
2.100000e-01	1.760386e+01	1.764659e+01	-.002427
2.200000e-01	2.307069e+01	2.305615e+01	.000630
2.300000e-01	3.083829e+01	3.074866e+01	.002907
2.400000e-01	4.245904e+01	4.247880e+01	-.000465
2.500000e-01	6.141160e+01	6.160833e+01	-.003203
2.600000e-01	9.635500e+01	9.607394e+01	.002917
2.700000e-01	1.794970e+02	1.796841e+02	-.001042
2.800000e-01	5.985117e+02	5.984283e+02	.000139

Printed in the United States of America. Available from
National Technical Information Service
US Department of Commerce
5285 Port Royal Road
Springfield, VA 22161

Microfiche $3.00

001-025	4.00	126-150	7.25	251-275	10.75	376-400	13.00	501-525	15.25
026-050	4.50	151-175	8.00	276-300	11.00	401-425	13.25	526-550	15.50
051-075	5.25	176-200	9.00	301-325	11.75	426-450	14.00	551-575	16.25
076-100	6.00	201-225	9.25	326-350	12.00	451-475	14.50	576-600	16.50
101-125	6.50	226-250	9.50	351-375	12.50	476-500	15.00	601-up	

Note: Add $2.50 for each additional 100-page increment from 601 pages up.